Final Report

Enceladus Life & Mechanism Explorer Orbiter

AE3200 Design Synthesis Exercise

Group 02

Delft University of Technology

TU Delft

This page is intentionally left blank.

Final Report

Enceladus Life & Mechanism Explorer Orbiter

by

Group 02

Student Name	*Student Number*
Farris Al-Rawi	5253683
Alice Girardello	5214742
Jeroen Hilker	5333008
Elena Moro	4784308
Sherif Nafie	5213363
Jochem van der Ouw	5206049
Visini Pathirana	5294959
Christian Plevier	5041120
Matyas Toulemonde	5113458
Nelson Wierzbinski	5508479
Hidde Zwart	5332885

Issue	*Amendment*	*Date*
V2.0	Final report	28/01/2025

Course:	AE3200 Design Synthesis (2024/25 Q2)
Tutor:	Ir. B. Zandbergen
Coaches:	Dr. F. Oliviero, E. Wiegert
Project Duration:	11 November 2024 - 30 January 2025
Faculty:	Faculty of Aerospace Engineering

Cover image: Own work.

TU Delft

Changelog

Table 1: Changelog table.

Date	Version	Changed Items and Details
22/01/2025	1.0	Draft.
28/01/2025	2.0	Whole report: grammar and phrasing checks. Nomenclature: added TBR acronym. Section 4.6: added the mass of the launch vehicle adapter to the total launch mass. Also added it to other tables specifying the launch mass. Section 4.7: Added this section, it describes the overall design process with 2 diagrams. 1 showing the system design process, and the other giving a basic overview of an iteration cycle. Chapter 5: small fixes following feedback in particular to specify better the hoppers data rate requirement subsection 5.3.5: added subsection to present reviewers concerns and add beamwidth calculations Chapter 6: modified Figure 6.1 to include PDU redundancy, added explanations to clarify margins and V&V procedure. Chapter 7: Appended with disclaimer about pointing performance. Chapter 8: Added in the recommendations the potential usage of a pump-fed configuration, rather than a pressure-fed configuration. Chapter 9: modified Section 9.2 to include final structure mass with system margin and modified Section 9.3 to include LVA connection and outer structure dimensions. Chapter 17: In subsection 17.2.1 changed reported spacecraft cost incl. payload in SCEA-ISPA Joint Annual Conference and Training Workshop slide from $3\,\mathrm{G\$}$ to $2\,\mathrm{G\$}$. Removed margin of ESA / NASA and instead used RSE in subsection 17.2.3. Replaced estimates with ESA / NASA margin with estimate plus RSE in Table 17.5. Added recommendation for a split of cost estimation into kick stage and orbiter estimation in Section 17.4. Added a comment on kickstage separation mass in Chapter 10

Executive Overview

Mission Description

Saturn's icy moon Enceladus has long been a candidate for possible alternative life in the solar system. This is due to its sub-surface ocean and hydrothermal activity, causing geyser-like plumes on its South Pole. To investigate the possibility of life on Enceladus, the Enceladus Life and Mechanisms Explorer (ELMO) has been conceived. ELMO's mission is to transport several payloads to an orbit around Enceladus to investigate the possibility of life. The payload includes several instruments that will map Enceladus' surface and magnetic field. Additionally, once arrived at Enceladus, 2 hoppers will separate from the spacecraft and autonomously explore the geysers on Enceladus' South Pole.

Driving Requirements

The customer has outlined numerous requirements for the mission, but during the design process, it was determined that only a handful of them drive the design. The driving requirements are presented in Table 2.

Table 2: Driving requirements

ID	Description
USR-SYS-01	The spacecraft shall be compatible with the Ariane 64 launch vehicle. The launch vehicle is considered to put the spacecraft on an Earth escape trajectory. The maximum launch mass for the Ariane 64 is 9600 kg.
USR-SYS-02	The orbiter reliability (including payload) shall be equal or better than 0.75 for EoM.
USR-SYS-06	The orbiter (including payload) shall cost equal or less than 750 M$ (FY 2025).
USR-SYS-07	The orbiter shall be able to perform transfer flight correction manoeuvres of total size $1200\,\mathrm{m/s}$ (high-thrust option).
USR-SYS-08	The orbiter shall be able to provide for a delta-V equal or better than $4.6\,\mathrm{km/s}$ (high-thrust option) in order to achieve the desired orbit around Enceladus.
USR-SYS-09	The orbiter shall be able to perform orbit control when in mission orbit about Enceladus to the extent of $200\,\mathrm{m/s}$ or better.
USR-PLD-06	The HRC shall only operate in regions that are sunlit
USR-MIS-07	The orbiter shall comply with the Space Debris Guidelines of the Committee on the Peaceful Uses of Outer Space

Mission and System Overview

A summary of the most important features of the ELMO orbiter design is presented in Table 3.

Table 3: Mission overview

Parameter	Description
Production completion Date	2035
Date at Enceladus	2043-2044
Launcher	Ariane A64
Transfer time	$8\,\text{years}$
Trajectory	Earth - Venus - Venus - Earth - Jupiter - Saturn - Enceladus
Time at Enceladus	$100\,\text{days}$ nominal, consumables up to 1 year
ΔV for transfer flight	$1200\,\text{m/s}$
ΔV for insertion into Enceladus orbit	$4600\,\text{m/s}$
ΔV for orbital maintenance	$200\,\text{m/s}$
Orbit type around Enceladus	$100\,\text{km}$ altitude polar dawn-dusk orbit
Science-transmission orbit split	$30\,\%$ science, $70\,\%$ transmission
Solar availability	$100\,\%$
Earth availability	$100\,\%$
Time window for $100\,\%$ availability	August 2042 - March 2051 February 2058 - April 2065
Mass of the kick stage (1st stage)	Dry mass of $921.6\,\text{kg}$ and wet mass of $8503.9\,\text{kg}$ incl. $20\,\%$ system margin
Mass of the orbiter (2nd stage)	Dry mass of $1633\,\text{kg}$ and wet mass of $4870.7\,\text{kg}$ incl. $20\,\%$ system margin
Total Mass	Dry mass of $2554.6\,\text{kg}$ and wet mass of $13\,374.7\,\text{kg}$ incl. $20\,\%$ system margin
Estimated total spacecraft cost	$2613\,\text{M\$}$ incl. $30\,\%$
Propellant tank dimensions	Each stage has 2 spherical propellant tanks. The radius of the propellant tanks are $0.73\,\text{m}$ and $0.97\,\text{m}$ for the orbiter and kick stage respectively.
Propellant	Fuel: Monomethylhydrazine (MMH) Oxidiser: Dinitrogen tetroxide (N2O4) Pressurizing gas: Helium (He)
Solar array dimensions	4 solar array wings, each being $3\text{x}8\,\text{m}$, composed of 3 panels each for a total area of $85.5\,\text{m}^2$
Solar cell efficiency	$37\,\%$
Solar array angle of incidence	$26.7°$
Total power generated at EOL	$219\,\text{W}$ at $26.7°$ angle of incidence (science mode) and $245\,\text{W}$ at $5°$ angle of incidence (transmit mode).
Antenna diameter and band	Main antenna: $3.5\,\text{m}$ (Ka and X-band) Hopper antenna $0.5\,\text{m}$ (S-band)
Data transmission rate	$381\,\text{kbps}$
ADCS actuators and sensors	4 Reaction wheels 24 Thrusters for desaturation 1 IMU 2 Sun sensors 4 star trackers

Mass Reduction Strategies

The most challenging aspect of the design was to match the high ΔV requirements with the stringent mass requirements of the Ariane A64 launcher. Many strategies were devised to minimize the mass. State-of-the-art solar cells with high efficiency were selected for the solar array to reduce its area and mass, as well as a strong but light honeycomb structure for its back panel support. Due to high pressures within the propellant tanks, a spherical shape was chosen for them, reducing their thickness. CFRP was chosen for the helium tanks instead of the standard titanium, reducing their mass. Furthermore, a truss was chosen instead of a cylindrical shell for the main structure of the orbiter.

Another way of saving mass is by reducing the power requirements of the subsystems, as it reduces the required solar array area and therefore solar array mass. For this reason, having a passive thermal system was insisted upon. With a combination of multi-layer-insulation (MLI), radioisotope thermo-electric heaters (RTH) and louvers, it was possible to have a passive thermal subsystem. This system caters to the frigid environment around Saturn and to the hot one close to Venus. For ADCS, power requirements were minimized by opting for long slew times to reduce reaction wheel size. The instruments onboard the ELMO orbiter produce a high amount of data that needs to be sent back to Earth. This high data rate and large distance to Earth causes the communications subsystem to require a lot of power and a large antenna diameter. Using the Ka-band instead of the X-band reduces the power of the subsystem. Furthermore, a science orbit and transmission orbit split was chosen, dedicating 70% of the orbits to transmitting data to Earth and 30% for science data collection.

The orbit design has been optimized to maximize Sun and Earth availability. The chosen polar dawn-dusk orbit ensures that the spacecraft is never eclipsed by Enceladus. Furthermore, due to the inclination of Enceladus' orbit, there exists a time window (2042-2051) where Enceladus is never eclipsed by Saturn. This mission will be performed in this ideal time window and will therefore have a 100% Earth and Sun availability, compared to 67% in the worst case orbit. This causes 3 improvements: firstly, this allows the solar array to continuously collect power, eliminating the need for a battery specifically for eclipses and reducing the peak power production. Secondly, this allows the communications antenna to continuously send data to Earth, reducing power requirements. Lastly, having the spacecraft continuously exposed to the sun helps heating it in the cold Saturnian environment, minimizing the amount of RTH used in the thermal subsystem. These improvements lead to the reduction of mass in the spacecraft. Within other subsystems, smaller decisions were made in an attempt to comply with the mass requirement. In the end, it was not possible to do this as the ELMO orbiter's final wet mass is $13\,374.7\,\mathrm{kg}$, which is above the maximum of $9600\,\mathrm{kg}$ of the Ariane A64 launcher.

A picture of the final design can be found below. The MLI was removed to show the internal outline.

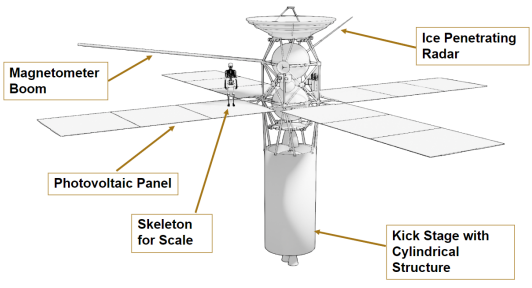

Figure 1: Deployed two-stage configuration of the ELMO orbiter with subsystem elements indication.

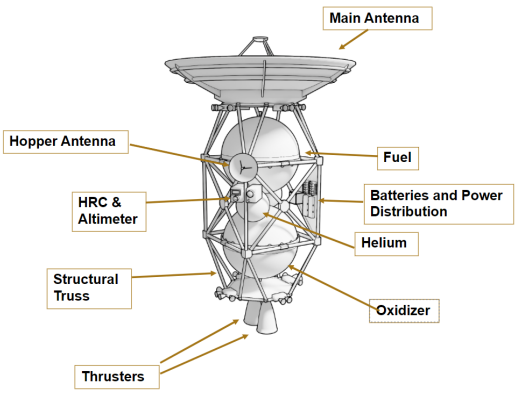

Figure 2: Deployed upper stage of the ELMO orbiter with subsystem elements indication.

Reliability Improvement Strategy

Since ELMO is set to travel for 8 years with no possible maintenance, reliability must be considered during its design. One of these considerations is that there should be no single point of failure in the design. For this reason, there is a backup antenna dish that can be used to receive the necessary commands from Earth to re-establish connection in case of the main antenna dish failure. Each stage has 2 engines, such that the spacecraft can still propel itself in case of an engine failure. All ADCS components are duplicated. Structural components are an exception to this rule, as duplicating those would cause too much of a mass increase. To mitigate structural risks, they will be extensively tested. Another large reliability consideration is the reduction of mechanisms. ELMO does not use a solar array drive mechanism, instrument pointing mechanism or antenna pointing mechanism. This causes the solar arrays to be at an angle of incidence of 26.7°, which increases its mass. it was decided that this was a sufficient gain in reliability to afford a mass increase after performing a trade-off.

Requirement Compliance and Recommendations

This feasibility study concludes that at this stage of the design, 4 out of the 46 requirements cannot be met. These are the mass (USR-SYS-01) and cost (USR-SYS-06) requirements, and compliance with the safety and space debris requirements (USR-MIS-06, USR-MIS-07). The mass requirement could not be met, as the total launch mass is 13.5 tons (including a 20% system margin) compared to the 9.6 tons stated by the Ariane A64 launcher requirement. Furthermore, the cost requirement of $750\,\mathrm{M\$}$ could not be respected as the current best cost estimate of the spacecraft is $2613\,\mathrm{M\$}$. However, this was expected since similar missions usually cost several billions of dollars. Per request of the customer, compliance with the end-of-life aspect of the safety and space debris requirements were set aside. This decision is justified as this would require a significant additional ΔV. Finally, it was uncovered that when ELMO is performing its mission around Enceladus, the south pole of Enceladus will not be sunlit until October 2054, making it impossible for the high-resolution camera to observe the area of interest.

Several recommendations can be made to solve these problems. Firstly, the high mass of the spacecraft can be accommodated by selecting another launch vehicle. For example, the Falcon Heavy has the capability of sending 16.8 tons to Mars, which should be enough to send ELMO towards Venus. The high cost of the mission can be mitigated by involving other parties, such as QUEST, a Uranus Orbiter mission concept, and COMPASS, a Jovian orbiter mission concept. As these missions have some similarities with ELMO, the development costs could be shared.

Several reasons have been found to delay the launch of the spacecraft. Firstly, this serves to satisfy the lighting condition requirement. Delaying the launch by roughly 15 years would render it possible to observe the South Pole of Enceladus in sunlit conditions. Delaying the launch was also deemed necessary since 2035 seems like an overly optimistic completion date, given historic space missions. Delaying by 15 years also means that Saturn will be $1\,\mathrm{AU}$ closer to the sun, meaning 20% more power can be generated per unit area, reducing solar array area. Finally, a delay would allow new technologies to be developed, such as lighter materials and more efficient solar cells, reducing the overall mass of the spacecraft.

Finally, some recommendations can be given to future feasibility studies. The risk for micrometeorite collisions should be investigated. The effect of Saturn's E ring was neglected in this study, but might be worth considering in a later study. Lastly, the decision to delay solar array deployment can cause some risk that should be considered in more detail.

Contents

Nomenclature

Abbreviations

Abbreviation	Definition
ADCS	Attitude Determination and Control Subsystem
ARW	Angular Random Walk
ATP	Authority To Proceed
AU	Astronomical Unit
CDH, C&DH	Command and Data Handling Subsystem
COM	Communication Subsystem
CoM	Centre of Mass
COSPAR	Committee for Space Research
COTS	Commercial Off-The-Shelf
DoD	Depth of Discharge
DSN	Deep Space Network
EOL	End of Life
EoM	End of Mission
EPS	Electrical Power System
ELMO	Enceladus Life and Mechanisms Explorer
ESA	European Space Agency
FBS	Functional Breakdown Structure
FFD	Functional Flow Diagram
FY	Fiscal Year
HGA	High Gain Antenna
HRC	High-Resolution Camera
IMU	Inertial Measurement Unit
MEC	Mechanism Subsystem
MGA	Medium Gain Antenna
MLE	Most Likely Estimate
MLI	Multi-Layer Insulation
MMH	Monomethylhydrazine
N/A	Not applicable
N_2O_4	Dinitrogentetraoxide
LCC	Life Cycle Cost
LEO	Low Earth Orbit
LGA	Low Gain Antenna
LILT	Low-Intensity Low-Temperature
PEBD	Planetary Exploration Budget Database
PLD	Payload Subsystem
PMU	Power Management Unit
PPP	Planetary Protection Policy
PRP	Propulsion Subsystem
QPSK	Quadrature Phase Shift Keying
RAM	Random Access Memory
RRS	Reliability, Risk and Safety
RTG	Radioisotope Thermo-electric Generator

Abbreviation	Definition
RTH	Radioisotope Thermo-electric Heater
SA	Solar Array
SPF	Single-Point Failure
STR	Structures Subsystem
TBR	To be reviewed
TRC	Thermal and Radiation Control Subsystem
TWTA	Traveling Wave Tube Amplifiers
V&V	Verification and Validation

Symbols

Symbol	Definition	Unit
A	Area	m^2
a	Albedo factor	-
B	Bandwidth	Hz
B_r	Data rate	bps
C	Channel capacity	bps
c	Speed of light	m/s
C_r	Reflectivity coefficient	-
D	Diameter	m
d	Distance	m
$\frac{E_b}{N_0}$	Ratio of energy per bit to noise power spectral density	dB
$EIRP$	Effective isotropic radiated power	dBW
f	Frequency	Hz
$\mathbf{I}$	Spacecraft inertia matrix	$kg \cdot m^2$
G	Gain	-
G	Solar flux	W/m^2
H	Momentum	$N \cdot m \cdot s$
I_{sp}	Specific Impulse	s
Ka	Absorption factor	-
k_B	Boltzmann constant ($1.380649 \cdot 10^{-23}$)	J/K
L	Transmission loss	dB
m	Mass	kg
n	moles	mol
P	Power	W
Q	Planetary infrared radiation	W/m^2
q	Heat flux	W
S	Surface area	m^2
SNR	Signal to noise ratio	-
T	Temperature	K
R	Gas constant	$J/mol/K$
r	Orbital radius about Enceladus	m
α	Angle of incidence	deg
α	Absorptivity	-
Δq	Change in heat	W
Δt	Simulation time step	s
ΔV	Delta-V	m/s

Symbol	Definition	Unit
ϵ	Emissivity	-
η	Efficiency	-
λ	Wavelength	m
ν	Poisson's ratio	-
ρ	Surface density	kg/m^2
ρ	Volume density	kg/m^3
ρ	Angular radius	rad
μ	Gravitational parameter	m^3/s^2
$\boldsymbol{\tau}$	Torque	$N \cdot m$
$\boldsymbol{\omega}$	Spacecraft angular velocity	rad/s
$\dot{\boldsymbol{\omega}}$	Spacecraft angular acceleration	rad/s^2

1 Introduction

The pursuit of life beyond our planet has intrigued humankind for centuries, long before the dawn of space exploration. While it is often considered a far concept that can only exist light years away, evidence has shown that there are possibilities for life to thrive much closer to home. Of the many moons that orbit Saturn, the Cassini spacecraft found evidence of hydrothermal activity and methane in the geyser-like plumes on the South Pole of Enceladus. Since these are vital elements of life as humans know it on Earth, Enceladus quickly became one of the most interesting bodies in the solar system to search for life. The Enceladus Life and Mechanism Explorer (ELMO) orbiter aims to travel to Enceladus to investigate for biosignatures and signs of life, as well as to map its surface, by carrying five scientific payload instruments and two hopper vehicles to be deployed on the icy moon's South Pole.

The mission is composed of two main elements. Firstly, an orbiter platform, to host and carry payloads to Enceladus, which will also serve as a communication relay between the hopper vehicles on the icy moon's surface and Earth. The orbiter platform carries on board a suite of five scientific instruments to analyse the surface of Enceladus. Secondly, the mission also includes two hopper vehicles, which will be released on Enceladus' surface from the orbiter and will investigate its surface plumes of water vapour at the South Pole. The hoppers also function as miniature laboratories and can analyse plume samples on-board. The data that they collect is sent to the orbiter and shall be relayed back to Earth.

The study presented in this report investigates the feasibility of the design within specific constraints. The report begins with an overview of the payloads in Chapter 2, followed by a thorough mission analysis in Chapter 3 where the data acquisition and transmission plan will be explained, alongside the main orbital considerations. In Chapter 4, the spacecraft will be presented in its entirety on a system level. The spacecraft analysis will continue from Chapter 5 until Chapter 12 where every subsystem of the ELMO orbiter will be described. In Chapter 13, the sustainable development plan for the ELMO orbiter will be presented, as well as some end-of-life considerations.

Chapter 14 will propose a sensitivity analysis of how some key design parameter changes could affect the spacecraft on a system level. Chapter 15 will focus on the future developments needed to realize the ELMO mission, from design to testing all the way up until launch. Chapter 16 will focus on exploring the risks and reliability of the mission and spacecraft design, while Chapter 17 will present a cost overview and market analysis. Lastly, Chapter 18 will wrap up the report by defining the feasibility of the study and offering recommendations for future development, as well as some options for design exploration. An overview of the main outcomes of the study will then be given in the conclusion, in Chapter 19.

2
Payload Description

The goal of the ELMO mission is to search for signs of life on the surface, and to map and characterize the icy moons surface. This chapter shall describe each element of the payload and its contribution to the mission goal. In Section 2.1, each of the scientific instruments is described. Then, in Section 2.2, a description of the hopper vehicles, along with their characteristics, is given.

2.1. Scientific Instruments

There are 5 scientific payload instruments that can be found on the spacecraft. A description of each instrument can be found below. Table 2.1 summarises the instruments with respect to their mass, power, data rate, and cost.

Ice Penetrating Radar

The Ice Penetrating Radar (IPR) is designed to characterize the sub-surface structure of the ice sheets of Enceladus with depths of up to $30\,\mathrm{km}$. The IPR is the most complex onboard instrument, as well as the most expensive, having a cost of $25M (*FY 2019*). Its antenna extends out of the spacecraft by $16\,\mathrm{m}$ in its deployed state. The IPR, including its electronics, has a total mass of $28\,\mathrm{kg}$. It has a required pointing accuracy of 0.1°. It has an average active power consumption of $18\,\mathrm{W}$ and an idle power consumption of $1\,\mathrm{W}$. The IPR has a data rate of $5\,\mathrm{Mbps}$.

Enceladus Laser Altimeter

The Enceladus Laser Altimeter (ELA) is designed to map the topology of the surface. It sits in the payload bay of the spacecraft and has a total mass of $13\,\mathrm{kg}$. It has a pointing accuracy of $10''$ and a cost of $10M (*FY 2022*). It has an active power consumption of $25\,\mathrm{W}$ and an idle power consumption of $2\,\mathrm{W}$. The ELA has a data rate of $12.5\,\mathrm{kbps}$.

High Resolution Camera

The High Resolution Camera (HRC) is responsible for surface imaging and topology, and sits within the payload bay. By integrating HRC imagery with ELA data, the Enceladus surface data can be mapped with extremely high precision. The HRC has a total mass of $22\,\mathrm{kg}$ and a pointing accuracy of 0.1°. The HRC costs $16M (*FY 2022*). Its power consumption is $40\,\mathrm{W}$ when active and $6\,\mathrm{W}$ when in idle mode. The HRC has an produces a data rate of $40\,\mathrm{MB}$ per image. The field of view of the HRC lense is 12°.

Tri-Axis Accelerometer

The Tri-Axis Accelerometer (TAA) shall be used to measure the gravity field produced by Enceladus. It shall also sit within the payload bay of the spacecraft and has a mass of $0.5\,\mathrm{kg}$, and has a sample rate between $12.5\,\mathrm{Hz}$ and $50\,\mathrm{Hz}$. The TAA has a power consumption of $1\,\mathrm{W}$ in active mode and $0\,\mathrm{W}$ in idle. The TAA costs $1M (*FY 2022*). The TAA has a data rate of $3.6\,\mathrm{kbps}$.

Tri-Axis Magnetometer

The Tri-Axis Magnetometer (TAM) is responsible for measuring the magnetic field produced by Enceladus. In order for readings to not be obscured by magnetic fields produced by the spacecraft, the

TAM shall be placed on a boom to distance it from the spacecraft body. The TAM has a mass of $3.1\,\mathrm{kg}$, whilst the boom has a mass of $0.1\,\mathrm{kg}$ per meter and must be at least $6\,\mathrm{m}$ outboard. It has a pointing accuracy of less than $5\,\mathrm{mrad}$ and an active power consumption of $4\,\mathrm{W}$ and a idle power consumption of $0\,\mathrm{W}$. The TAM costs $1M (*FY 2019*), and has a sample rate between $10\,\mathrm{Hz}$ and $80\,\mathrm{Hz}$. The TAM has a data rate of $5.76\,\mathrm{kbps}$.

Table 2.1: Summary of the characteristics of the 5 payload instruments. The harness mass is neglected for the TAM. Costs are all given for fiscal year 2025 and calculated using [1]

Instrument	Mass (kg)	Power (W)		Data Rate	Cost ($M)
		Active	Idle		
IPR	28	18	1	$5\,\mathrm{Mbps}$	30.85
ELA	13	25	2	$12.5\,\mathrm{kbps}$	10.78
HRC	22	40	6	$40\,\mathrm{Mb}$ per image	17.25
TAA	0.5	1	0	$3.6\,\mathrm{kbps}$	1.08
TAM	3.1	4	0	$5.76\,\mathrm{kbps}$	1.08

2.2. Hopper Vehicles

The spacecraft shall carry 2 spherical hopper vehicles to Enceladus, where they will be deployed to the South Pole at an altitude of $100\,\mathrm{km}$, as is stated by requirement USR-MIS-08. Both hoppers have a volume of $0.7\,\mathrm{m}^3$. The hopper vehicles have a mass of $86\,\mathrm{kg}$, and $99\,\mathrm{kg}$, as well as a cost of $27.2M (*FY 2010*), and $34.1M (*FY 2010*), respectively. The mechanism for the hopper release is investigated in Section 10.4. The hopper vehicles shall act autonomously on the surface and thus will not require any commands from the spacecraft. Figure 2.1 shows a visual representation of the hopper vehicles.

Figure 2.1: A rendering of a hopper vehicle. Taken from the project document [2].

The purpose of the hopper vehicles is to search for signs of life on the surface and transmit scientific data to the spacecraft. Once deployed to the surface, the hopper vehicles will search for geysers and insert themselves into jet plumes in order to take samples of the subsurface oceans contents. After analysing the water contents in an onboard laboratory, the data generated shall be relayed to the spacecraft. The hoppers are equipped with transmitter antennas that operate on the S-band at a frequency of $2\,\mathrm{GHz}$. Each hopper produces $2.95\,\mathrm{Gb}$ per Earth day and is capable of transmitting a maximum data rate of $4\,\mathrm{Mbps}$ when the spacecraft is in view. Both hopper vehicles have an antenna elevation angle of $10°$.

The hopper vehicles are critical to the search-for-life aspect of the mission, as the spacecraft payload instruments themselves does not have the capabilities to detect signs of life, but are rather designed for characterising Enceladus itself. Although they are critical for the success of the ELMO mission, the specifics of the hopper vehicle design is to be further investigated at a later time.

3
Mission Analysis

This chapter describes the operations planning of ELMO at Enceladus and all astrodynamics concerning ELMO's trajectory and orbit and starts with an overview of all payload requirements in Section 3.1. Following this, the launch and transfer phase will be explained in Section 3.2. The mission profile is explained in Section 3.3 and a description of the chosen orbit is given in Section 3.4. Two important values used during the design process are determined in this chapter, such as Saturn's orbital altitude in Section 3.5 and the Sun and Earth Availability in Section 3.6. The coverage visualization is verified for accuracy in Section 3.7 and a problem concerning Enceladus' south pole illumination is presented in Section 3.8

3.1. Requirements and Constraints

In this section the requirements and constraints are discussed. First the requirements are given with their coding convention, followed by the changelog of the requirements.

3.1.1. User requirements

The user requirements, as derived from the reader [2], form the basis of our design. These requirements have been listed in Table 3.2 and are categorized and coded according to the conventions found in Table 3.1.

Table 3.1: Requirement Coding Convention

Category	Description
User Requirements (USR)	• **USR-MIS-XX:** Mission-related requirements. • **USR-SYS-XX:** System-level requirements. • **USR-PLD-XX:** Payload-related requirements. • **USR-COM-XX:** Communication-related requirements.
ELMO Requirements (ELM)	• **ELM-UMXX-[Subsystem]-XX:** Flows down from USR-MIS-XX. • **ELM-USXX-[Subsystem]-XX:** Flows down from USR-SYS-XX. • **ELM-UPXX-[Subsystem]-XX:** Flows down from USR-PLD-XX. • **ELM-UCXX-[Subsystem]-XX:** Flows down from USR-COM-XX.

Category	Description
Subsystem Codes	• **PRP:** Propulsion • **ADC:** Attitude Determination and Control (ADCS) • **COM:** Communication • **CDH:** Command and Data Handling • **EPS:** Electrical Power System • **PLD:** Payload • **STR:** Structure • **TRC:** Thermal and Radiation Control • **MEC:** Mechanism • **RRS:** Reliability, Risk, and Safety • **CST:** Cost

Table 3.2: Updated User Requirements

ID	Description
USR-SYS-01	The spacecraft shall be compatible with the Ariane 64 launch vehicle. The launch vehicle is considered to put the spacecraft on an Earth escape trajectory. The maximum launch mass for the Ariane 64 is $9600\,\mathrm{kg}$.
USR-SYS-02	The orbiter reliability (including payload) shall be equal to or better than 0.75 for EoM.
USR-SYS-03	The orbiter operational life shall be extendible to 1 year, considering consumable reserves.
USR-SYS-04	Orbiter position accuracy (knowledge) shall be better or equal to $1\,\mathrm{km}$.
USR-SYS-05	The spacecraft shall withstand a radiation dose of at least $50\,\mathrm{krad}$ over its lifetime.
USR-SYS-06	The orbiter (including payload) shall cost equal to or less than $750\,\mathrm{M\$}$ (FY 2025).
USR-SYS-07	The orbiter shall be able to perform transfer flight correction maneuvers of total size $1200\,\mathrm{m/s}$ (high-thrust option).
USR-SYS-08	The orbiter shall provide a delta-V equal to or better than $4.6\,\mathrm{km/s}$ (high-thrust option) to achieve the desired orbit around Enceladus.
USR-SYS-09	The orbiter shall perform orbit control in mission orbit around Enceladus to the extent of $200\,\mathrm{m/s}$ or better.
USR-MIS-01	The orbiter shall be delivered ready for launch in 2035.
USR-MIS-02	The orbiter transfer flight duration shall not exceed $8\,\mathrm{years}$.
USR-MIS-03	The transfer orbit shall be of a similar trajectory to Cassini.
USR-MIS-04	The orbiter shall orbit at an altitude between $100\,\mathrm{km}$ and $500\,\mathrm{km}$, in a retrograde circular orbit.
USR-MIS-05	The orbiter operational life in mission orbit (science life) shall be at least $100\,\mathrm{days}$.
USR-MIS-06	A safety policy in accordance with ECCS-Q-ST-40C shall aim to eliminate hazards during manufacturing, operation, and end-of-life stages, protecting personnel, property, and the environment.
USR-MIS-07	The orbiter shall comply with the Space Debris Guidelines of the Committee on the Peaceful Uses of Outer Space.

ID	Description
USR-MIS-08	The Hopper vehicles shall be deployed at an altitude of $100\,\mathrm{km}$.
USR-MIS-09	The HRC shall image the entire southern hemisphere of Enceladus at least once, with regular revisits to detect variations.
USR-PLD-01	Scientific instruments shall be active for $15\,\%$ of the operational mission time.
USR-PLD-02	The orbiter shall supply a maximum power of $97.5\,\mathrm{W}$ to the payload.
USR-PLD-03	The orbiter shall contain a payload of $251.6\,\mathrm{kg}$ (excluding the magnetometer harness).
USR-PLD-04	The magnetometer sensors shall be mounted on a boom at least $6\,\mathrm{m}$ outboard from any other spacecraft component.
USR-PLD-05	The payloads shall experience a radiation dose of no more than $10\,\mathrm{krad}$.
USR-PLD-06	The HRC shall operate only in sunlit regions.
USR-PLD-07	The orbiter shall provide a pointing accuracy of at least $10\,\mathrm{arcsec}$ or better.
USR-PLD-08	The orbiter shall provide a pointing stability of $0.5\,\mathrm{arcsec/sec}$ or better.
USR-PLD-09	The maximum spacing of magnetometer data points shall not exceed $2\,\mathrm{km}$ in the along-track and across-track directions.
USR-PLD-10	The maximum spacing of accelerometer data points shall not exceed $2\,\mathrm{km}$ in the along-track and across-track directions.
USR-PLD-11	The payload operational temperature range shall be limited to $-30\,°\mathrm{C}$ to $65\,°\mathrm{C}$ unless specified otherwise.
USR-PLD-12	The HRC shall point in the nadir direction with a ground resolution of $20\,\mathrm{m}$ at most.
USR-PLD-13	The Enceladus Laser Altimeter shall point in the nadir direction.
USR-PLD-14	The EPS shall not supply power to the Hopper vehicles before deployment.
USR-PLD-15	The hoppers shall be deployed near the south pole of Enceladus.
USR-PLD-16	The orbiter shall facilitate a minimum elevation angle of $10°$ for communication with the hoppers.
USR-PLD-17	The spacecraft shall securely contain Hopper 1.
USR-PLD-18	The spacecraft shall securely contain Hopper 2.
USR-PLD-19	The spacecraft shall securely contain a customer-specified IPR.
USR-PLD-20	The spacecraft shall securely contain a customer-specified HRC.
USR-PLD-21	The spacecraft shall securely contain a customer-specified ELA.
USR-PLD-22	The spacecraft shall securely contain a customer-specified tri-axis magnetometer.
USR-PLD-23	The spacecraft shall securely contain a customer-specified tri-axis accelerometer.
USR-COM-01	The orbiter shall communicate with the ground station using ESA or NASA Deep Space Network in X-band or Ka-band (S-band as backup).
USR-COM-02	The orbiter shall communicate with the hoppers using S-band.
USR-COM-03	The orbiter shall allow for science downlink in Ka-band.
USR-COM-04	The orbiter shall allow for uplink in X-band, keeping downlink as a backup option.
USR-COM-05	The orbiter shall communicate with Earth using S-band as a backup option.

3.1.2. Requirements changelog

During the design process, some requirements have been updated either at the customers request, or to improve the feasibility of the design. The updated requirements and, where applicable, their old descriptions have been listed in Table 3.3. The updated requirements are a part of the user requirements listed in Table 3.2.

Table 3.3: Updates to User Requirements

ID	Original Description	New Description
USR-SYS-01	The spacecraft shall be compatible with the Falcon 9 and the Ariane 62/64 launchers. The launch vehicle is considered to put the spacecraft on an Earth escape trajectory. The maximum launch mass for the Falcon 9 is limited to 3100 kg, for Ariane 64 to 9600 kg, and for A62 to 2600 kg.	The spacecraft shall be compatible with the Ariane 64 launch vehicle. The launch vehicle is considered to put the spacecraft on an Earth escape trajectory. The maximum launch mass for the Ariane 64 is 9600 kg.
USR-MIS-06	A safety policy in accordance with ISO 14300-2 shall be established that aims to eliminate hazards associated with the manufacturing, operation (including end of life) as well as personnel, other property, and the environment.	A safety policy in accordance with ECCS-Q-ST-40C shall be established that aims to eliminate hazards associated with the manufacturing, operation (including end of life) as well as personnel, other property, and the environment.
USR-PLD-01	-	Scientific instruments shall be active 15% of the operational mission time.
USR-PLD-18	The spacecraft shall have the capacity to accommodate and securely contain two Hopper 2 vehicles.	The spacecraft shall have the capacity to accommodate and securely contain a Hopper 2 vehicle.
USR-COM-03	The orbiter shall allow for science down-link in X-band.	The orbiter shall allow for science down-link in Ka-band.

3.2. Launch and Transfer Phase

Although the launch and transfer phase are not the main focus of the feasibility study, there are still several key functions that the spacecraft must perform during the launch and transfer phase of the ELMO mission.

After separation from the launch vehicle adapter, the spacecraft may experience tumble. The MGA shall be the primary antenna used for Earth communications thanks to its increased field of view, which helps to provide consistent communication while tumbling. Once the spacecraft communicates with ground systems and determines its angular velocity, it may begin its de-tumbling manoeuvres, making use of its reaction control wheels and thrusters. The spacecraft must also perform health checks, and relay its diagnostics reports to Earth. These diagnostics reports should also be stored onboard to potentially be analysed in the future.

Throughout the transfer phase, the spacecraft shall follow the same trajectory as for the Cassini-Huygens mission, as seen in Figure 3.1. The transfer flight shall take approximately 8 years and

initially falls toward the Sun before performing several flybys and gravity assists to put the spacecraft onto a Saturn intercept trajectory.

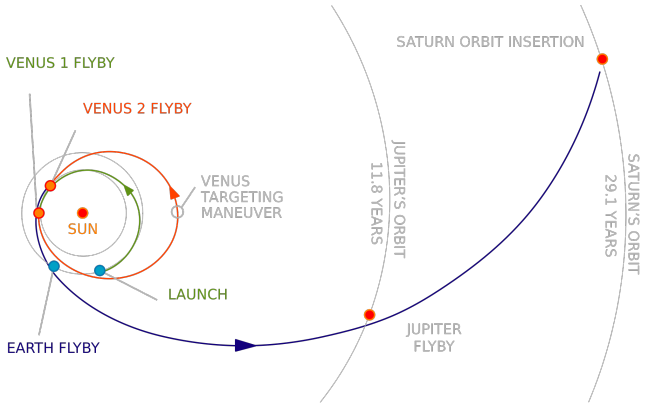

Figure 3.1: Interplanetary trajectory for the Cassini-Huygens mission. Dates have been removed. [3]

The spacecraft must also perform trajectory checks on a consistent basis in order to ensure that its flight path is optimal. To perform these checks it shall utilize its 2 sun sensors and 4 star sensors, with additional verification from ground-based systems. When performing the Venus flybys, the spacecraft experiences its peak solar flux. In order to maintain thermal equilibrium, the HGA will be used to effectively shield a large portion of the spacecrafts area. A more in-depth analysis on the thermal management near Venus can be found in subsection 11.1.2. The solar array deployment will occur at a later point in the transfer phase, although this point has not been specifically defined. When on approach to Enceladus, there shall also be an opportunity to image the full moon using the HRC.

3.3. Mission Profile

The mission profile is driven by the requirements found in Table 3.4

Table 3.4: Requirements driving the mission profile

Requirement ID	Description
USR-MIS-08	The Hopper vehicles shall be deployed at an altitude of 100 km.
USR-MIS-10	The HRC shall image the entire southern hemisphere of Enceladus at least once, with regular revisits to detect variations.
USR-PLD-01	Scientific instruments shall be active 15% of the operational mission time.

The most simple profile that the mission could take would be to immediately begin with science data collection as to fulfil requirement USR-PLD-01. After that, all recorded data could be transmitted to Earth for the remaining duration of the mission. However, this simple profile produces a number of flaws. In the event that the spacecraft suffers a catastrophic failure during the data collection phase, no science data will have been transferred to Earth. As well as this, significant onboard data storage would be required. This profile would also conflict with requirement USR-MIS-10 by significantly reducing the payload instruments ability to measure seasonal variations on the surface of Enceladus.

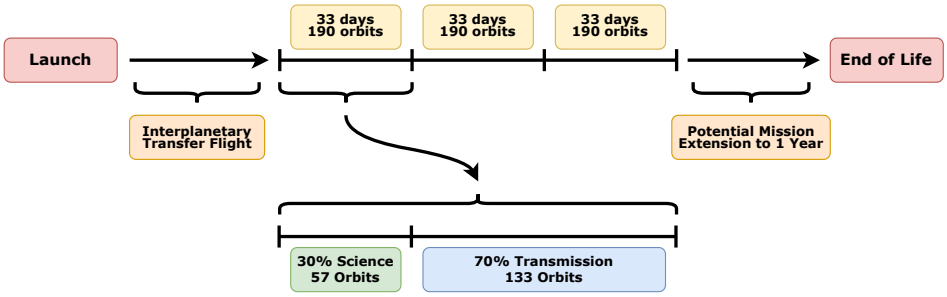

Figure 3.2: The mission profile and breakdown of science and transmission orbits in each batch. Values are rounded to the nearest whole number.

To resolve these issues, it was decided that the mission would be divided into 3 identical batches, with each batch having its own data collection and transmission phases. This helps to reduce the aforementioned risk in the event of a systems failure. The s/c onboard data storage is also significantly reduced. The value of 3 was decided to also reduce the number of slewing manoeuvres that would be performed by the ADCS (Chapter 7). Each batch shall start with data collection for the first $30\,\%$ of the batch time. The latter $70\,\%$ of the batch shall consist of data transmission to Earth. Orbits dedicated to data collection are hereby referred to as ”science” orbits. Similarly, orbits dedicated to transmission are hereby referred to as ”transmission” orbits. Note that both orbits share identical parameters but serve different purposes. An explanation of the science orbits and transmission orbits can be found below in 3.3.1 and 3.3.2, respectively.

The s/c shall orbit Enceladus in a polar orbit at an altitude of $100\,\mathrm{km}$. This allows for high resolution data from the onboard instruments, as well as the fact that the hopper vehicles must be deployed at $100\,\mathrm{km}$, given by requirement USR-MIS-08. The orbital period around Enceladus at $100\,\mathrm{km}$ is $15\,197\,\mathrm{s}$, or roughly $4.22\,\mathrm{h}$.

When transitioning between science orbits and transmission orbits, the ADCS is responsible for slewing the spacecraft accordingly. During science orbits, the HRC and ELA must point in the Nadir direction, in accordance with USR-PLD-12 and USR-PLD-13. During transmission orbits, the HGA is pointed at Earth, and the aforementioned payload instruments no longer point Nadir. The slew manoeuvre is analysed in further detail in Chapter 7.

Given the HRC field of view, and the orbital altitude of $100\,\mathrm{km}$, a coverage visualization could be made to check whether the USR-MIS-10 is fulfilled. The HRC coverage for one batch (57 orbits) can be seen below in Figure 3.3. It can be seen that the entire southern hemisphere is covered, and that the South Pole is covered multiple times per batch. Note that the heat map has a cap at 5 passes for visualisation reasons. Certain latitudes near the South Pole reach significantly higher amounts of passes, providing more detail about the regions closer to the polar extremes.

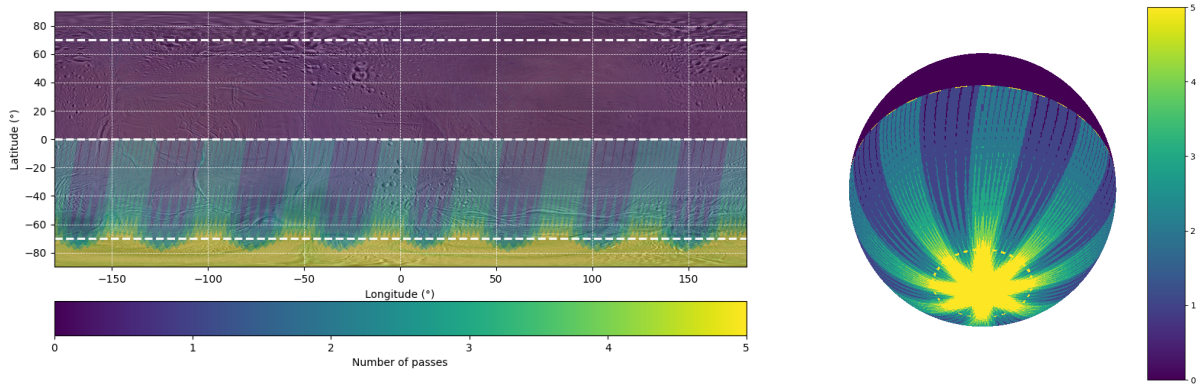

Figure 3.3: A 2D as well as a 3D visualization of the HRC coverage for a single batch. The spherical plot is viewed from below the equator to expose the South Pole. White dashed lines mark the equator as well as the positive and negative $70°$ latitude, where both poles are defined.

3.3.1. Science Orbits

Science orbits are fully dedicated to data collection. Requirement USR-PLD-01 states that the onboard instruments must be active for $15\,\%$ of the mission duration. As the science orbits make up $30\,\%$ of the mission timeline, onboard science instruments should be active for half of each science orbit. As the south pole is the region of significance on Enceladus, it was decided that the onboard instruments would only be active over the southern hemisphere of the Saturnian moon, and thus for $50\,\%$ of the orbital period. This is also consistent with USR-MIS-10. The exception to this is for the accelerometers and magnetometers, which shall be active throughout the entire orbit to accurately map the gravitational and magnetic fields of Enceladus, respectively. Both have a relatively low power and data rate, hence do not significantly impact the mission. The maximum spacing between accelerometer and magnetometer data points are at $11.5\,\mathrm{m}$ and $14.4\,\mathrm{m}$, respectively. This is based on their minimum sampling frequency of $12.5\,\mathrm{Hz}$ for the accelerometer and $10\,\mathrm{Hz}$ for the magnetometer [2], as well as an orbital velocity of $143.9\,\mathrm{m\,s^{-1}}$. This is sufficient for requirements USR-PLD-10, USR-PLD-11, which state that both should have an along-track spacing of equal or less than $2\,\mathrm{km}$. A ground resolution of $4\,\mathrm{m}$ was calculated for the HRC based on [4], satisfying the USR-PLD-12 requirement as well.

Communication with the hopper vehicles only occurs near the south pole, where both hopper vehicles shall be deployed. Given the hopper antennas minimum elevation angle of $10°$, and the s/c orbital altitude of $100\,\mathrm{km}$, the communication time with each hopper is $2991\,\mathrm{s}$. Communication with the hopper vehicles is done on the S-band at a frequency of $2\,\mathrm{GHz}$ using the MGA.

To calculate the data generated per science orbit, an analysis of the payload instruments and the hopper vehicles is performed. It is assumed that slew manoeuvres for orbital maintenance do not impact data acquisition as they shall only be performed above the equator, while all major payload instruments are idle. Table 3.5 shows the steps taken to calculate the data generated by each hopper and scientific instrument. Note that the IPR only generates data for $10\,\%$ of its active time due to its duty cycle. For the HRC, the data generated was calculated using a different method as its data generation is given on a per image basis, rather than time. Firstly, the image length on the surface of Enceladus was found using the HRCs field of view, as well as the orbital altitude. Then, using the polar circumference of Enceladus, it was calculated that a total of just under 219 images were required to capture the area below the spacecraft with a $10\,\%$ overlap between images for the southern hemisphere. Given that each image produces $4.2\,\mathrm{MB}$ after compression, this results $7.34\,\mathrm{Gb}$ of data generated each science orbit.

As for the hopper vehicles, it is assumed that they only produce scientific data when the spacecraft is out of view, and that no scientific data is produced when transmitting to the spacecraft. Given by the fact that each hopper vehicle produces $2.95\,\mathrm{Gb}$ per day, it is calculated that the data rate transmitted by each hopper vehicle to the spacecraft is $279\,\mathrm{kbps}$.

Table 3.5: All data producing mission elements and their activity and data generated per science orbit.

	Data Rate	Time Active	Data Generated
Ice Penetrating Radar	5 Mbps	7598 s	3.8 Gb
Enceladus Laser Altimeter	12.5 kbps	7598 s	94.9 Mb
High Resolution Camera	-	7598 s	7.34 Gb
Tri-Axis Accelerometer	3.6 kbps	15 197 s	54.7 Mb
Tri-Axis Magnetometer	5.76 kbps	15 197 s	87.5 Mb
Hopper 1	279 kbps	2991 s	415.7 Mb
Hopper 2	279 kbps	2991 s	415.7 Mb
Total Data Generated	-	-	12.21 Gb

Similarly, Table 3.6 is used to calculate the average power consumption per payload instrument, which shall help to inform the EPS power production requirement. The total average payload power is calculated to be $51\,\mathrm{W}$ during science orbits. The maximum payload power is calculated to be $88\,\mathrm{W}$, whilst the spacecraft is below the southern hemisphere.

Table 3.6: All payload instruments and their activity and power consumption per science orbit.

	Power (Active/Idle)	Time Active	Average Power
Ice Penetrating Radar	18 W / 1 W	7598 s	9.5 W
Enceladus Laser Altimeter	25 W / 2 W	7598 s	13.5 W
High Resolution Camera	40 W / 6 W	7598 s	23 W
Tri-Axis Accelerometer	1 W / 0 W	15 197 s	1 W
Tri-Axis Magnetometer	4 W / 0 W	15 197 s	4 W
Total Average Power	-	-	51 W

3.3.2. Transmission Orbits

Transmission orbits are fully dedicated to Earth transmissions. In order to transmit the high amounts of data produced by the payload and the hopper vehicles, the spacecraft is equipped with a $3.5\,\mathrm{m}$ diameter HGA that shall operate in the Ka-band at a frequency of $32\,\mathrm{GHz}$ to comply with deep space network (DSN) standards [5]. Calculations show that during the mission lifetime, the Earth will be in view of the spacecraft for 100% of the orbit time. These calculations can be found in Section 3.6. This means that transmission can occur over the course of the entire orbit.

Given that $12.21\,\mathrm{Gb}$ of data are produced per science orbit, and that there are 57.3 science orbits per batch, a total of $700.35\,\mathrm{Gb}$ is produced per batch. This helps to inform the required on board data storage. With just under 133 orbits dedicated for science, it can be calculated that the data rate to be transmitted to Earth must be $0.381\,\mathrm{Mbps}$, when accounting for time lost due to slew manoeuvres and orbital maintenance burns.

There are several redundancies in the communications architecture. Firstly, the HGA is equipped with two transmitters: One in the Ka-band and one in the X-band. In the event that a transmitter fails, the other can be used. In the event of HGA dish failure, the S-band MGA may be used, however at

significantly reduced data rates for the same power consumption. Calculations for the X-band HGA and S-band MGA data rates can be found in Chapter 5.

3.4. Orbit Description

The chosen orbit of ELMO around Enceladus is a polar dawn-dusk orbit at an altitude of $100\,\mathrm{km}$. Since the south pole must be imaged, it makes sense to use a polar $100\,\mathrm{km}$ orbit. Next, the orientation of the orbit should be determined. For this, a dawn-dusk orbit is chosen. This type of orbit ensures that ELMO is never eclipsed by Enceladus. This reduces the required solar array area, increases communications bitrate and allows the spacecraft to receive more heat from the sun in the frigid Saturnian environment. The orbit is visualized in Figure 3.6. The yellow hemisphere represents the sunlit side of Enceladus and the grey hemisphere represents the dark side of Enceladus.

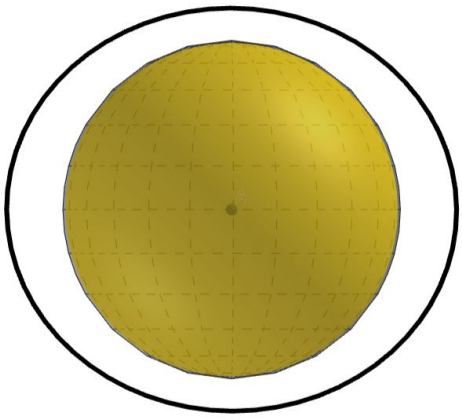

Figure 3.4: Front view

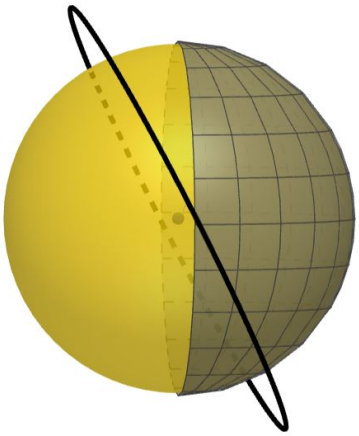

Figure 3.5: Side view

Figure 3.6: Orbit of ELMO around Enceladus

Enceladus has an inclination α of $26.7°$, which means that a polar orbit around Enceladus would be tilted by $26.7°$ with respect to the Sun. It needs to be checked whether this tilt doesn't cause eclipse time. One can conclude that the spacecraft is not eclipsed if $(h + r_{enc}) \cdot cos(\alpha) > r_{enc}$, Where h is the altitude of ELMO's orbit ($100\,\mathrm{km}$) and r_{enc} is Enceladus' polar radius ($248\,\mathrm{km}$). The evaluated formula is $311km > 248km$. Since this result is true, it can be deduced that Enceladus will not eclipse this orbit.

One concern was raised about precession. If this orbit would process, it is possible that the spacecraft would become eclipsed at some point. However, it was concluded that this is not the case. Nodal precession due to the J2 effect (biggest effect) can be quantified by the rate of change of the longitude of the ascending node $d\Omega/dt$. However, this quantity is proportional to $cos(i)$. Since the inclination is 90 degrees, it means that the cosine term vanishes and that no nodal precession takes place.

The requirements specify that ELMO must orbit Enceladus between $100\,\mathrm{km}$ and $500\,\mathrm{km}$. It was decided to set the orbit at the lowest orbital altitude allowed by the requirements. This was done for three reasons. Firstly, the hoppers must be deployed at $100\,\mathrm{km}$ anyway, so maintaining that altitude avoids unnecessary manoeuvrers. Secondly, being closer to the surface allows for a higher ground resolution. Lastly, a polar $100\,\mathrm{km}$ orbit is much more stable than a polar $500\,\mathrm{km}$ orbit as seen in Figure 3.9.

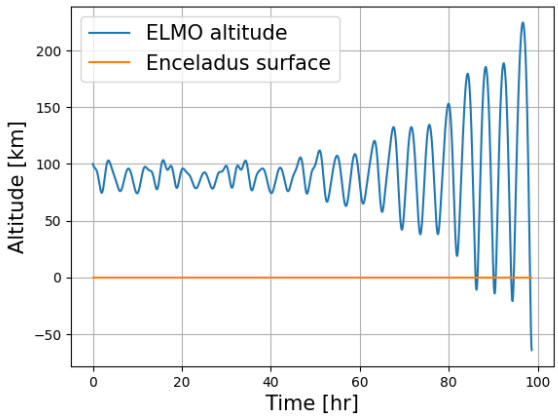

Figure 3.7: Orbital stability of ELMO at 100km

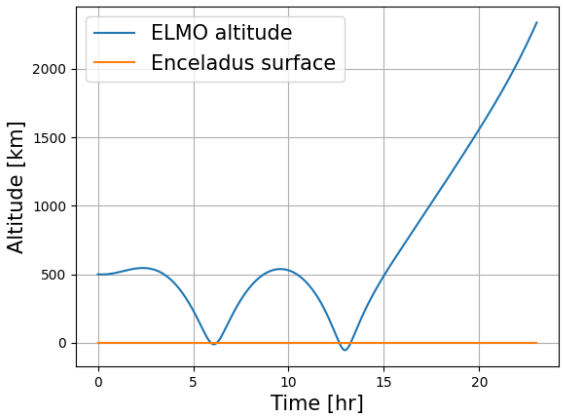

Figure 3.8: Orbital stability of ELMO at 500km

Figure 3.9: Orbital stability analysis of ELMO for two different starting altitudes

The two figures show that a polar $100\,\mathrm{km}$ orbit slowly diverges and hits Enceladus' surface after 85 hours. In contrast, the polar $500\,\mathrm{km}$ orbit hits the surface after merely 6 hours. This means that maintaining the $500\,\mathrm{km}$ orbit would require much more ΔV than maintaining the $100\,\mathrm{km}$ orbit. The simulation also predicts that a retrograde equatorial orbit is stable (not requiring orbital maintenance) at any altitude between $100\,\mathrm{km}$ and $500\,\mathrm{km}$. However, similar prograde orbits are less stable. It is worth investigating these orbits in further studies if less emphasis is given on the south pole of Enceladus.

3.5. Saturn's Orbital Altitude

Due to the eccentricity of Saturn, its distance from the sun varies between $9.07\,\mathrm{AU}$ and $10.07\,\mathrm{AU}$, which due to the inverse square law causes a $20\,\%$ difference in solar flux between Saturn's perihelion and aphelion. It is therefore necessary to find Saturn's distance to the sun at the moment ELMO is supposed to conduct its mission on Enceladus, which is around 2043. The method for this is to first calculate the mean anomaly, then the true anomaly and finally the distance to the sun. Mean anomaly can easily be calculated from the time.

$$M = \frac{2\pi}{T}(t - t_p) \tag{3.1}$$

where T is the orbital period of Saturn ($29.45\,\mathrm{years}$). t_p is the time of periapsis, which is 2032.91 or 29 November 2032. A more accurate approximation of true anomaly is derived in Appendix A. This can be used to find the orbital altitude of Saturn as a function of time.

$$r = \frac{a(1 - e^2)}{1 + ecos(M + 2esin(M))} \tag{3.2}$$

Plotting this equation results in Figure 3.10

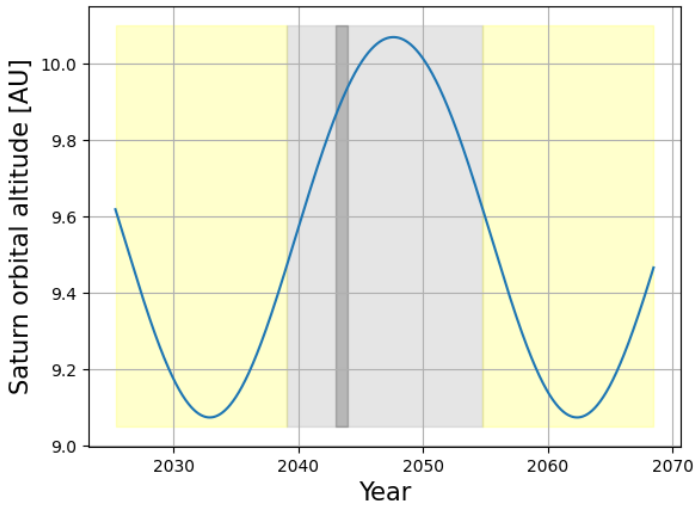

Figure 3.10: Saturn orbital distance over time

Apart from seeing Saturn's orbital altitude over the years, it is indicated when the south pole is illuminated. Yellow means illuminated, grey means not illuminated and the black strip is when ELMO is expected to perform its mission if launched in 2035. The fact that the mission is performed during a dark period of Enceladus's south pole is further elaborated in Section 3.8. Saturn also seems to be close to its aphelion during the mission. To account for a possible delay of the mission, it was signalled to the power, thermal and communications subsystems to design for the worst-case scenario distance of $10.07\,\mathrm{AU}$.

3.6. Sun and Earth Availability

Due to the inclination of the Saturn system of $26.7°$, there exists an opportunity to time the mission such that ELMO performs its mission during a period where it is never eclipsed by Saturn. These preferred time intervals will be shown in this section. The detailed calculations are put in Appendix A.

Enceladus' orbit was projected to 3 different perspectives. First, is the sun's perspective, relevant to the power and thermal subsystem. Second and third are Earth's left and right perspectives, which are two extremal positions of the Earth 6 months apart. This is relevant to the communications subsystem. The 3 projections are plotted in 4 different timestamps in Figure 3.15

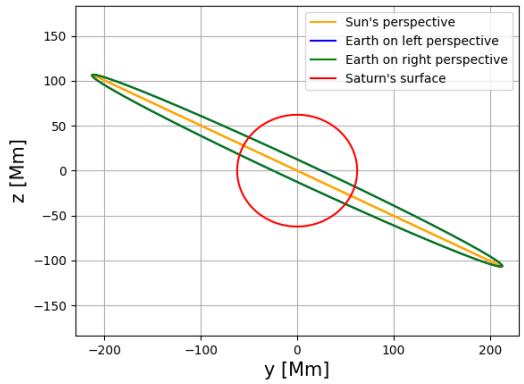

Figure 3.11: Orbit of Enceladus on February 2039 during the equinox

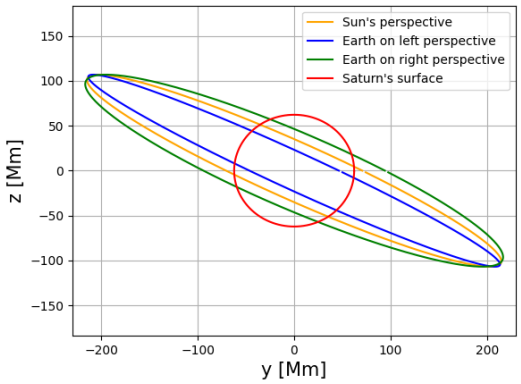

Figure 3.12: Orbit of Enceladus on July 2040 with significant eclipse time

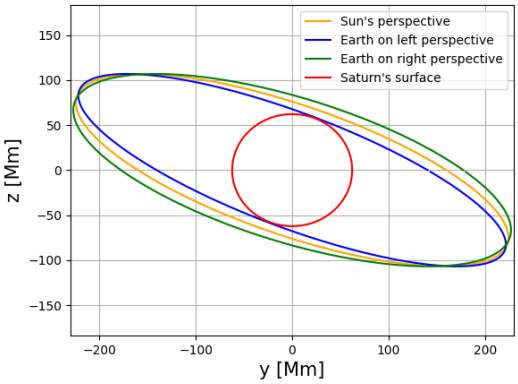

Figure 3.13: Orbit of Enceladus on August 2042 which is the first date with no eclipse time

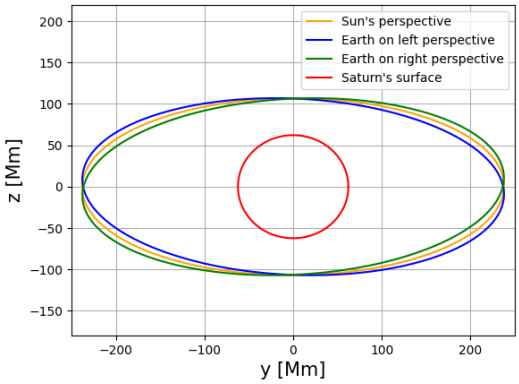

Figure 3.14: Orbit of Enceladus on November 2046 during the Saturn solstice

Figure 3.15: Orbit of ELMO around Enceladus. Units are Megameters (1000 km)

From the plots above, it can be seen that there is no full earth and sun availability until august 2042. Afterwards, the availability becomes $100\,\%$ due to the absence of eclipse time. Considering that ELMO will operate between 2043 and 2044, it can be concluded that the spacecraft will have $100\,\%$ availability. The availability over time can be summarized in one plot:

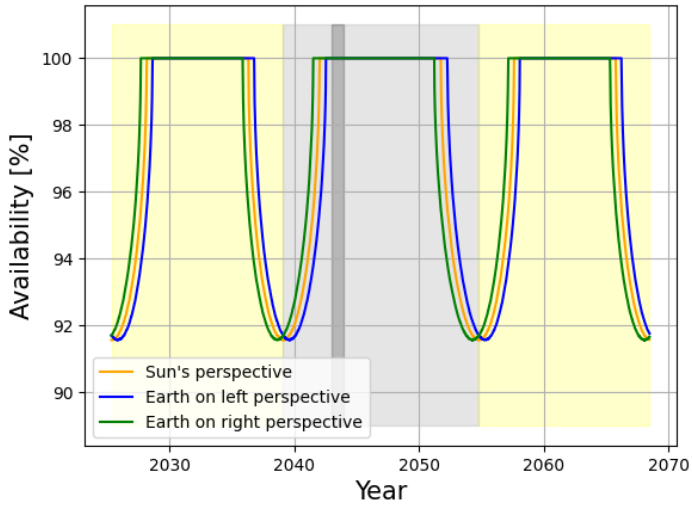

Figure 3.16: Earth and Sun availability over time

Apart from seeing the Earth and Sun availability over the years, it is indicated when the south pole is illuminated. Yellow means illuminated, grey means not illuminated and the black strip is when ELMO is expected to perform its mission if launched in 2035. The fact that the mission is performed during a dark period of Enceladus's south pole is further elaborated in Section 3.8. The fact that the transition times between illuminated and non-illuminated south poles coincide with the predicted equinoxes verifies all calculations made so far. Even if the spacecraft launch is delayed for several years, it is still likely that ELMO's operations would occur in the $100\,\%$ availability period. Therefore, all subsystem design with $100\,\%$ Earth and Sun availability, drastically optimizing the design. In case of major delays, it should be remembered that the following 2 mission operation intervals have $100\,\%$ availability:

- August 2042 - March 2051
- February 2058 - April 2065

3.7. Verification of Enceladus Coverage Visualization

The Enceladus coverage visualization is made by first constructing a 2D array representing Enceladus' surface. The array is iterated for every row (each row representing a latitude) by adding 1 to all areas of Enceladus covered by the high-resolution camera. The latitude is defined as 0 on the south pole and π at the north pole. For each latitude, the range of longitudes covered by the HRC is calculated using Equation 3.3

$$covered = \lambda_0 + \frac{T_{sat}}{T_{enc}}\phi \pm \frac{W}{2}cosec(\phi) \tag{3.3}$$

W is the swath width, λ_0 is the starting longitude at the south pole. ϕ is the latitude. T_{sat}/T_{enc} is the ratio between the orbital period of the satellite and the orbital period of Enceladus, which is the same as the rotational period of Enceladus due to tidal locking. This term accounts for the rotation of Enceladus while the spacecraft is orbiting around it. The cosecant term accounts for the distortion due to the spherical coordinate system. The cosecant function is the right trigonometric function to model the extreme distortion at the poles ($\phi = 0$ and $\phi = \pi$) and no distortion at the equator ($\phi = \pi/2$). The visualization method can be checked by setting up a hypothetical scenario where $T_{sat} = T_{enc}$. In this hypothetical scenario, the coverage by the 2 orbits would perfectly match, meaning only uncovered and double-covered area would exist. Furthermore, it can be verified whether the cosecant function is the correct one by visually determining whether the swath width is constant on the spherical 3D projection. This hypothetical scenario is shown in Figure 3.19

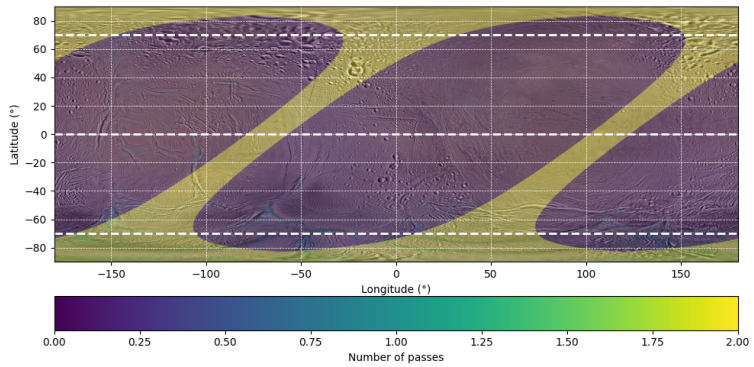

Figure 3.17: Coverage flat projection

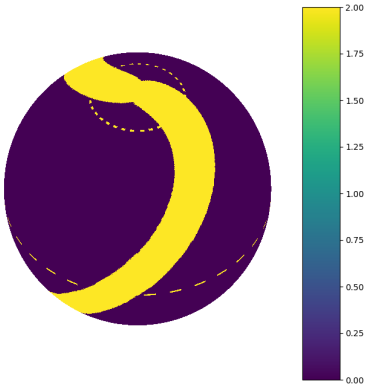

Figure 3.18: Coverage spherical projection

Figure 3.19: Verification of Enceladus coverage plots

The plots indeed show the predicted behaviour. Two slanted columns can be seen with a coverage number of 2, meaning both orbits covered both columns (one going south-to-north, one going north-to-south). On the spherical projection, a constant swath width can indeed be seen, except for at very high latitudes, where non-linear effects take place. However, these effects do not change the conclusions made using these plots. These plots are therefore verified to be correct.

3.8. Enceladus South Pole Illuminance

During mission analysis, it was discovered that when ELMO will perform its mission in 2043-2044, that the area of interest (the south pole of Enceladus) will not be illuminated by the sun. In fact, Due to the long orbital period of Saturn and its inclination, the Enceladus' South pole will be in the dark until October 2054. Enceladus' orbit has an inclination of 0 degrees in the Saturn system. Enceladus is also tidally locked to Saturn. This means that Enceladus has the same axis of rotation as Saturn. Since Saturn's rings also orbit at an inclination of 0 degrees, one can deduce that when the bottom of Saturn's rings are visible, the South pole of Saturn is illuminated and, therefore, the South pole of Enceladus is illuminated. Two of Saturn's equinoxes (when the rings appear like a line) can be found exactly: 11 August 2009 and 6 May 2025. Saturn's elliptical orbit causes the interval between between equinoxes to oscillate between 15.7 years and 13.7 years. In Figure 3.20 it seems that the period between 2009 and 2025 was a period where the North pole of Saturn is visible and subsequently the South pole of Enceladus not being illuminated. Using all the previous information, one can extrapolate the data to future dates:

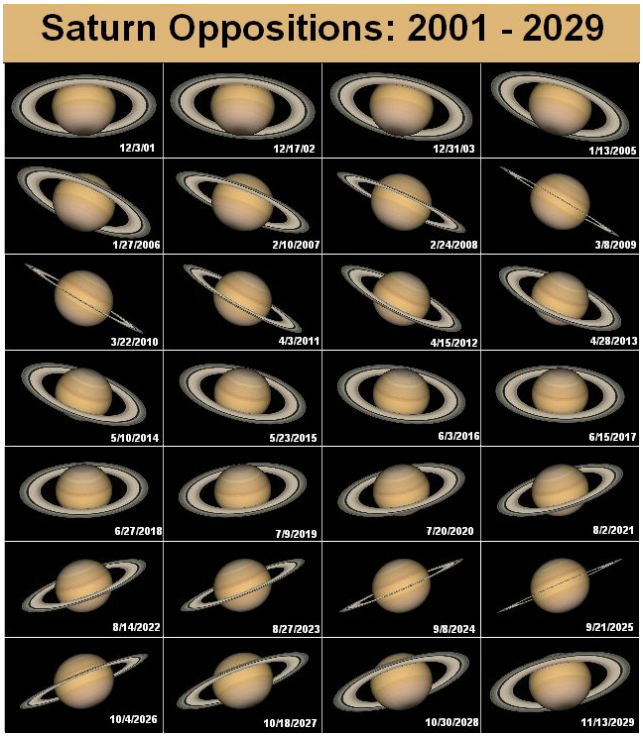

Figure 3.20: Orientation of Saturn from Earth over time

- August 2009 - May 2025: South pole not illuminated
- May 2025 - January 2039: South pole illuminated
- January 2039 - October 2054: South pole not illuminated
- October 2054 - July 2068: South pole illuminated

From this, it can be deduced that if ELMO launches in 2035 and subsequently performs its mission between 2043 and 2044, it will observe Enceladus' south pole while it is in the dark. However, after a discussion with the customer, this problem was solved by setting aside the requirement of sunlit conditions at the south pole, and will therefore not be a major problem.

4
System Overview

In this chapter the system overview will be presented. First, the functional diagrams are presented in Section 4.1. Next, Section 4.2 will describe the most critical and design driving requirements. Section 4.3 will present the trade-off methodology and criteria which have been used in the most important design decisions. Using this methodology, the final system design can start in Section 4.4. In this section the most important design decisions and considerations are presented along with the system configuration and the margin methodology and philosophy. This final design then results in a power budget, presented in Section 4.5 followed by the mass budget in Section 4.6. At the end of this chapter, the overall design has been layed out in Section 4.7.

4.1. Functional diagrams

In this section, the Functional Flow Diagram (FFD) and Functional Breakdown Structure (FBS) are presented. The FBS provides an in-depth visualization the spacecrafts main functions and subfunctions, whilst the FFD provides the same functions but in a sequential manner consistent with what would be done during nominal mission.

These diagrams provide a basis for the most critical functions that the spacecrafts subsystems should be capable of, as well as guiding the requirements for each subsystem. The FBS and FFD can be found below.

Perform ELMO Mission

- Reach Enceladus — F1
  - Sustain Launch Accelerations — F1.1
  - Sustain Launch Vibrations — F1.2
  - Separate From Launch Vehicle Adapter — F1.3
  - Check System Health — F1.4
    - Check EPS — F1.4.1
    - Check ADCS — F1.4.2
    - Check T&RC — F1.4.3
    - Test Payload Instruments — F1.4.4
    - Log Diagnostics Report — F1.4.5
  - Perform De-Tumbling — F1.5
  - Establish Earth Communication — F1.6
    - Provide Power to Comms — F1.6.1
    - Select Antenna (HGA, MGA) — F1.6.2
    - Point Antenna to Ground Station — F1.6.3
    - Transmit/Receive Telemetry Data — F1.6.4
  - Verify Nominal Trajectory — F1.7
  - Maintain Nominal Trajectory — F1.8
    - Calculate Required Correction — F1.8.1
    - Orient Spacecraft For Burn — F1.8.2
    - Activate Propulsion Subsystem — F1.8.3
  - Perform Gravity Assists — F1.9
  - Maintain Thermal Equilibrium — F1.10
    - Orient HGA for Thermal Shielding Near Sun — F1.10.1
    - Measure Onboard Temperatures — F1.10.2
    - Determine Temperature Gradients — F1.10.3
    - Adjust Thermal Controls — F1.10.4
  - Deploy Solar Array — F1.11
  - Separate From Kick Stage — F1.12
    - Terminate Kick Stage via Saturn Impact Trajectory — F1.12.1
  - Inject Spacecraft Into Mission Orbit — F1.13
- Perform Enceladus Operations — F2
  - Deploy Hopper Vehicles — F2.1
    - Enter Hopper Deployment Mode — F2.1.1
    - Activate Hopper Deployment Mechanism — F2.1.2
      - Acquire **TBR** Slew Rate — F2.1.2.1
    - Establish Communication with Hoppers — F2.1.3
      - Synchronize Communication Parameters — F2.1.3.1
    - Assess Hopper Vehicle Status — F2.1.4
  - Maintain Mission Orbit — F2.2
    - Monitor Orbital Parameters — F2.2.1
      - Activate ADCS Sensors/Actuators — F2.2.1.1
    - Plan Orbital Maintenance Burns — F2.2.2
      - Compute Required Delta-V — F2.2.2.1
    - Perform Trajectory Correction Burns — F2.2.3
    - Log Orbit Adjustment for Analysis — F2.2.4
  - Transmit Data to Earth — F2.3
    - Point HGA to Earth — F2.3.1
    - Prepare Data for Transmission — F2.3.2
      - Activate High Speed Data Links — F2.3.2.1
      - Determine Data Transmission Sequence — F2.3.2.2
    - Provide Power to Communication Subsystem — F2.3.3
      - Allocate Power from Non-Essential Subsystems — F2.3.3.1
    - Verify Succesful Data Transmission — F2.3.4
      - Receive Confirmation From Earth — F2.3.4.1
    - Log Transmission Anomalies — F2.3.5
  - Acquire Scientific Data — F2.4
    - Point Payload Bay to Nadir — F2.4.1
      - Activate ADCS — F2.4.1.1
      - Calculate Required Attitude Change — F2.4.1.2
      - Perform Slew Manouvre — F2.4.1.3
      - Perform Momentum Dumping — F2.4.1.4
    - Activate Payload Instruments — F2.4.2
      - Provide Power to Instruments — F2.4.2.1
      - Monitor Instrument Status — F2.4.2.2
      - Deploy Magnetometer Boom — F2.4.2.3
      - Deploy Ice Penetrating Radar — F2.4.2.4
    - Acquire Hopper Data — F2.4.3
      - Activate MGA — F2.4.3.1
      - Establish Hopper Data Link — F2.4.3.2
      - Download Hopper Data — F2.4.3.3
    - Store Scientific Data — F2.4.4
      - Assign Memory For Instrument Data — F2.4.4.1
      - Ensure Data Redundancy — F2.4.4.2
      - Perform Error-Handling — F2.4.4.3
      - Format and Package Data — F2.4.4.4
      - Monitor Storage Systems — F2.4.4.5
      - Activate High Speed Data Links — F2.4.4.6
- End-of-Life — F3
  - Perform **TBR** Manoeuvre — F3.1

LEGEND

- Level 1 — Fx
- Level 2 — Fx.x
- Level 3 — Fx.x.x
- Level 4 — Fx.x.x.x

Function ID

- Reach Enceladus (F1)
  - Sustain Launch Accelerations (F1.1)
  - Sustain Launch Vibrations (F1.2)
  - Separate from Launch Vehicle Adapter (F1.3)
  - Check System Health (F1.4)
    - AND
      - Check EPS (F1.4.1)
      - Check ADCS (F1.4.2)
      - Check T&RC (F1.4.3)
      - Test Payload Instruments (F1.4.4)
      - Log Diagnostics Report (F1.4.5)
  - Perform De-Tumbling (F1.5)
  - Establish Earth Communication (F1.6)
    - Provide Power to Comms (F1.6.1)
    - Select Antenna (HGA, MGA) (F1.6.2)
    - Point Antenna to Ground Station (F1.6.3)
      - IF
        - Uplink Mode
          - Receive Telemetry Data (F1.6.4)
        - Downlink Mode
          - Transmit Telemetry Data (F1.6.5)
  - Verify Nominal Trajectory (F1.7)
  - Maintain Nominal Trajectory (F1.8)
    - Calculate Required Correction (F1.8.1)
    - Orient Spacecraft For Burn (F1.8.2)
    - Activate Propulsion Subsystem (F1.8.3)
  - Perform Gravity Assists (F1.9)
  - Maintain Thermal Equilibrium (F1.10)
    - IF
      - Near sun conditions
        - Orient HGA for Thermal Shielding Near Sun (F1.10.1)
    - Measure Onboard Temperatures (F1.10.2)
    - Determine Temperature Gradients (F1.10.3)
    - Adjust Thermal Controls (F1.10.4)
  - Deploy Solar Array (F1.11)
  - Separate from Kick Stage (F1.12)
    - Terminate Kick Stage via Saturn Impact Trajectory (F1.12.1)
  - Inject Spacecraft into Mission Orbit (F1.13)
- Perform Enceladus Operations (F2)
  - Deploy Hopper Vehicles (F2.1)
    - Enter Hopper Deployment Mode (F2.1.1)
      - Acquire **TBR** Slew Rate (F2.1.2.1)
    - Execute Hopper Deployment Mechanism (F2.1.2)
      - Synchronise Communication Parameters (F2.1.3.1)
    - Establish Communication with Hoppers (F2.1.3)
    - Assess Hopper Vehicle Status (F2.1.4)
  - Maintain Mission Orbit (F2.2)
    - Monitor Orbital Parameters (F2.2.1)
      - Activate ADCS Sensors (F2.2.1.1)
      - Compute Orbit Deviation (F2.2.2.1)
    - Plan Orbital Maintenance Burns (F2.2.2)
      - Activate ADCS (F2.3.1.1)
      - Calculate Required Attitude Change (F2.3.1.2)
      - Perform Slew Manouvre (F2.3.1.3)
      - Perform Momentum Dumping (F2.3.1.4)
    - Perform Trajectory Correction Burns (F2.2.3)
    - Log Orbit Adjustment for Analysis (F2.2.4)
  - Acquire Scientific Data (F2.3)
    - Point Payload Bay to Nadir (F2.3.1)
    - Activate Payload Instruments (F2.3.2)
      - Provide Power to Instruments (F2.3.2.1)
      - Monitor Instrument Status (F2.3.2.2)
      - Deploy Magnetometer Boom (F2.3.2.3)
      - Deploy Ice Penetrating Radar (F2.3.2.4)
      - Activate MGA (F2.3.3.1)
      - Establish Hopper Data Link (F2.3.3.2)
      - Download Hopper Data (F2.3.3.3)
    - Acquire Hopper Data (F2.3.3)
    - Store Scientific Data (F2.3.4)
      - Assign Memory For Instrument Data (F2.3.4.1)
      - Ensure Data Redundancy (F2.3.4.2)
      - Perform Error-Handling (F2.3.4.3)
      - Format and Package Data (F2.3.4.4)
      - Monitor Storage Systems (F2.3.4.5)
      - Activate High Speed Data Links (F2.3.4.6)
  - Transmit Data to Earth (F2.4)
    - Point HGA to Earth (F2.4.1)
    - Prepare Data for Transmission (F2.4.2)
    - Provide Power to Communication Subsystem (F2.4.3)
    - Verify Succesful Data Transmission (F2.4.4)
      - Allocate Power from Non-Essential Subystems (F2.4.3.1)
      - Receive Confirmation from Earth (F2.4.4.1)
      - Activate High Speed Data Links (F2.4.2.1)
      - Determine Data Transmission Sequence (F2.4.2.2)
    - Log Transmission Anomalies (F2.4.5)
- End-of-Life (F3)
  - Perform **TBR** Manouvre (F3.1)

LEGEND

- Level 1 — Fx
- Level 2 — Fx.x
- Level 3 — Fx.x.x
- Level 4 — Fx.x.x.x
  - **Function ID**

4.2. System Requirements

When designing a spacecraft, the top priority is to meet the requirements. As some requirements have a larger impact on the design than others, a subset of design driving, critical requirements was selected and presented in Table 4.1. This subset of the user requirements found in Chapter 15, acts as the basis to which this system has been designed. This section will treat the requirements which had the largest impact on the final design of ELMO.

Table 4.1: Design Driving System Requirements

ID	Description
USR-SYS-01	The spacecraft shall be compatible with the Ariane 64 launch vehicle. The launch vehicle is considered to put the spacecraft on an Earth escape trajectory. The maximum launch mass for the Ariane 64 is 9600 kg.
USR-SYS-02	The orbiter reliability (including payload) shall be equal or better than 0.75 for EoM.
USR-SYS-06	The orbiter (including payload) shall cost equal or less than 750 M$ (FY 2025).
USR-SYS-07	The orbiter shall be able to perform transfer flight correction manoeuvres of total size $1200\,\mathrm{m/s}$ (high-thrust option).
USR-SYS-08	The orbiter shall be able to provide for a delta-V equal or better than $4.6\,\mathrm{km/s}$ (high-thrust option) in order to achieve the desired orbit around Enceladus.
USR-SYS-09	The orbiter shall be able to perform orbit control when in mission orbit about Enceladus to the extent of $200\,\mathrm{m/s}$ or better.
USR-MIS-03	The transfer orbit shall be of a similar trajectory to Cassini.
USR-MIS-06	A safety policy in accordance with ECCS-Q-ST-40C shall be established that aims to eliminate hazards associated with the manufacturing, operation (including end of life) as well as personnel, other property, and the environment.

As mentioned, these requirements have proved most critical for the design. The reason for their criticality lies in their combination. USR-SYS-01, for example, is very reasonable, as the relatively heavy, and similar Cassini spacecraft weighed under $6\,\mathrm{tons}$[6]. The reason for the criticality of this requirement are requirements USR-SYS-07, USR-SYS-08 and USR-SYS-09 which, when their effect is combined, require the spacecraft to have $6000\,\mathrm{m/s}$ of ΔV (delta-V). As the spacecraft mass grows exponentially with ΔV, and this required ΔV budget is very large in comparison to similar orbiters such as the Cassini orbiter, which had a ΔV budget of only about $2400\,\mathrm{m/s}$[7].

As will be explained in more detail in Chapter 17, the models used for the cost estimation rely on mass as their input. Since the mass of this orbiter will likely be very high due to the previously mentioned ΔV budget, the cost requirement USR-SYS-06 will also prove critical. These along with USR-MIS-03 and USR-MIS-06, which specify reliability and sustainability, will drive the design of the orbiter. These last mentioned will be treated in Chapter 16 and Chapter 13 respectively.

4.3. Trade-off methodology and criteria

In this section the trade-off methodology and criteria will be treated. Starting with the selection of the criteria and their reasoning, then the weights will be presented followed by the evaluation of the method.

4.3.1. Trade-off criteria

To effectively design for the requirements mentioned in Section 4.2, a trade-off method was developed. This trade-off method will act as the basis for the system wide decision making process when simpler methods do not result in a very clear preferred option. The criteria used in the trade-off have been summed up below.

- **Mass**: Measures how well the option meets the system launch mass requirement (USR-SYS-01). Lower mass is preferred because it directly impacts launch feasibility and subsystem sizing.
- **Data Rate**: Assesses the ability to meet the science collection and transmission requirement (USR-PLD-01). Higher data rates are preferred, which often necessitate increased power and communication subsystem capacity.
- **Cost**: Evaluates total orbiter cost (USR-SYS-06). Lower costs are preferred as they ensure adherence to budget constraints, enabling mission approval.
- **Reliability**: Considers the likelihood of meeting reliability requirements (USR-MIS-03). Higher reliability is preferred to maximize mission success probability.
- **Technology Readiness**: Measures the feasibility of achieving delivery schedule targets (USR-MIS-01). Higher readiness is preferred to minimize development risk and delays.
- **Sustainability**: Addresses environmental and planetary protection considerations (USR-MIS-06). Lower environmental impacts are preferred for regulatory compliance and long-term ethical stewardship.

The relative weights of these trade-off criteria can be found in Table 4.2.

Table 4.2: Trade-off Criteria Weights

Criterion	Weight
Mass	0.30
Data Rate	0.15
Cost	0.25
Reliability	0.15
Technology Readiness	0.10
Sustainability	0.05

In this trade-off the mass criterion has been assigned the highest weight due to its overarching effect on some of the other criteria, whilst also stressing the importance of the launch mass requirement as early estimations indicated this requirement would prove critical. Data rate will be of importance to meet the science collection and transmission requirement, the challenge of which has been explained in Chapter 5. To avoid double counting, no power criterion was chosen as power is reflected in data rate due to the high power used by the communication subsystem. Cost has been assigned a high weight to reflect the highly critical cost requirement. Considering current cost models use mass-based parametric estimations, the lower cost of design options might not be reflected correctly in the trade-off. This is taken into account in the trade-off leading to improved cost perfomance once better models are used. As an example Radioisotope Thermoelectric Generators (RTGs) have a much higher cost than the heavier photovoltaics, even though current estimation methods would prefer the RTGs. The described trade-off method will account for this, favouring photovoltaics with regards to the cost criterion.

As an unreliable spacecraft is of no use, a weight of 0.15 was chosen for the reliability criterion. In the current design phase reliability could be difficult to assess, however, due to its importance this

weight was chosen. The weights assigned to technology readiness and sustainability are lower to reflect their less critical requirements. Designing with technology readiness in mind is very straight forward as selecting well-proven fully developed methods allows for confidence in a design whilst mitigating development risks and possible extra costs. Sustainability has been assigned the lowest weight due to its non-critical requirement, and the specific customer request to not incorporate any end of life planning in the system. These criteria along with their weights have been approved by the team and customer, and thus have been used in all large system wide design decisions.

4.3.2. Trade-off evaluation

The trade-off process consists of the following simple steps:

First for every criterion for all design options a score is chosen from 1 to 5:

- Score 1: Very poor performance
- Score 3: Adequate performance
- Score 5: Excellent performance

To calculate the overall performance of a design option, all scores are multiplied with the weights corresponding to their criteria and added up. The design with the highest final score will be chosen.

As some design options might score very similar scores, a sensitivity analysis will be performed to ensure robustness of the result. Thus the second step of the trade-off will be to conduct this as follows:

- Identify most influential criteria
- Simulate performance improvements by independently increasing the scores of competing options by one point for these criteria
- Asses whether the overall ranking changes

Significant changes in the rankings during this analysis indicate some options are closely matched. Further analysis is advised if this is the case. The final design selection will be based on this final scoring, and will take customer preferences into account where applicable.

4.4. Final System Design

In this section the final system design will be presented starting with the chosen system configuration. Secondly the most impactful design choices and conducted trade-offs are treated. At last the use of margins will be carefully be explained.

4.4.1. System Configuration

To illustrate the final design some engineering drawings of the full orbiter, and its launch configuration are presented in Figure 4.1 and Figure 4.2.

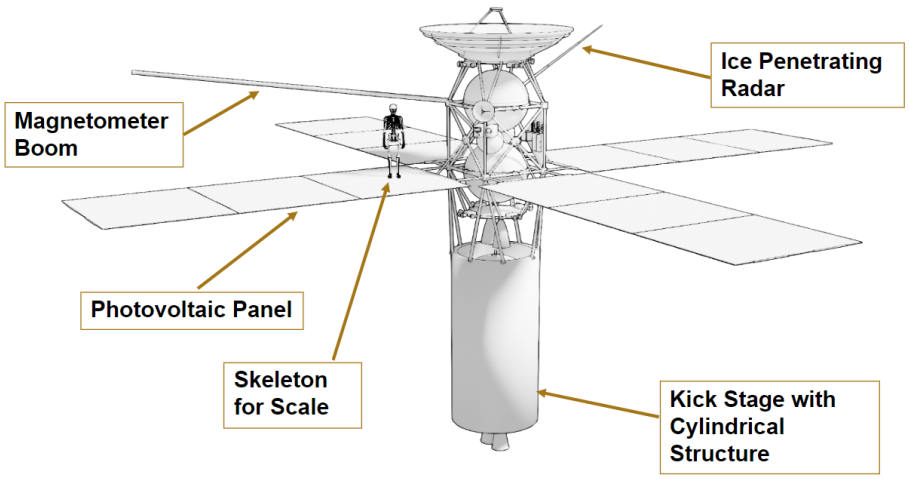

Figure 4.1: Configuration with arrows for subsystem indication

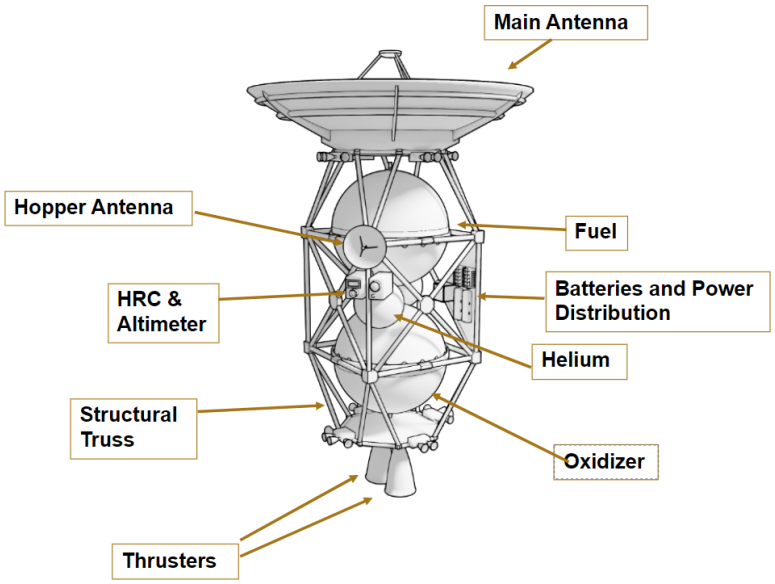

Figure 4.2: Configuration with arrows for subsystem indication

The driving factors of the shape of the main spacecraft body are the spherical propellant tanks. Each stage has a fuel and oxidizer tank that are stacked on top of each other. It is crucial that they are vertically stacked instead of next to each other to avoid a centre of mass deviation (since the oxidizer and fuel have different densities). This explains the length of the spacecraft. Both the main antenna and the solar arrays are fixed and pointed the same direction. This is possible due to the large distance of Saturn to the Earth and the Sun, which is 10 times larger than the distance between the Earth and the Sun. The maximal $5.7°$ of angular separation this causes in the sky does not effect the solar array power output significantly. The solar array is composed of 4 wings, each with 3 panels separated by a hinge. This configuration results in some outward pointing solar cells in the stowed configuration. Allowing for power generation in this stowed configuration, the use of which is detailed in the next section. The width of the solar arrays were maximized to fit into the Ariane A64 launcher. The launcher's payload bay diameter is $4.6\,\mathrm{m}$ and therefore allows for a 4-wing design with each wing being $3\,\mathrm{m}$ wide (with a bit of margin for vibrations during launch). This was verified geometrically by inscribing a square inside a circle and ensuring that the main body of the spacecraft fits inside the square. One last consideration was to put the spacecraft's electronics in between the orbiter's fuel

and oxidizer tank as this could reduce the radiation dosage reaching the electronics[1].

4.4.2. Design Choices and trade-offs

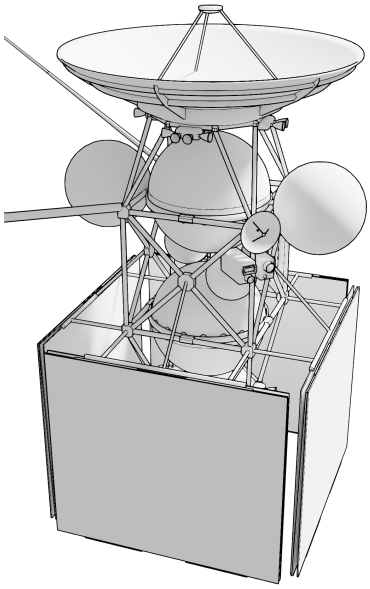

Figure 4.3: The orbiter with spheres representing the attachment points of the hoppers.

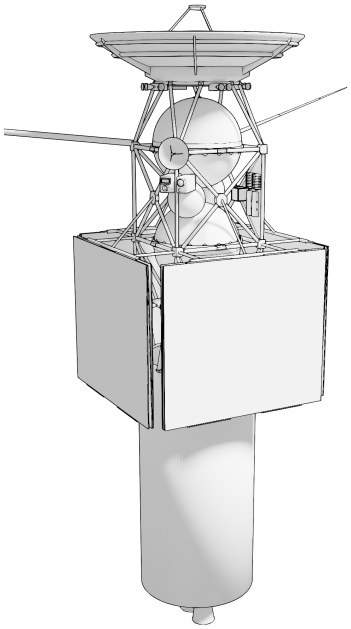

Figure 4.4: The orbiter in launch configuration

To achieve the design shown in the previous subsection a lot of design options were considered, many of which were investigated in detail to be traded off to comply with the most harsh requirements mentioned in Section 4.2. The most notable design options considered were regarding the propulsion subsystems and Electrical Power Subsystems (EPS). Due to the enormous ΔV requirement a kick stage was considered in parallel to a single stage orbiter. The kick stage would harbour large mass improvements for the price of extra cost and some increased technological development. As mentioned in Chapter 3, ELMO will make its journey to the very distant Enceladus. As the intensity of the sunlight at this destination will be about a hundredth of that at Earth, the cheap and easy Photo Voltaic panels (PV panels) will generate barely any power, requiring very large and heavy panels to comply with the power requirements of the orbiter. As this would pose multiple problems for other subsystems and the mass requirement Radioisotope Thermoelectric Generators (RTG) were considered, posing a possible solution to the mass and size problems of PV panels at a high cost and low availability. Since both these trade-offs had such enormous impact on the design, all 4 combinations were carefully considered in a single, large trade-off, the results of which are found in Figure 4.5.

[1] Note that the current models do not account for this.

Weight	0.3	0.15	0.25	0.15	0.1	0.05	1
Criterion	Mass	Data rate	Cost	Reliability	Technlogy Readiness	Sustain ability	**NUMERICAL SCORES**
Kick-stage & RTG	5	5	1	4	2	3	**3.45**
Single-stage & RTG	3	5	1	3	2.5	2	**2.7**
Kick-stage & PV	3	3	3	3.5	3.5	4	**3.18**
Single-stage & PV	1	3	3	2	4	3	**2.35**

Figure 4.5: Numerical scores for some design concepts based on weighted criteria.

The preferred design of the aforementioned trade-off, by quite some margin, was the design harbouring a kick stage and RTGs. As this trade-off was so influential on the design, the customer was informed on its results. Leading to their decision to choose the less-optimal, but more available and sustainable option using a kick stage and PV panels, leading to the configuration found inFigure 4.1.

The choice of PV panels had big implications on the mass of the spacecraft whilst also increasing the toll on other subsystems, mainly increasing the Mass Moment Of Inertia (MMOI) which lead to larger Attitude Determination and Control Systems (ADCS), this problem has partially been mitigated by the selection of 4 PV wings, instead of more commonly used 2 or 3 wing designs. This ADCS reduction was very valuable in keeping the subsystem as small as possible, as it is one of the systems requiring the most power. To omit some more of this high power usage a trade-off was done to increase the time available for slewing manoeuvres. The current ADCS system is designed to slew $90\,^{\circ}$ in $3000\,\mathrm{s}$, taking time out of the available transmission time. This solution lowered the mass and power usage of the ADCS significantly, as explained further in Chapter 7.

As the mass of the spacecraft by this point did not meet the requirements, numerous attempts have been made to improve ELMO's mass performance. Because of its enormous mass, the propulsion system was investigated. This investigation resulted in possible mass savings in the shape of propellant tanks. A successful trade-off was conducted, resulting in two identical spherical tanks for the both the orbiter and the kick stage. These tanks and their advantages have been treated in more detail in Chapter 8. The largest drawback of this decision was the inability of the current models to incorporate the propellant tanks in the structure, with as a minor drawback a little bit larger spacecraft, which still fits well within the bounds of the launch vehicle. The gain in structural performance of integrating the fuel tanks in the structure has been discarded due to the little gain to be made as changing the propellant tank shape quickly results in total mass gain. It is advised that future studies revise this choice once better structural models are available.

To further lower the mass, truss structures were investigated for both the kick stage and the orbiter. Since the propellant tanks are spherical, and the Thermal and Radiation Control subsystem (TRC) had little use for a structural shell as radiation protection or thermal control due to its small thickness this decision was incorporated in the final design as mentioned in Chapter 9. All these design choices resulted in the partial configuration found in Figure 4.4, the full configuration is found in Figure 4.1.

The TRC could not be optimized using the structure, however, since it was projected to be very heavy due to the close passage to the sun mentioned in Chapter 3 an unconventional design option was considered. Since the PV cells degrade very quickly in full sunlight, during coast they would point perpendicular to the solar rays most of the time. This would result in a single side of the spacecraft being in full view of the sun, requiring lots of thermal control. It was realised, if the PV panels would not deploy until far in the coast, the main High Gain Antenna (HGA) could be used as an effective heat shield without degrading and overheating the PV cells during the closest passage to the sun. This un-deployed configuration is illustrated in Figure 4.4. Note that the spacecraft will be tilted slightly

with respect to the sun, to prevent the focal point of the HGA coinciding with the vital electronics of the communication system as the HGA will not have a pointing mechanism itself. This design option was discarded as this mechanism would save too little EPS mass to make up for a loss in reliability and cost.

When it comes to pointing, the engines will be pointing through the centre of mass of the spacecraft. Since the centre of mass will change when propellant is used and mechanisms are deployed the thrust vectors of the main engines will create relatively large torques. To mitigate this problem three design concepts were investigated, namely increasing the size of the ADCS to counteract these torques using its thrusters, thrust vectoring using extra thrusters with thrust differential or to have a gimbal. After careful consideration both the ADCS and thrust vectoring system using extra thrusters deemed too heavy and complex, resulting in the gimbal design option to be chosen. A similar gimbal to Cassini's gimbal will be used[8].

4.4.3. Kick Stage

The choice of adding a kick stage to ELMO was driven by the low launch mass requirement relative to the high ΔV requirement. It was found in a preliminary analysis that implementing a kick stage could reduce total system mass by up to 35%.

While several commercially available kick stages exist such as the L9.7 and L10 manufactured by Arianespace [9] and the Fregat manufactured by NPO Lovachkin [10]. Other upper stages exist however most kick stages either use solid propellants which cannot be reignited or cryogenic propellants which cannot be stored for long missions. The L9.7, L10, and Fregat all use hypergolic storable propellants which makes them potentially usable for a mission such as ELMO, however, all 3 are designed as second stages for the Ariane 5 and Soyuz which makes them particularly heavy. These stages have masses of 10.9, 11.2, and 11.68 tonnes respectively [10][9]. These masses alone already exceed the launch mass requirement for ELMO, as such, it was decided to exclude these commercially available kick stages.

Additionally, all commerciality available kick stages studied for this design included independent ADC, communications, and C&DH subsystems which allowed them to act as autonomous spacecraft. These subsystems exist on kick stages to allow them autonomy in performing end of life manoeuvres as they are most often used in Earth orbit where space debris is a major concern[2]. Since it was requested by the customer that end of life should not be considered in this design phase for ELMO, it was decided that a new propulsive kick stage should be designed for this mission. As these autonomous subsystems increase the dry mass of the kick stage, this further reinforces the decision that ELMO's kick stage should be bespoke to this mission and should depend on the orbiter for as many functions as possible. While L9.7, L10, and Fregat have dry mass to propellant ratios on the order of 15-18%, the kick stage designed in this report has a more advantageous ratio of 12%. The final kick stage design only possesses subsystems for structures, propulsion, and mechanisms (stage separation and engine gimbals).

The kick stage is pictured in Figure 4.1. In the current configuration, the kick stage cannot perform an autonomous end of life, the implications of this are discussed further in Section 13.2.

4.4.4. Margin Methodology and Philosophy

Because engineering designs can never account for every variation or uncertainty, margins are applied as an essential buffer during the design process to lower the risk of required redesign after a small change. The importance of these early design margins is best illustrated using Table 4.3. This table contains data on the masses of different spacecraft by ATP (Authority To Proceed) and by launch. This table shows the importance of incorporating adequate margins to ensure the spacecraft can meet performance and launch vehicle constraints, despite the inevitable projected changes.

[2] It should be noted that these kick stages are also not qualified for long term deep space missions.

Table 4.3: Mass Growth from ATP to Launch [9]

Program	Span (months)	ATP Mass (kg)	Launch Mass (kg)	% Growth
Pioneer Venus	52	292	374	28
Scatha	25	360	396	10
FLTSATCOM	50	645	840	30
Magellan	72	830	1032	25
HEAO-2	60	2223	3016	36
HEAO-3	60	2313	2722	18
Mars Observer	71	827	1125	36
Average	-	-	-	27

As this feasibility study is similar to ESA studies, the team opted to used ESA's margin philosophy [11]. The main margins used in this study have been the subsystem and system margins. Below some subsystem margins have been given. All subsystem components will have one of the following three margins applied.

- **'Off the shelf' components**, $5\,\%$ margin on mass and power.
- **'Off the shelf' components requiring minor modifications**, $10\,\%$ margin on mass and power.
- **Newly designed parts, or parts requiring major redesign**, $20\,\%$ margin on mass and power.

After summing up the all subsystem masses and power, a final system margin of $20\,\%$ is applied. All subsystems will be designed for the final mass and power including all margins. An example of the margins and their application is given in Table 4.4.

Table 4.4: Example on the application of subsystem and system level margins

Subsystem Margins	Margin	Example Initial Mass [kg]	Mass After Margin [kg]
Off the shelf component	5%	10	10.5
Off the shelf components with minor modifications	10%	15	16.5
Newly designed systems, or parts requiring major re-design	20%	20	24
Total subsystem mass	-	45	51
System margin and final mass	20%	51	61.2

Note that this same margin convention applies to the estimated power. After the system margin application, the resulting final masses and power requirement are distributed to the subsystems.

4.5. Power Budget

The power budget is summarised in Table 4.5. The design of the power system is presented in Chapter 6, and it takes into account the total average power for both modes. Here the peak power is presented as a sum, but the EPS design assumes that the peaks do not occur simultaneously, so the different cases are evaluated separately.

Table 4.5: The ELMO orbiter's power budget.

Item	Communication mode			Science mode		
	Average power [W]	Peak power [W]	Peak duration [s]	Average power [W]	Peak power [W]	Peak duration [s]
Payload	10.5	-	-	46.2	52.5	7560
Comms	53.17	-	-	14.4	-	-
ADCS	62.41	76	3000	62.41	76	3000
CDH	58.8	-	-	58.8	-	-
Thermal	-	-	-	-	-	-
Mechanisms	-	-	-	-	-	-
Propulsion	-	70	0.03	-	70	0.03
Total	185	146	-	182	198	-
Margin	20	20	-	20	20	-
Total with margin	222	175	-	218	238.2	-

These quantities were compared to statistical estimates done using other interplanetary spacecraft [12], in addition to the JUICE and Ulysses missions. The main features of the ELMO orbiter, namely its deployable hopper vehicles, the large communication system and its solar array, are considered to be the main reasons behind these differences, alongside the early stage of the design. A summary of the power distribution percentages, taking into account the ELMO orbiter's average power needs, can be found in Table 4.6.

Table 4.6: Power Budget Percentages Breakdown

Subsystem	Communication	Science	ELMO Average	Other Missions
Payload	6%	25%	12%	25%
Comms	29%	8%	23%	25%
ADCS	34%	34%	34%	10%
CDH	32%	32%	32%	10%
Thermal	-	-	-	20%
Mechanisms	-	-	-	8%
Propulsion	-	-	-	2%

4.6. Mass Budget

This section discusses the mass budget of the final design. The budget is given in Table 4.7.

Table 4.7: Mass Budget for Orbiter and Kick Stage

Subsystem	Subsystem Orbiter Mass [kg]	Subsystem Kick Stage Mass [kg]
Structures	61	173
Mechanisms	51	22
Communications	118	-
Command and Data Handling	45	-
Electrical Power Systems	318	-
Propulsion Systems	249	534
Attitude Determination and Control Systems	46	-
Thermal and Radiation Control	141	-
Payload	265	-
Harness	68	38
Orbiter / Kick Stage Dry Mass	1361	768
Dry Mass Including System Margin	1633	922

When comparing to other spacecraft of the same type, the orbiter has an atypical mass distribution. Namely the Electrical Power System (EPS) and Propulsion masses are very high, with a relatively large Thermal and Radiation Control (TRC) subsystem. As mentioned in Section 4.4, the EPS mass is linked to using photovoltaic panels for its power generation and the very large propulsion system mass can be linked directly to the ΔV requirements mentioned in Section 4.2. The large TRC mass stems from the two extreme thermal environments the spacecraft needs to overcome. Note that aside these setbacks and high masses, some of the other subsystems are performing very well. The Attitude Determination and Control Subsystem (ADCS) and structures specifically have a lot lower mass then what is expected in spacecraft of similar size. Table 4.8 illustrates these differences further by comparing the mass fractions of a parametric estimation, JUICE and Cassini. The total mass of the system including the launch vehicle adapter explained in Chapter 9, can be found in Table 4.9.

Table 4.8: Mass Distribution Comparison Across Missions. Note the mechanism mass fraction of the ELMO orbiter has been added to structures

Subsystem	Zandbergen [%]	JUICE [%]	Cassini [%]	Average [%]	ELMO [%]
Payload	N/A	10.8	14.4	12.4	12.4
Structure	23.0	34.7	19.6	26.7	14.4
Thermal Radiation and Control	4.8	6.1	2.7	4.3	6.6
Electrical Power Systems	22.4	18.6	12.4	15.3	14.9
Communications	7.7	4.9	2.4	3.6	5.5
Attitude Determination and Control Systems	8.0	4.6	10.4	7.4	2.2
Propulsion	19.0	12.4	28.8	20.2	36.8
Harness	9.8	7.9	6.0	6.8	5.0
Command and Data Handling	5.3	N/A	3.3	3.3	2.1

Table 4.9: Mass Breakdown of Orbiter and Kick Stage

Parameter	Mass [kg]
Orbiter Dry Mass	1633
Orbiter Propellant	3238
Orbiter Wet Mass	4871
Kick Stage Dry Mass	922
Kick Stage Propellant	7582
Kick Stage Wet Mass	8504
Total Dry Mass	2555
Total Wet Mass	13375
Launch Vehicle Adapter	80
Launch Mass	13455

From this table it can be found that the launch mass does not comply with the requirement for launch vehicle compatibility, USR-SYS-01. The total system mass is about $4\,\mathrm{tons}$ over the maximum mass requirement of $9600\,\mathrm{kg}$. This enormous mass has mostly accumulated from the very large ΔV requirement mentioned in the start of this chapter, as propellant mass outweighs dry mass by a factor of 4, and the propulsion dry mass is more than a third of the total dry mass. For reference, Cassini's propellant outweighed its dry mass by less than a factor of 1.5[6].

Some straightforward mass-savings are still projected, such as those outlined in Chapter 11 and Chapter 12. Although these savings will likely have a large compounding effect, as explained in Chapter 14, it is concluded that the USR-SYS-01 requirement cannot be met.

As mentioned in subsection 4.4.4, large margins have been applied in the current design of the orbiter. As explained in this section, these margins have been applied for good reason. Since the USR-SYS-01 requirement of maximum mass has not been met, an analysis was performed on the system

without the $20\,\%$ system margin. As it is very unlikely that this design will not grow in mass, there is no confidence in this design, hence it acts as an experiment to design for requirement compliance. The final masses of this experiment are given in Table 4.10. This design also does not comply with the USR-SYS-01 requirement. As just subsystem inputs have changed, the team is confident this requirement can be met with minimal redesign.

Table 4.10: Mass breakdown of orbiter and kick stage computed without the system margins.

Parameter	Mass [kg]
Total Dry Mass	1844
Total Wet Mass	9887

4.7. Design Process

In this section the overall design process is explained.

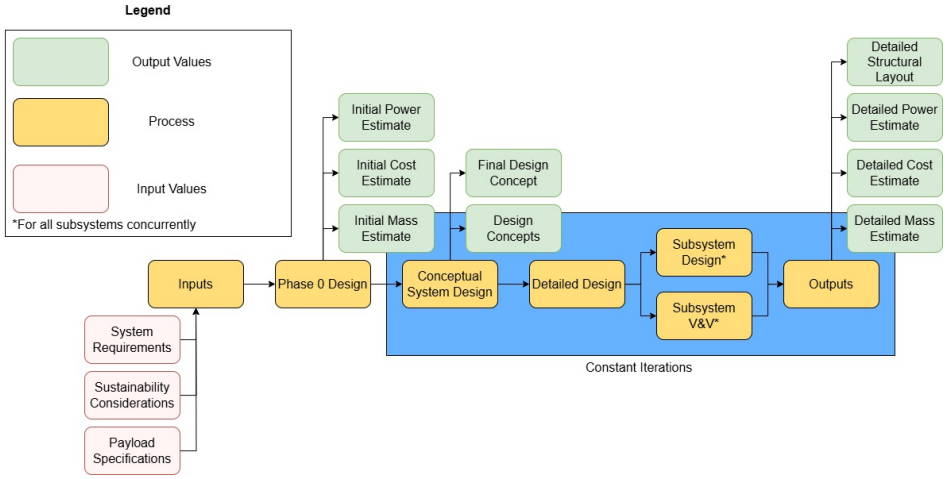

Figure 4.6: System Design Process

Figure 4.6 shows the design process used by the ELMO team for the system design of the spacecraft. At the start of the project several inputs were received which led to a level 0 design, which was done to create reliable initial estimates. After this conceptual system design, detailed design and subsystem design were all performed on an iterative basis, meaning that the outcomes of all the design steps were put back into the design until convergence was reached. Once convergence was reached for every step the output values and methods for the final report were frozen and put into the report.

Figure 4.7 describes the basic iteration cycles. After any change in value, this value is entered in the system parameter dashboard where the system margin is re-applied before the value is passed to the subsequent subsystem. The $\Delta P > x$ and $\Delta m > y$ gates refer to the significance of changes in power and mass respectively. Depending on the desired level of accuracy the threshold for re-iteration are set. An example is $x = 1\,\mathrm{W}$ and $y = 1\,\mathrm{kg}$. In this case the iterations between ADCS and EPS will stop when changes are lower than $1\,\mathrm{W}$. The same is true for the cycle between structures and propulsion for $1\,\mathrm{kg}$. If after sufficient convergence is reached the spacecraft dimensions have changed significantly, the configuration is updated, followed by an updated T&RC system before the iteration restarts.

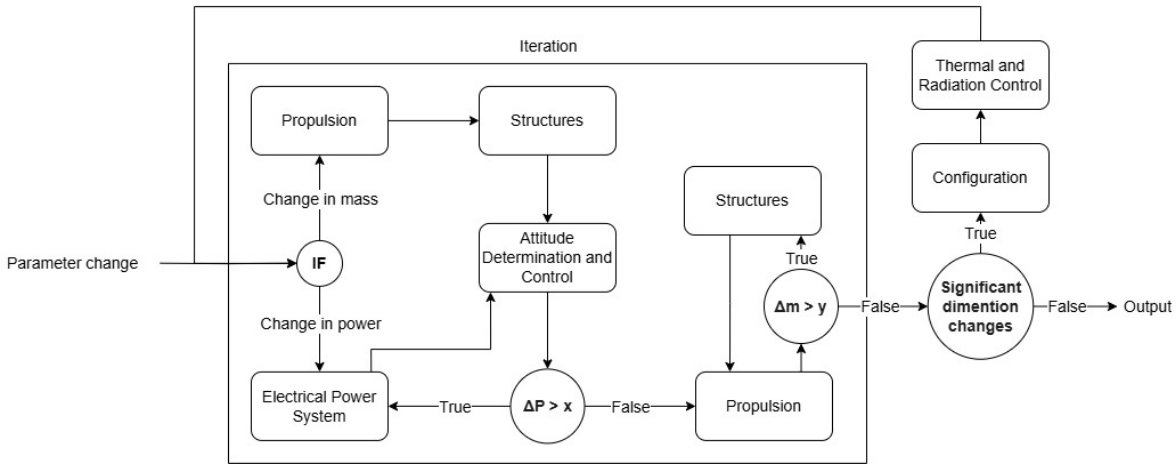

Figure 4.7: Figure describing basic iteration cycles

Note that no iteration cycle is the same as it all depends on the desired level of accuracy and on the input, however the general structure is the same. In these iterations not only mass and power are communicated from subsystem to subsystem but also the dimensions of, for example, solar panels or propellant tanks.

The paths shown in the figure have been chosen as, by experience, the subsystems connected by arrows influence each other the most. For example, changes in the propulsion not only change the mass, but also the propellant tank dimensions. This has a much larger effect on structures than any other subsystem, thus structures logically follows from propulsion. Using the same logic, ADCS is the only subsystem with an arrow towards EPS as it is the only where power changes during iterations[3].

[3] In our current models, however if T&RC models change in power this is accounted for, as can be seen in the figure. Other subsystems do not require power for now.

5
Communications

This chapter presents the design of the communication subsystem of ELMO which needs to meet the requirements presented in Section 5.1. The criticality of this subsystem in the orbiter's design lies in its power consumption, dependent on the far distance between ELMO and Earth and directly proportional to the amount of data gathered by payload and hoppers. The latter is evaluated from the mission planning outlined in subsection 3.3.1 and subsection 3.3.2. The overall system characteristics at this stage are presented in Section 5.2, where the communication flow diagram is included. All link budgets are summarised in Section 5.3, containing the methods used to design the subsystem, which are verified and validated.

5.1. Subsystem Requirements

From the user requirements in Table 3.2 the subsystem requirements are derived. The numbers used in the subsystem requirements were derived from the customer requirements in combination with the deep space network (DSN) bands specifications in [5] as well as the critical science downlink data rate downflowing from USR-PLD-01. The communication subsystem of ELMO was therefore designed following the requirements in Table 5.1.

To evaluate the data rate in ELM-UP01-COM-01, the science and transmission orbits defined in Chapter 3 were used. With $12.2\,\mathrm{Gbit}$ of data per science orbit and 57 orbits per science batch, ELMO must transmit the full data during each 133-orbit transmission batch. After subtracting $516\,000\,\mathrm{s}$ for slewing and orbital correction manoeuvres (taken out of the total transmission time), the resulting data rate is $381\,\mathrm{kbps}$.

Table 5.1: Communication subsystem requirements.

ID	Title	Description
ELM-UC01-COM-01	DSN Ka-band frequency	Ka-band transmission to and from Earth shall be done at frequency of 32 GHz
ELM-UC01-COM-02	DSN X-band frequency	X-band transmission to and from Earth shall be done at frequency of 8.4 GHz
ELM-UC01-COM-03	DSN S-band frequency	S-band backup transmission to and from Earth shall be done at frequency of 2 GHz
ELM-UC01-COM-04	DSN Ka-band bandwidth	Ka-band transmission to and from Earth shall make use of a 5.2 MHz bandwidth
ELM-UC01-COM-05	DSN X-band bandwidth	X-band transmission to and from Earth shall make use of a 1.4 MHz bandwidth
ELM-UC01-COM-06	DSN S-band bandwidth	S-band backup transmission to and from Earth shall make use of a 0.4 MHz bandwidth
ELM-UC02-COM-01	Antenna to communicate with hoppers	COM shall be provided with an antenna operating on S-band for the hopper 4Mbps data rate in uplink during orbits at Enceladus

ELM-UC03-COM-01	Antenna for science downlink	COM shall be provided with an antenna operating on Ka-band for science downlink to Earth during orbits at Enceladus
ELM-UC04-COM-01	Backup antenna for downlink	COM shall allow for downlink to Earth using X-band in case the Ka-band is not available during orbits at Enceladus
ELM-UC04-COM-02	Antenna for uplink	COM shall allow for uplink from Earth using an X-band during orbits at Enceladus
ELM-UC05-COM-01	Antenna for emergency	COM shall allow communication with Earth using an S-band antenna in case of emergency during transfer and orbits at Enceladus
ELM-UC05-COM-02	Antenna redundancy	COM shall be provided with at least 2 independent antennas to allow for backup communication with Earth at all times
ELM-UP01-COM-01	Science data rate	HGA on Ka-band shall allow for a downlink data rate of 381 kbps when in 100km orbit at Enceladus
ELM-US01-COM-01	HGA diameter	HGA dish shall have a diameter smaller than 4.6m

5.2. Subsystem Overview

The subsystem provides ELMO with two fixed antenna assemblies to modulate and send signals for downlink to Earth as well as receive uplink data from the hoppers and Earth on different bands, to meet the requirements in Table 5.1. The main antenna is a high gain parabolic antenna (HGA) operating as a baseline in Ka-band for downlink and in X-band for uplink. The second antenna is a medium gain parabolic antenna (MGA) operating in S-band, which has the baseline function of communicating with the hoppers on the surface of Enceladus for the uplink of measurements data.

Additionally the antennas will be used to measure the Doppler shift of the radio signals transmitted from or to the spacecraft. By analysing the frequency shift due to the relative motion of the spacecraft, the spacecraft's velocity can be determined. This information, combined with other positional data from ADCS sensor suite, helps the determination of the spacecraft's position.

The biggest challenge for this subsystem is the downlink of the large volume of data acquired during the mission, requiring a $381\,\mathrm{kbps}$ science data rate, ELM-UP01-COM-01 therefore drives the design. For the smaller antenna ELM-UC02-COM-01 is driving, as the maximum hopper's transmission data rate is set to be $4\,\mathrm{Mbps}$. The subsystem key design figures, that influence the system design, are presented in Table 5.2, following the methods in Section 5.3, while the parameters of the communication link segments further evaluated in subsection 5.3.2 are summarised in Table 5.3.

For all communication bands, quadrature phase shift keying (QPSK) modulation scheme is chosen due to its efficient use of bandwidth and robustness in noisy environments. To ensure a balance between data rate, error performance, and adequate space within the selected bandwidth, the signal-to-noise ratio $\frac{E_b}{N_0}$ figure is selected within the typical ranges of QPSK [13].

Table 5.2: Communication entire subsystem design figures. Subsystem margin applied following [11] on single components.

Mass m	**Peak Power** P	**Mass with Margin** $14.4\,\%$	**Peak Power with Margin** $19.8\,\%$	**Antenna Dish Diameter**
$103\,\mathrm{kg}$	$43.4\,\mathrm{W}$	$118\,\mathrm{kg}$	$53.2\,\mathrm{W}$	$3.5\,\mathrm{m}$ HGA $0.5\,\mathrm{m}$ MGA

Table 5.3: Communication main parameters of different link segments, depending on selected band.

Parameter		Unit	Value Ka-band	Value X-band	Value S-band
Signal	Frequency	[GHz]	32	8.4	2
	Bandwidth to/from Earth	[MHz]	5.2	1.4	0.4
	Bandwidth from Hopper	[MHz]	-	-	4
ELMO	Gain HGA	[dBi]	59.4	47.8	-
	Gain MGA	[dBi]	-	-	15.2
	Antenna Noise Temperature	[K]	150	200	230
Ground	Gain DSN	[dBi]	86.1	74.5	63.0
	Antenna Noise Temperature	[K]	22	12.3	19.1

The antenna dish sizing is performed in subsection 5.3.3, but the subsystem is composed of multiple elements which need to provide the transmission of data. For the HGA assembly a double band transceiver is selected as well as two traveling wave tube amplifiers (TWTA) for both X and Ka-band transmissions. Similarly for the MGA an S-band transceiver and a S-band TWTA are chosen. ELMO will also be provided with a redundancy for each of these items. Table 5.4 contains the breakdown of all components considered. The transmitter-amplifier combination is responsible to transform the electrical power from EPS into a transmittable radio frequency (RF) signal modulated with the data bit stream stored on board. In the receiver section the transceiver allows for decoding the information sent by either the DSN ground station or the hoppers on Enceladus. Figure 5.1 illustrate the links ELMO is designed to establish as well as the signal flow for downlink of science.

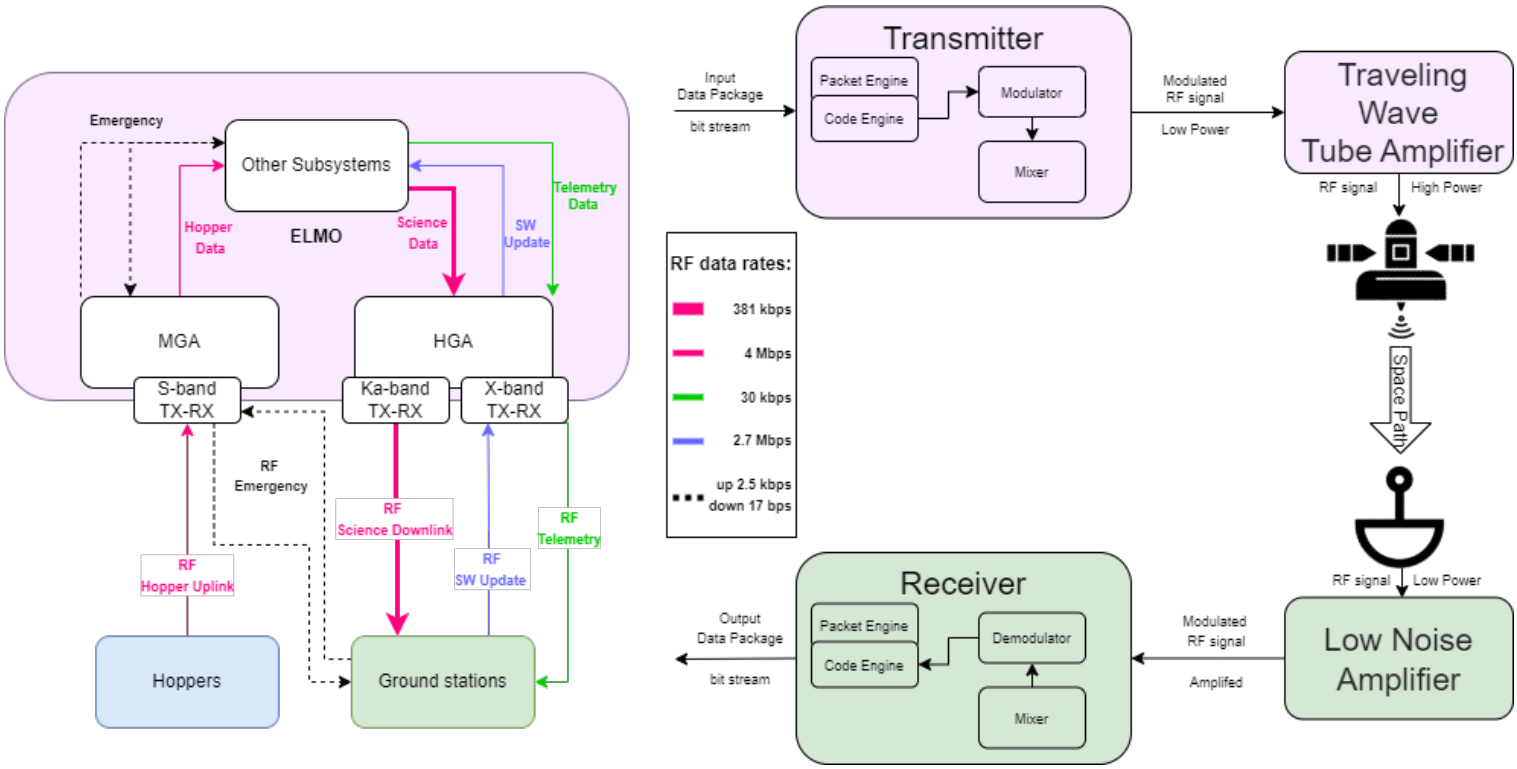

Figure 5.1: Communication flow diagram. On the left the link flows, operated on different bands between ELMO, the DSN ground stations and the hoppers, with estimated achievable data rates. On the right the downlink communication flow from ELMO to Earth.

Table 5.4: Subsystem components with corresponding and masses and sources.

Item	Quantity	Mass/unit [kg]	Source
High Gain Antenna			
HGA Dish	1	52.9	-
Transponder Ka&X-band	2	2.5	T-748 L3Harris[14]
Ka-band Amplifier TWTA	2	2.67	Dual TWT Thales [15] (mass[16])
X-band Amplifier TWTA	2	0.9	86160Hx Stellant Systems [17]
Medium Gain Antenna			
MGA Dish	1	1.1	-
Transponder S-band	2	2.1	μSGLS-100 Space Micro [18]
S-band Amplifier TWTA	2	1.3	8412HXR Stellant Systems [19]
Additional Subsystem component			
Radio Frequency Distribution Network	1	30	conservative estimation [20] [21]

5.3. Design Method

This section outlines the design process to size the communication subsystem. subsection 5.3.1 summarises all the assumptions and input parameters, subsection 5.3.2 presents the link budgets and the power estimation while subsection 5.3.3 discusses the method used to perform the antenna dish sizing. Finally, subsection 5.3.4 briefly presents the verification and validation procedures.

5.3.1. Assumptions and Design Inputs

The subsystem requirements in Table 5.1 consider the modification of the user science transmission requirement, which changed from downlink in X-band to downlink in Ka-band during the design process due to the infeasibility of transmitting the high data rate from Enceladus' far location. This change was implemented to improve the link budget parameters as, according to Professor S. Speretta [personal communication, January 8, 2025], the increased frequency leads to increased gain G of the same transmitter antenna as well as an increased $\frac{G}{T}$ of the receiving DSN dish. Equation 5.1 is therefore used to evaluate the antenna gains from the assumed one in X-band to the Ka-band value, using the DSN frequency [5] of respectively $8.4\,\mathrm{GHz}$ and $32\,\mathrm{GHz}$ for f_1 and f_2.

$$G_{f_2} = G_{f_1} + 20log_{10}\left(\frac{f_2}{f_1}\right) \quad [dB] \tag{5.1}$$

This assumption needs to be evaluated in further studies as, in reality, the performance of the subsystem and the DSN could be lower. The other assumptions and related input parameters are presented in Table 5.5.

Table 5.5: Assumptions for communication subsytem design.

Assumption/Input	Rationale/Recommendations
DSN full availability during transmit orbits	The evaluation of the science data rate was done considering that the availability of the DSN on ground was continuous during the transmit orbits on the X-band [1] [22]. Due to the modification of a user requirements during the design process, specifically, having the downlink to Earth be in Ka-band instead of X-band, this evaluation would no longer be valid. It is therefore recommended to reassess the amount of time ELMO can be transmitting to Earth at the selected band and bandwidth. Lower amount of data acquisition will then be necessary to keep the same design.
Constant distance from Earth d=$11.07\,\mathrm{AU}$	In reality this will be variable but the maximum distance between Earth and Saturn was considered a suitable worst case estimation for evaluating the transmission losses Section 3.5.
Gain of ground receiving dish in X and S-band $G_X = 74.5\,\mathrm{dBi}$ $G_S = 63.0\,\mathrm{dBi}$	From the DSN manual [23] as an average of all the best performing antennas corresponding to the band. In reality gains variate depending on the antenna in view during transmission and on its size.
Antenna noise temperature for X and S-band receiver ground $T_X = 12.3\,\mathrm{K}$ $T_S = 19.1\,\mathrm{K}$	From the DSN manual [23] as an average of all the temperatures corresponding to the band. These in reality depend on the selected ground antenna
Antenna noise temperature for Ka-band receiver ground $T_{Ka} = 22\,\mathrm{K}$	To further increase the link performance this low temperature was considered attainable with new technologies[2], while in reality low temperatures are in the $30\,\mathrm{K}$ to $35\,\mathrm{K}$ range.[24] [25]
Ground EIRP transmitter for S, X and Ka bands $EIRP_S = 135\,\mathrm{dBm}$ $EIRP_X = 145\,\mathrm{dBm}$ $EIRP_{Ka} = 134\,\mathrm{dBm}$	The values of EIRP are taken from the DSN specifications, [23] for X, S and Ka bands. These are values that in reality are antenna specific but just a single value was considered per band to evaluate the link budget.
The hopper transmission gain $G_{hopper} = 13\,\mathrm{dB}$	To evaluate the link between ELMO and the hoppers the parameter was assumed in the range of existing probes antennas [26]. Once the communication system of the hopper will be known a new link budget should be performed.
Additional losses L_x per band $L_{Sband} = 1\,\mathrm{dB}$ $L_{Xband} = 1.4\,\mathrm{dB}$ $L_{Kaband} = 2.2\,\mathrm{dB}$	Considering optimal weather conditions and how the frequency increase causes a greater susceptibility to atmospheric and cosmic absorption, these are reasonable estimations[27].
The ELMO HGA should be designed for a gain in X-band $G_X = 47.8\,\mathrm{dBi}$	Cassini, as a similar mission, had a 4 meter antenna with a gain of $47.2\,\mathrm{dBi}$[15]. According to the Expert D. Jameux [personal communication, January 13, 2025] a slightly higher gain is considered reachable within similar mission spacecraft development for even smaller dishes.

[1] NASA, "Deep Space Network Complexes," https://www.nasa.gov/directorates/somd/space-communications-navigation-program/dsn-complexes/

[2] https://esoc.esa.int/content/cool-tech-almost-double-deep-space-data

The ELMO MGA should be designed with G_{Ka} =39.3 dBi D_{dish} =0.5 m	This is heritage from the Juice mission MGA [3]. It is taken as a reasonable reference for a long distance communication optimised medium gain antenna for icy moon orbiters. Further studies should consider including also low gain omnidirectional antennas (LGA) for emergency transmission during the long transfer phase (where distance from earth is smaller), de-tumbling and safe mode.
ELMO transmission cable losses L_{cable} =0.7 dB	Estimation to account for the cable losses of the RF power transmitted to the antenna. Further investigation would be necessary to evaluate the correctness of the estimation.
An electrical power to RF power efficiency of 0.2 for the HGA and 0.15 for the MGA	This is a reasonable power conversion efficiency for lightweight systems [28]. In future development the efficiency of the developed items should be assessed and updated. If such efficiency will not be attainable at the required transmit power the amount of data acquired will need to decrease in order for ELMO to meet the requirements.
ELMO reception noise temperature for S,X,Ka-bands T_S =230 K T_X =200 K T_{Ka} =150 K	Reflecting typical conditions for deep-space communications, considering factors such as the spacecraft's environment around Enceladus, the operational frequency bands, and the expected performance of onboard communication systems[29][30]. Further analysis on actual temperatures need to assess better the reception performance.

5.3.2. Link Budgets and Power Sizing

Sizing of the link budgets is crucial to ensure the selected design meets the communication requirements. The required transmitted power P_{TX} can be derived from Equation 5.3 by evaluating the link budget in Equation 5.2[31]. The link budget relates the transmitter and receiver parameters with the data rate B_r. The term $\frac{E_b}{N_0}$ is the ratio of the energy per bit to the noise power spectral density, it represents the bit error rate achievable with the selected RF modulation. L_{FSL} is the free space loss that can be computed with Equation 5.4 while L_x accounts for additional atmospheric losses and possible scintillation effect.

$$\frac{E_b}{N_0} = EIRP_{TX} - L_{FSL} - L_x + \frac{G}{T}_{RX} - 10log_{10}(k_B \cdot B_r) \quad [dB] \tag{5.2}$$

$$EIRP_{TX} = P_{TX} + G_{TX} - Loss_{cable} \quad [dBW] \tag{5.3}$$

$$L_{FSL} = 20log_{10}(4\pi) + 20log_{10}(d) - 20log_{10}(\lambda) \quad [dB] \tag{5.4}$$

The transmitted power relates to the power consumption of the subsystem during communications depending on the efficiency of the transmitter-amplifier combination, transforming the electrical power into RF power. Given the link budgets are assessed, a further check must be performed to ensure that the channel capacity can cover the corresponding data rate. This check is provided by the Shannon-Hartley theorem Equation 5.5. In case this condition is not met and a higher bandwidth B is not an option, it is possible to increase $\frac{E_b}{N_0}$ by choosing a different error correction, or a completely different modulation scheme. Following this analysis the bandwidth for the S-band communication with the hoppers is set to be 4 MHz, higher than the DSN forced bandwidth considered for downlink to Earth.

[3] SENER, "JUICE's Medium Gain Antenna Subsystem (MGAMA)" https://www. group.sener/en/project/juices-medium-gain-antenna-subsystem-mgama/

$$C = B \cdot log_2(1 + SNR) = B \cdot log_2\left(1 + \frac{B_r}{B} \cdot 10^{\frac{1}{10} \cdot \frac{E_b}{N_0}}\right) \quad [bps] \tag{5.5}$$

The most critical link budget is given by ELM-UP01-COM-01, due to the high data rate of 381.31 $Mbps$ the Ka-band downlink is used to size the subsystem power consumption and performance. The science data transmission link is summarised in Table 5.6, the imposition of the data rate together with the system parameters and design assumptions in subsection 5.3.1 results in a required transmitted RF power of $8.67\,\mathrm{W}$ which to be transmitted consumes $43.4\,\mathrm{W}$.

Table 5.6: Link budget, science transmission from ELMO to Earth using HGA on Ka-band. Positive attenuations.

Science Downlink to Earth			
Segment	**Parameter**	**Value**	**Note**
ELMO	EIRP [$\mathrm{dB\,W}$]	68.1	P_{Tx} + G_{TX} - 0.7
ELMO	E_b/N_0 [dB]	1.4	Modulation QPSK
ELMO	$-10log(k_B \cdot B_r)$ [dB]	172.8	Data rate = 381 kbps
Path	Free Space Loss [dB]	306.9	Ka-band
Path	Additonal Losses [dB]	2.2	
Ground	G/T [$\mathrm{dB/K}$]	72.7	
-	Margin [dB]	3	

A similar procedure is followed in Table 5.7 to evaluate the downlink data rate to Earth achievable using other bands, assuming the system will provide the same amount of electrical power to the transmitter of either the MGA or HGA. In case of failure of the Ka-band transceivers, X-band will be used as a backup, however it is important to notice that the amount of data that can be transferred to Earth is more than 100 times smaller. If the HGA fails the S-band will be used but again, the data rate is drastically lowered.

Table 5.7: Link budget, transmission from ELMO to Earth using HGA for X-band and MGA for S-band. Positive attenuations and maximum data rate backup downlink from Enceladus orbit.

Downlink to Earth X-band			
Segment	**Parameter**	**Value**	**Note**
ELMO	EIRP [dB W]	56.6	P_{Tx} + G_{TX} - 0.7
ELMO	E_b/N_0 [dB]	4.3	Modulation QPSK
ELMO	$-10log(k_B \cdot B_r)$ [dB]	184	**Data rate = 30.4 kbps**
Path	Free Space Loss [dB]	295	
Path	Additonal Losses [dB]	1.4	
Ground	G/T [dB/K]	63.6	
-	Margin [dB]	3	
Downlink to Earth S-band			
Segment	**Parameter**	**Value**	**Note**
ELMO	EIRP [dB W]	21.9	P_{Tx} + G_{TX} - 0.7
ELMO	E_b/N_0 [dB]	1.4	Modulation QPSK
ELMO	$-10log(k_B \cdot B_r)$ [dB]	216	**Data rate = 17.4 bps**
Path	Free Space Loss [dB]	283	
Path	Additonal Losses [dB]	1	
Ground	G/T [dB/K]	50.2	
-	Margin [dB]	3	

The MGA of ELMO has the function to communicate with the hoppers on the surface of Enceladus, in particular for the uplink of the science data. Following requirement ELM-UC02-COM-01 and subsection 5.3.1 the link budget is evaluated in Table 5.8.

Table 5.8: Link budget, science transmission from hoppers to ELMO using MGA on S-band. Positive attenuations.

Science Uplink from Hoppers			
Segment	**Parameter**	**Value**	**Note**
Hopper	EIRP [dB W]	-10.8	P_{Tx} + G_{TX} - 0.7
Hopper	E_b/N_0 [dB]	1.4	Modulation QPSK
Hopper	$-10log(k_B \cdot B_r)$ [dB]	163	Data rate = 4000 kbps
Path	Free Space Loss [dB]	138	S-band
Path	Additonal Losses [dB]	0.5	
ELMO	G/T [dB/K]	-8.45	
-	Margin [dB]	3	

To evaluate the performance of the subsystem Table 5.9 provides the link parameters for uplink from Earth done on the three bands and the corresponding data rate. This evaluation clearly shows that the HGA X-band is the favorable choice for the transmission from the DSN to ELMO, this is due to the higher transmitted power and lower losses in comparison with Ka DSN antennas.

Table 5.9: Link budget, transmission from Earth to ELMO using MGA for S-band and HGA for X-band and Ka-band. Positive attenuations and maximum data rate uplink to Enceladus orbit.

Uplink from Earth S-band			
Segment	**Parameter**	**Value**	**Note**
Ground	EIRP [$\mathrm{dB\,W}$]	105	
Ground	E_b/N_0 [dB]	4.3	Modulation QPSK
Ground	$-10log(k_B \cdot B_r)$ [dB]	195	**Data rate = 2.51 kbps**
Path	Free Space Loss [dB]	283	
Path	Additonal Losses [dB]	1	
ELMO	G/T [$\mathrm{dB/K}$]	-8.45	
-	Margin [dB]	3	
Uplink from Earth X-band			
Segment	**Parameter**	**Value**	**Note**
Ground	EIRP [$\mathrm{dB\,W}$]	115	
Ground	E_b/N_0 [dB]	4.3	Modulation QPSK
Ground	$-10log(k_B \cdot B_r)$ [dB]	164.3	**Data rate = 2.71 Mbps**
Path	Free Space Loss [dB]	295	
Path	Additonal Losses [dB]	1.4	
ELMO	G/T [$\mathrm{dB/K}$]	24.7	
-	Margin [dB]	3	
Uplink from Earth Ka-band			
Segment	**Parameter**	**Value**	**Note**
Ground	EIRP [$\mathrm{dB\,W}$]	104	
Ground	E_b/N_0 [dB]	4.4	Modulation QPSK
Ground	$-10log(k_B \cdot B_r)$ [dB]	175	**Data rate = 233 kbps**
Path	Free Space Loss [dB]	307	
Path	Additonal Losses [dB]	2.2	
ELMO	G/T [$\mathrm{dB/K}$]	37.6	
-	Margin [dB]	3	

5.3.3. Antenna Sizing and Mass Estimation

The MGA that ELMO is provided with is heritage from the Juice mission [4], therefore its diameter of $0.5\,\mathrm{m}$ is fixed. However, the parabolic antenna dish sizing was performed with the following method for the HGA. As per assumption the gain G of ELMO HGA is selected to be $47.8\,\mathrm{dB}$ in X-band. Equation 5.7 derived from Equation 5.6 [12] allowed to calculate the corresponding dish diameter of $3.5\,\mathrm{m}$, which meets the ELM-US01-COM-01 requirement. A_p is the physical parabolic area, λ the wavelength of $0.036\,\mathrm{m}$ for X-band and η the antenna efficiency of 0.6 which is considered a reasonable estimation [32] [33].

$$G = \frac{4 \cdot \pi}{\lambda^2} \cdot A_e = \frac{4 \cdot \pi}{\lambda^2} \cdot \eta \cdot A_p = \frac{4 \cdot \pi}{\lambda^2} \cdot \eta \cdot \frac{\pi \cdot D^2}{4} = \eta \cdot \left(\frac{\pi \cdot D}{\lambda}\right)^2 \tag{5.6}$$

[4] SENER, “JUICE’s Medium Gain Antenna Subsystem (MGAMA)” https://www. group.sener/en/project/juices-medium-gain-antenna-subsystem-mgama/

$$D = \lambda \cdot \pi \cdot \sqrt{\eta \cdot 10^{G/10}} \quad [m] \tag{5.7}$$

To evaluate the mass of the two antenna dishes Equation 5.8[12] is used, assuming a density ρ_A of $5.5\,\mathrm{kg\,m^{-2}}$, for achievable lightweight antennas [34] [35], reaching the $52.9\,\mathrm{kg}$ estimation for the HGA and $1.1\,\mathrm{kg}$ for the MGA, which is within the ranges of other existing spacecrafts[15].

$$M_{antenna} = \rho_A \cdot S_{antenna} = \rho_A \cdot \pi \cdot \left(\frac{D}{2}\right)^2 \quad [kg] \tag{5.8}$$

5.3.4. Verification and Validation

The methods discussed in subsection 5.3.2 and subsection 5.3.1 were implemented in a spreadsheet. Given that the underlying formulas are well-established and widely used in literature, the method was verified by using input parameters from [36], for which the numerical outputs are known. The consistency between the calculated and expected results serves as verification of the correctness of the link budget formula implementation. To further validate the link budget calculations, Cassini downlink data from [37][38] was used. By inputting the X-band frequency, gain, and data rate from the mission specifications, the model outputs a $27\,\mathrm{W}$ RF power. The $35\,\%$ difference from the expected $20\,\mathrm{W}$ value can be attributed to the assumptions listed in Table 5.5, as well as the standard theoretical link margin of $3\,\mathrm{dB}$ (without which the resulting Cassini power would be $13.5\,\mathrm{W}$). Additionally, some parameters from the Cassini link data, which were not readily available, may have differed from the assumed values. For future studies, it is recommended to re-evaluate the validity of the assumptions underlying the used method.

5.3.5. Review update

Following further discussions and review of the results, as stated before, the assumptions in Table 5.5 need to be re-examined to guarantee reliable links. Experts stated that the driver requirement of $381\,\mathrm{kbps}$ should not be attainable given the distance of Enceladus from Earth and implementing realistic DSN performance. Moreover it is worth to mention that the size of the HGA is not higher than $3.5\,\mathrm{m}$, as for example Cassini's, to allow for a lighter subsystem as well as to not generate shadow on the wings of the solar panels, which, due to the launcher size constraints, could not be placed further from the main orbiter structure.

As missing from previous calculations in the chapter Equation 5.9 from [36] is used to estimate the beamwidth (angle across which the gain is within $3\,\mathrm{dB}$ of its peak) for both HGA and MGA at different frequencies. θ results in Table 5.10 are within the limitation of the spacecraft pointing accuracy in subsection 7.2.3 and within the 10 arcsec requirement.

$$\theta = \frac{21}{f_{GHz} D} \tag{5.9}$$

Table 5.10: Beamwidths of ELMO antennas.

Antenna	Band	Beamwidth θ
HGA	Ka-band	0.19 [°]
HGA	X-band	0.71 [°]
MGA	S-band	21 [°]

6
Electrical Power System

This chapter will outline the design of the electrical power subsystem (EPS). The chapter will begin by presenting the subsystem requirements in Section 6.1. The overall system characteristics will be presented in Section 6.2, alongside the electrical diagram. In Section 6.3, the solar array design will be presented, while in Section 6.4 and Section 6.5 the power storage and distribution systems will be presented. Lastly, in Section 6.6, the methods used for calculations will be verified and validated using comparable missions.

6.1. Subsystem Requirements

The ELMO orbiter's power system was designed in accordance with the requirements defined in Table 6.1.

Table 6.1: EPS requirements.

ID	Title	Description
USR-PLD-14	Hopper Power Usage	The EPS shall not supply any power to the Hopper vehicles before their deployment
ELM-US03-EPS-01	Solar Array Operational Lifetime	The orbiter's solar array shall be able to produce power for 9 years.
ELM-UP01-EPS-01	Spacecraft Power Need During Science	The EPS shall be able to supply the orbiter with at least $182\,\mathrm{W}$ of power during science data collection with an angle of incidence of 26.7 degrees.
ELM-UP01-EPS-02	Spacecraft Power Need During Operations	The EPS shall be able to supply the orbiter with at least $185\,\mathrm{W}$ of power during communication to Earth with an angle of incidence of 5 degrees.

6.2. Subsystem Overview

The electrical power system serves four main functions: power generation, power storage, power distribution and power regulation. The ELMO orbiter EPS was designed to fulfil all these functions, as well as comply with the requirements defined in Section 6.1. The main design challenge for this system was the large distance from the sun, which reduced the power produced per squared meter. Power generation decreases with distance to the Sun, and at almost 10 AU, the ELMO orbiter is in unfavourable solar irradiance conditions. In previous stages of design, RTGs were considered, but they were removed from the design due to their high costs and limited availability. The key specifications of the EPS are given in Table 6.2.

Table 6.2: EPS fact sheet.

EPS mass	Mass margin	EPS mass with margin	Power generated (science, EOL)	Power generated (transmit, EOL)	Battery capacity	Array area
279 kg	14.2 %	318 kg	219 W	245 W	824 W − hr	85.5 m^2

To account for the spacecraft having two stages, the power system of the orbiter includes a power line for each of the propellant feed systems. The power line to the kick stage is doubled up for redundancy, with umbilical connections that get shorted and cut once separation occurs. The spacecraft's electrical diagram is given in Figure 6.1. As per USR-PLD-14, the hoppers are not included in the power distribution system.

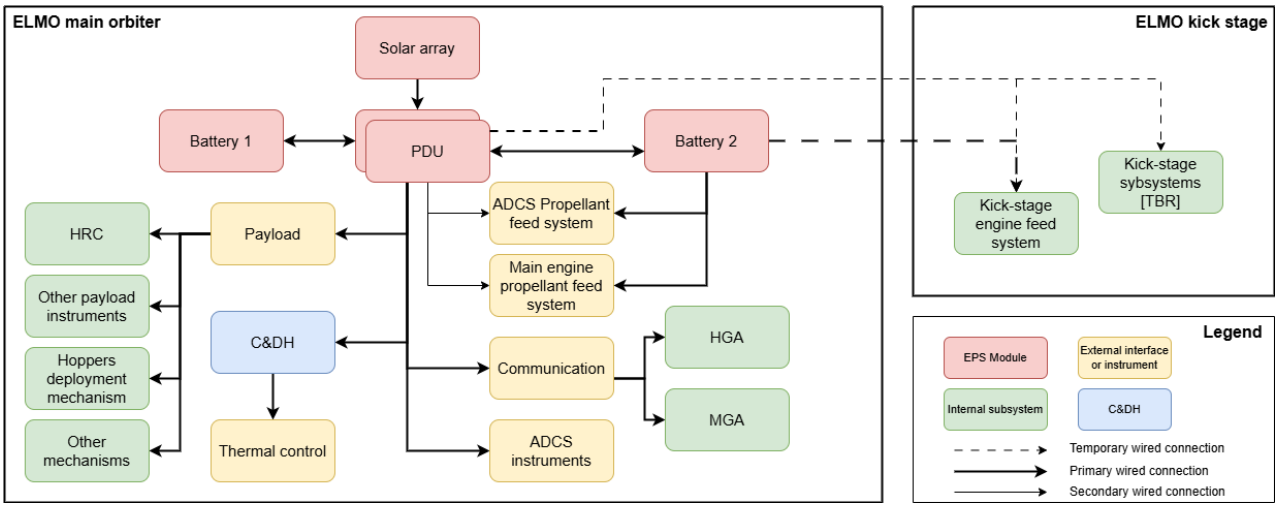

Figure 6.1: Electrical diagram for the ELMO orbiter. Elements not included are beyond the scope of the study.

For the ELMO orbiter EPS design, it is assumed that the yearly cell degradation is half of that of a solar cell in LEO, and that the radiation environment in Saturn is less harsh than around Jupiter. It is also assumed that the density of the back panel support density matches that of JUICE, with an added margin for design changes. Furthermore, it is assumed that any work on the stringing scheme for the solar array will be done in later design phases. These assumptions are discussed further in the following sections.

6.3. Power Generation

The ELMO orbiter's solar array covers the power generation function of the EPS. This element of the EPS was designed with the most demanding mission section in mind, which is the science orbits. During this phase, the spacecraft shall generate $218\,\mathrm{W}$ (ELM-UP01-EPS-01), which is the amount of power necessary for all operations during science data collection with a design margin of 20%. The angle of incidence on the solar panels during science data collection will be $26.7°$, as illustrated previously in Section 3.4. Due to the large angle of incidence, this phase of the mission requires a larger area than the communication phase, therefore it was chosen as the design case. In the following subsections, the main design elements will be explained, alongside their method, and a summary will be given at the end.

6.3.1. Solar Cells and Required Area

To determine the required solar cell area, a method found in literature was used [36]. The SpectroLab XTE-LILT cells were chosen, due to their large efficiency in low-intensity low-temperature (LILT)

conditions [39]. These cells have flight heritage and they were used on Juno. The relevant cell information is presented in Table 6.3.

Table 6.3: Summary of values of the SpectroLab XTE-LILT cells.

Item	Description	Value	Unit
η_{cell}	Average cell efficiency[39]	37%	-
A_{cell}	Cell area[39]	27	cm^2
ρ_{cover}	Cover glass density[40]	2.60	g/cm^3
t_{cover}	Cover glass thickness [41]	0.30	mm
m_{cell}	Cell only mass, without cover glass[39]	1.42	g
d_{cell}	Cell inherent degradation [36][p. 397]	0.77	-

Using the data presented above, the power output per squared metre of cell surface $P_{cell_{BOL}}$ in W/m^2 can be calculated using Equation 6.1.

$$P_{cell_{BOL}} = \eta_{cell} \cdot I_d \cdot d_{cell} \cdot cos(\alpha_{array}) = 3.48 W/m^2 \tag{6.1}$$

Where I_d is the solar irradiance at Saturn calculated at a distance of $10.1\,\mathrm{AU}$ ($13.8\,\mathrm{W/m^2}$), α_{array} is the angle of incidence of $27.6°$. The other values come from Table 6.3. To $P_{cell_{BOL}}$, one must add the lifetime degradation L_d, which can be estimated with Equation 6.2.

$$L_d = (1 - degradation/year)^{satellitelife} = 0.83 \tag{6.2}$$

The degradation per year was estimated at 2%, taking half of what normally affects a LEO array [36], due to the higher degradation factors (i.e. atomic oxygen, space debris) to be found in LEO. It is important to note that this is a rough approximation and that further studies would need to be conducted to evaluate the impact of Saturn's E-ring, the material ejected by the plumes on Enceladus and other degradation effects to better evaluate the solar cells degradation. A simulation of the reduced solar irradiance is presented in Chapter 14, which offers more insight into this topic. The satellite life is 9 years, summing up the 8-year transfer, and the 100 days of nominal operation time, with the extension of up to a year to comply with ELM-US03-EPS-01.

By multiplying $P_{cell_{BOL}}$ and L_d, the end-of-life (EOL) power generated per square meter of cell $P_{cell_{EOL}}$ can be calculated to be equal to $2.89\,\mathrm{W/m^2}$. This number can then be used to calculate the total area of cells needed to generate enough power (ELM-UP14-EPS-01). The cell-only area of $75.3\,\mathrm{m^2}$ was then used to calculate the cover glass mass of $58.8\,\mathrm{kg}$, alongside t_{cover}, and ρ_{cover}. A_{cells} was also used to calculate the total mass of the cells m_{cells} of $35.9\,\mathrm{kg}$. A summary of the key masses and areas is given in Table 6.4. For further design, it is recommended to investigate lighter and or more efficient cells for the ELMO orbiter.

6.3.2. Back Panel Support

The total solar array area results in a total solar panel area A_{sa} of $85.2\,\mathrm{m^2}$, including an area factor of 1.13 in the cell-only area, calculated from JUICE and Europa-Clipper's solar array. The total back panel support mass is $170\,\mathrm{kg}$ A_{sa} was used to calculate the mass of the back panel and support structure, by using a density of $133\,\mathrm{kg/m^3}$, based on JUICE's ARA Mk4 array [41] with a 10% development margin added for possible design changes. This back panel features two CFRP plates and an internal honeycomb structure [41]. For JUICE and Europa-Clipper, a core thickness of $22\,\mathrm{mm}$ was used [41], but for ELMO it was reduced to $15\,\mathrm{mm}$, to reduce the overall array mass by reducing the

mass of its heaviest component. This reduction is based on the assumption that the lower radiation environment of Enceladus compared to Jupiter would allow for a slimmer design [42].

A structural analysis was performed to confirm the structural stability of the array with a back panel thickness of $15\,\mathrm{mm}$, by verifying the bending stress and the Euler critical buckling load of each wing. The solar array is approximated as a cantilever beam with a rectangular cross-section. The limiting factor is the bending moment at the root, $M = \frac{1}{2}\rho a L^2$. Here ρ is the linear mass density composed of the solar cell density, cell cover glass density and the structural density itself. L is the length of the solar array and a is the acceleration due to the spacecraft's thrusters. The bending stress can be calculated using $\sigma = MY/I$. Y is the maximum distance to the neutral axis ($Y = t/2$), and I is the area moment of inertia. Using a material density of $133\,\mathrm{kg/m^3}$ and thickness of $15\,\mathrm{mm}$, a bending stress of around $1\,\mathrm{MPa}$ was calculated. This stress can be supported by the honeycomb structure, which has a yield stress of $3.22\,\mathrm{MPa}$ [43].

Euler critical buckling load was also investigated since the solar array is stowed upright during launch. Because the solar array folds into 3 pieces, a characteristic length of $L/3$ is used. Using Young's modulus from Tounsi (2012) [43] yields an Euler critical load of $527\,\mathrm{kN}$, which is two orders of magnitudes larger than the $5.2\,\mathrm{kN}$ load on the solar array during launch. It is therefore safe to say that a solar array support structure thickness of $15\,\mathrm{mm}$ should support all loads experienced by the spacecraft. For further design, it is recommended to analyse this further and to investigate lighter, stronger and overall more efficient materials.

6.3.3. Solar Array Overview

The values obtained with the estimations presented in the previous sections can be found in Table 6.4.

Table 6.4: Overview of solar array estimation values.

Item	Mass [kg]	Area[m^2]
Solar cells	35.9	75.3
Cover glass	58.8	75.3
Back panel	170	85.2
Full array	265	85.2

The values calculated for the total solar array area and mass were reevaluated based on cell packing efficiency. This, along with the size requirements to fit in the launcher faring has resulted in the wing configuration presented in Figure 6.2. The configuration presents four wings made of three $3\,\mathrm{m}$ by $2.64\,\mathrm{m}$ panels each. Each panel is fitted with 2336 cells, for a total of 28032 SpectroLab XTE-LILT cells. Each cell has the standard size of $4\,\mathrm{cm}$ by $8\,\mathrm{cm}$. With this solar array, the ELMO orbiter can produce $219\,\mathrm{W}$ at EOL during science, and $245\,\mathrm{W}$ during communications, fulfilling ELM-UP01-EPS-01 and ELM-UP01-EPS-02. The final solar array size specifications are presented in Table 6.5, while subsection 4.4.1 explains in further detail the solar array configuration motivations. Note that the back panel margin has been put to 20% to include the assessment of the thinner support structure. Further design should take into account the packing efficiency and the stringing of cells together to avoid exceeding the battery's maximum voltage and current capabilities.

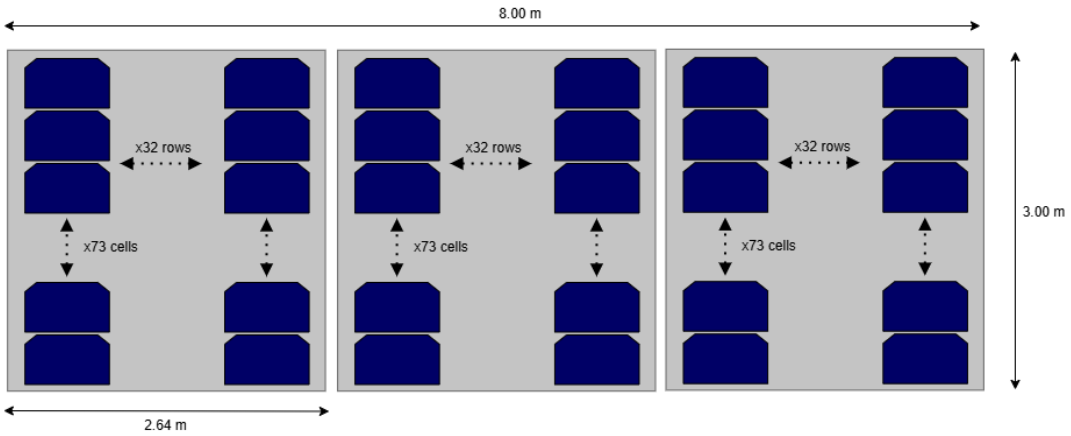

Figure 6.2: Configuration of each wing of the ELMO orbiter, with dimensions. The full length is rounded up to $8\,\mathrm{m}$ to account for hinges.

Table 6.5: Final mass and area values for the solar array, including margins.

Item	Mass [kg]	Mass margin	Mass with margin [kg]	Area [m^2]
Solar cells	37.8	5 %	39.7	75.7
Cover glass	59.3	5 %	62	75.7
Back panel	171	20 %	204.9	85.5
Full array	267	-	307	85.5

6.4. Power Storage

The power storage function of the EPS will be taken care of by the batteries. As shown in Section 3.6 ELMO will be in full sunlight during the nominal mission at Enceladus, therefore it does not need a battery designed for eclipse periods. The battery design is tailored to power peaks during the mission and power management during transfer to Enceladus. The transfer from Earth to Enceladus is beyond the scope of the study, so ELMO is assumed to follow a protocol of charging cycles and hibernation, similar to New Horizons or Rosetta[1].

Regarding ELMO, the battery was initially designed to cover the power peaks of $76\,\mathrm{W}$ for $3000\,\mathrm{s}$ for slewing. Considering a depth of discharge of 20% and transmission efficiency of 98% [44], the spacecraft needs a battery that can accommodate $175.93\,\mathrm{W}-\mathrm{hr}$. The formula used for the calculation of the battery capacity can be seen in Equation 6.3 [36]. Here P_{batt} is the power to be stored in the battery, $t_{storage}$ is the time, N_{batt} is the number of batteries (here is 1), DoD is the depth of discharge of 20%, and η_{batt} is the battery efficiency, taken to be 98% [44].

$$C_{batt} = \frac{P_{batt} \cdot t_{storage}}{N_{batt} \cdot DoD \cdot \eta_{batt}} = 106W - hr \tag{6.3}$$

Another use of the battery is during the mission's science phase. Data collection happens when flying above the south pole of Enceladus, leaving the northern hemisphere free of any payload usage. The battery is therefore charged in this phase such that it can provide half of the power to the payload peak later, when flying over the southern hemisphere. Using Equation 6.3, with P_{batt} being $46.2\,\mathrm{w}$, and $t_{storage}$ being $2.1\,\mathrm{h}$, one can then calculate $C_{battpld}$ to be $268\,\mathrm{W}-\mathrm{hr}$, which is leading compared to $C_{batt_{prop}}$ calculated earlier.

[1] https://pluto.jhuapl.edu/News-Center/News-Article.php?page=20170410, last accessed on 16/01/2025

A COTS battery was found to accommodate the required capacity and more, which is the Ibeos B50-412 (Figure 6.3). ELMO will carry two of these for redundancy. The Ibeos battery has a capacity of $412\,\mathrm{W}-\mathrm{hr}$ and can withstand up to $30\,\mathrm{kRad}$. This contrasts with USR-SYS-05, so a mitigation strategy was devised and it can be found in Chapter 11. It is important to note that the batteries are oversized to account for any possible needs during transfer, due to eclipses, hibernation and manoeuvres. The final values for the batteries on board are presented in Table 6.6.

Figure 6.3: The Ibeos B50 battery module.

Table 6.6: Overview of key battery sizing parameters. Values are given for 2 battery units with exception of the size.

Item	Mass[kg]	Mass margin	Mass with margin[kg]	Size[mm^3]	Capacity[$W-hr$]
Batteries	6	5%	6.3	147x90x185	824

6.5. Power Regulation and Distribution

The power management unit (PMU) will take care of regulating the power coming from the solar arrays and distributing it to the different subsystems according to their required voltage. ELMO has a relatively low power requirement compared to other interplanetary spacecraft, which means that, most likely, its voltage bus will be of $28\,\mathrm{V_{DC}}$ [45]. The power distribution system would also use direct energy transfer (DET), as it is the most efficient power transmission method [36]. The efficiency of this method can be taken to be up to 95% but as it is specific to the PMU design, it was not accounted for at the current design stage.

The PureLine Pearl Power Distribution unit was chosen as hardware for this stage of development (Figure 6.4[46]). This unit weighs $2.5\,\mathrm{kg}$, and it can handle input from 6 different panels. For this reason, and for redundancy, the ELMO orbiter will host two identical PMUs on board. This PMU provides an unregulated $22\,\mathrm{V}$-$38\,\mathrm{V}$ nominal voltage and ranges up to $1.5\,\mathrm{kW}$, which is oversized for the current design. With a similar philosophy as the battery choice, the PMU was selected with the transfer in mind, as each panel is expected to produce significantly higher amounts of power during manoeuvres in the inner solar system. A summary of the relevant sizing values for the PMUs is given in Table 6.7.

Figure 6.4: The PureLine Pearl Power Distribution unit.

Table 6.7: Overview of key PMU sizing parameters. Values are given for 2 units combined with exception of the size.

Item	Mass[kg]	Mass margin	Mass with margin[kg]	Size[mm^3]
PMU	5	5 %	5.25	395x125x65

6.6. Verification and Validation

To verify the method used to size the solar array, JUICE and Europa-Clipper were taken as examples. The back panel support density was extrapolated by removing cells and cover glass masses from the total mass and dividing by the volume of the array. A similar process was done to find the area factor that was used to estimate the non-cell area of each panel. Table 6.8 shows the main values used to verify the method illustrated in Section 6.3. This data was applied to the method in Section 6.3, producing the results in Table 6.9.

Table 6.8: Dataset used for validation of the calculation method [41][47]. ELMO's data is shown for comparison. Note that the angle of incidence on JUICE and Europa Clipper's solar array was not available.

Data	JUICE	Europa-Clipper	ELMO
Distance from Sun [AU]	5.03	5.46	9.97
Solar irradiance [W/m^2]	54.03	45.85	13.75
Solar cell	AzurSpace 3G28	AzurSpace 3G28	SpectroLab XTE-LILT
Cell efficiency	26.9 %	25.8 %	37 %
Cell area [cm^2]	32	32	27
Cell mass [g]	2.75	2.75	1.42
Support panel thickness [mm]	22	22	15
Array lifetime [y]	11.5	9.5	9
Support panel density [kg/m^3]	121	189	133
Angle of incidence [deg]	N/A	N/A	26.7
Power needed EOL [W]	766	728	218

Table 6.9: Values obtained applying the method used for ELMO on JUICE and Europa-Clipper.

Mission	Value Type	Array Mass [kg]	Array Area [m^2]
JUICE	Calculated value	359	97.6
	Real value	350	85
Europa-Clipper	Calculated value	567	109
	Real value	571	102

The verification values for JUICE and Europa-Clipper are not an exact match to the declared values [41]. The values calculated for Europa-Clipper are below 7.3% of difference from the real values, with the mass going below 1%. Regarding JUICE, the difference is larger, and it goes up to 15% in the case of the area, but it remains below 2.6% when it comes to the mass. The differences in values can be attributed to several reasons. The data on JUICE and Europa-Clipper's panels does not specify whether the numbers given include specific margins. Furthermore, as explained in Section 6.3, part of the method was obtained with approximations or comparisons. Overall, as the V&V values calculated are within a 20% margin, which is the largest margin used in the calculations of this chapter, the method can be considered sufficiently accurate for this stage of design.

7

Attitude Determination and Control System

The Attitude Determination and Control Subsystem (ADCS) of the ELMO is tasked with ensuring accurate orientation and stability, which are critical for the spacecraft's operations across all mission phases. During the operational lifetime, the ADCS fulfils stringent requirements for pointing accuracy and stability, enabling payload instruments to precisely observe Enceladus' surface and facilitate alignment for communications with Earth and for pointing the solar arrays towards the sun.

The key functions of the ADCS are summarized as follows:

1. **Attitude Stabilization**: Ensuring the spacecraft maintains a stable orientation to support consistent operations throughout all mission phases.
2. **Slewing**: Facilitating spacecraft reorientation for transitioning between operational modes and for alignment during orbital manoeuvres.

This chapter begins with the requirements and design drivers for the ADCS, followed by an overview of the subsystem's baseline configuration. It then details the methods used for modelling and component selection, leading to the final design and analysis of the subsystem.

7.1. Subsystem Requirements

In order to ensure that the ADCS design supports the spacecraft in meeting the mission's scientific and operational objectives, this section outlines its specific requirements and key design drivers that stem from system-level constraints. These requirements are tailored to the mission's unique challenges, such as the need for precise pointing of the HRC and a strict mass budget.

The ADCS must fulfil the following requirements:

Table 7.1: ADCS Requirements.

ID	Title	Description
USR-PLD-08	Pointing Stability	The spacecraft shall maintain pointing stability of less than 0.5 arcseconds per second.
USR-PLD-07	Pointing Accuracy	The spacecraft shall achieve a pointing accuracy of less than 10 arcseconds.
ELM-US03-ADC-01	Slews Between Transmission and Science Modes	The spacecraft shall be capable of performing slews between transmissions and science mode attitudes during the operational and extended lifetime.
ELM-US09-ADC-01	Slews for Orbital Correction Burns	The spacecraft shall perform slews for engine alignment at scheduled orbital correction burns.

Additionally, the design of the ADCS is driven by system-level considerations, including:

1. **Mass Optimization**: Mass is a critical constraint for the spacecraft, as outlined in Section 4.2.
2. **Reliability**: The ADCS should incorporate redundancy in its components to prevent single

points of failure (as per ELM-US02- RRS-02a), in alignment with the spacecraft's overall reliability strategy discussed in Section 16.2.

The ADCS subsystem is designed with these considerations in mind, whilst also adhering to the aforementioned requirements.

7.2. Subsystem Overview

With the subsystem requirements clearly defined and the main design drivers outlined, this section presents the subsystem design found to be optimal for meeting these criteria.

7.2.1. Trade-offs

Figure 7.1 illustrates the design option tree, showcasing all considered options for the ADCS design. The rationale behind the decision-making process is detailed below, with the primary objective being to adhere to the design drivers and requirements outlined in Section 7.1.

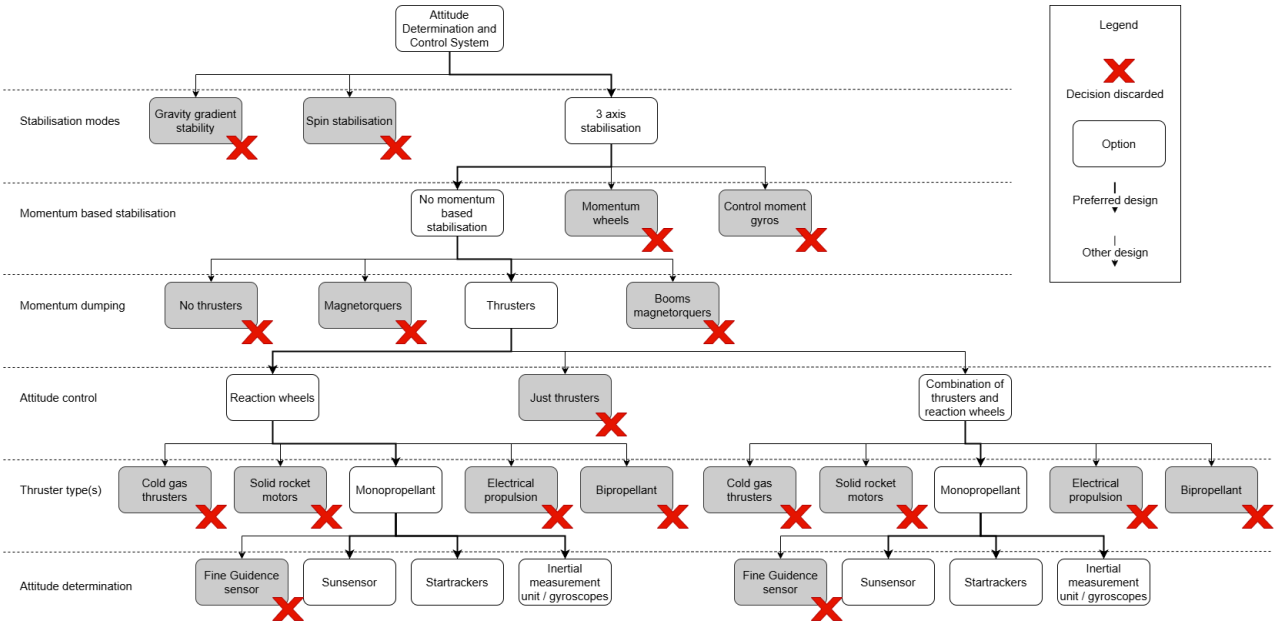

Figure 7.1: ADCS Design Option Tree highlighting the considered and discarded options in the design process.

To minimize mass in accordance with the design driver, the system employs reaction wheel based control. Thrusters are utilized exclusively for momentum dumping, thereby reducing the propellant mass requirements. This decision leverages the relatively low disturbance torques experienced characterized at the operational environment. The low gravity gradient of Enceladus, negligible magnetic field, and low solar radiation pressure due to the enormous distance from the Sun provide an opportunity for mass saving. To make use of this, the design utilizes long slew durations: $6000\,\mathrm{s}$ for orbital manoeuvre slews and correction burn slews and $2000\,\mathrm{s}$ for transitions between science and transmission orbit attitudes. These increased slew times enable the design to exploit the low-disturbance operational environment, minimizing propellant mass without necessitating oversized reaction wheels.

Spin stabilization and gravity gradient stabilization were excluded as they did not meet the pointing accuracy requirements [36]. Similarly, momentum wheel-based stabilization was dismissed due to its inability to comply with these accuracy requirements [36]. Other exclusions seen in the Design Option Tree were made based on misalignment with the primary objective of minimizing mass or their contribution to excessive system complexity.

7.2.2. Baseline Design

Building on the requirements and trade-offs discussed in subsection 7.2.1, this section details the baseline ADCS design tailored for the requirements and design drivers in Section 7.1. The final design is summarised in Table 7.2, which lists the selected components and their respective characteristics.

Table 7.2: ADCS list of equipment (mass and power values are in total for all units, with margins included).

Category	Component	Qty	Mass (kg)	Power (W)	Margin (%)
Reaction wheels	Bradford Space Reaction Wheel Unit W18E	4	21.8	32.0	5
Desaturation Thrusters	Arianegroup 1N Chemical Monopropellant Thruster	24	7.31	0	5
IMU	Airbus Defence and Space ASTRIX 120	1	6.83	18.9	5
Sun sensors	NewSpace Systems (NSS) Aquila-D02	2	0.08	0.32	5
Star trackers	O.C.E. Technology NST-2	4	0.55	4.20	5
Monopropellant	Hydrazine	N/A	5.81	0	5
Propellant Tank	Rafael Ltd PEPT-230	1	1.37	0	5
Electronics & Processing units	N/A	N/A	2.59	7.04	5
Total			**46.4**	**62.4**	

To meet the stringent pointing requirements outlined in Section 7.1, the sensor suite incorporates a high-performance IMU (ASTRIX 120), complemented by both star trackers and sun sensors. The IMU provides rapid updates, whereas the star trackers and sun sensors enable precise long-term orientation determination.

A pyramidal configuration of four reaction wheels has been selected to meet the design driver of eliminating single points of failure (Section 7.1). This arrangement provides redundancy by ensuring that the system can maintain full three-axis control even in the event of a single wheel failure. For momentum desaturation, 24 thrusters have been included, offering significant redundancy. Each axis of rotation requires two thruster pairs, one for clockwise and another pair for counter-clockwise burns—resulting in a total of 12 operational thrusters. To enhance reliability, a backup thruster is included for each operational one, doubling the total to 24. These thrusters use hydrazine monopropellant, which is known for its established reliability and predictable performance.

A dedicated allocation of 5% of the subsystem mass and 10% of its power budget has been reserved for supporting electronics and processing units, exclusive of the reaction wheel drive electronics. This ensures sufficient resources for the operation of additional control and processing systems, contributing to overall subsystem resilience and flexibility.

7.2.3. Pointing Performance

The ADCS pointing performance has been verified against the requirements of $10\,\mathrm{arcsec}$ accuracy and $0.5\,\mathrm{arcsec/s}$ stability (Section 7.1). Key contributors include the star trackers (O.C.E. Technology NST-2) and the Airbus ASTRIX 120 IMU, as well as the closed-loop control of the reaction wheels.

The NST-2 star trackers offer an absolute pointing knowledge of $3\,\mathrm{arcsec}$ (1σ) for pitch and yaw. With

updates provided at $10\,\mathrm{Hz}$, drift between updates can be neglected, ensuring an absolute pointing error of $3\,\mathrm{arcsec}$. The final accuracy remains $3\,\mathrm{arcsec}$, well below the $10\,\mathrm{arcsec}$ requirement (USR-PLD-07).

Short-term stability depends on the IMU's angular random walk (ARW $< 0.0016\,^\circ/\sqrt{\mathrm{h}}, 5.76\,\mathrm{arcsec}/\sqrt{\mathrm{h}}$). Over $0.1\,\mathrm{s}$, drift is estimated as:

$$\Delta_{\mathrm{drift}} = \mathrm{ARW} \cdot \sqrt{t} \approx 5.76\,\mathrm{arcsec}/\sqrt{\mathrm{h}} \cdot \sqrt{0.1\,\mathrm{s}} \approx 0.018\,\mathrm{arcsec}. \tag{7.1}$$

Assuming the reaction-wheel control loop operates with a typical conservative frequency of $0.3\,\mathrm{Hz}$ [48], the loop corrects disturbances within $\sim 3.3\,\mathrm{s}$, limiting rate errors. Conservatively, the rate error, including all contributors, is under $0.3\,\mathrm{arcsec/s}$, providing sufficient margin below the $0.5\,\mathrm{arcsec/s}$ requirement (USR-PLD-08) to account for neglected effects such as vibrations, reaction wheel inaccuracies, and other unmodelled disturbances. It should be noted that, following validation, it was found that these accuracy and stability figures seem to be somewhat ambitious and should be revised.

7.3. Sizing & Selection Method

To size and select the components found in the baseline ADCS design, a custom tool script was created to calculate the mission torque profile and momentum accumulation for various combinations of reaction wheels and thrusters. This script takes inputs such as the mission profile, system configuration, and operational requirements (e.g., pointing stability, slew rates) and outputs key parameters, including torque, momentum, power usage, and propellant mass. These outputs are used to optimise component selection for minimum mass and power usage.

7.3.1. Assumptions

Before proceeding with the modelling and analysis done by the ADCS tool, it is necessary to define the assumptions underlying the calculations. These assumptions simplify the design process by focusing on the most significant factors relevant to the mission while ensuring that the results remain accurate enough to extract meaningful results out of the tool.

The following assumptions are made for the ADCS design tool:

1. **Transfer Position Modelling**: During the transfer window, the spacecraft position is modelled as a straight line between key mission milestones. Specifically, for each milestone, the timestamp and distance (in astronomical units) are used, with a linear interpolation of distance versus time between milestones.
2. **Negligible Magnetic Disturbance at Enceladus**: Magnetic disturbance torque is assumed negligible within the operational environment at Enceladus due to its weak magnetic field.
3. **Negligible Gravity Gradient and Magnetic Disturbance During Transfer**: During the interplanetary transfer phase, both gravity gradient and magnetic disturbance torques are considered negligible.
4. **Negligible Aerodynamic Drag**: Aerodynamic drag is assumed to have no significant effect on the spacecraft due to the low-density environment in which it operates.
5. **Momentum Dumping Constraints**: Reaction wheel momentum dumps cannot be performed during slew manoeuvres. This imposes a minimum requirement on the maximum momentum storage capacity of the reaction wheels to ensure uninterrupted slews.
6. **Maximum Torque**: The peak torque must be able to be carried by a single reaction wheel. This imposes a minimum requirement on the maximum torque of the reaction wheels.
7. **Negligible Engine Misalignment Torque**: Any torques resulting from misalignment between the spacecraft's main engines and its centre of mass are assumed to be fully corrected by their gimbals.

8. **Circular Orbits Assumption**: The orbit of the spacecraft about Enceladus is assumed to have zero eccentricity.
9. **Fixed Bodies**: Enceladus, Saturn, Earth, and the Sun are assumed to be fixed at their starting positions, for the entire 365 days of extended operational lifetime.

7.3.2. Inertia Matrix Modelling

To accurately analyse the disturbance and slewing torque profiles that the ADCS must handle, the spacecraft's inertia matrix is modelled using a simplified geometric representation of its primary mass contributors.

The major mass contributors of the spacecraft, such as the solar panels, antenna, and structure, are represented using basic geometric primitives like cylinders, boxes, and cones. Each component's mass and dimensions are used to compute its individual contribution to the inertia matrix. Unaccounted mass, such as internal equipment or structural elements not explicitly modelled, is incorporated as a hollow cylinder of uniform density around the spacecraft bus. This ensures a conservative estimation by assuming that these masses are distributed farther from the centre of mass (CoM) than in reality.

The full inertia matrix of the spacecraft is derived by summing the contributions of all individual components, applying the parallel-axis theorem where necessary:

$$I_{\text{total}} = I_{\text{component}} + m \cdot d^2, \tag{7.2}$$

where $I_{\text{component}}$ is the inertia matrix of a component about its own CoM, m is the component's mass, and d is the displacement vector from the component's CoM to the spacecraft's CoM.

To account for uncertainties in the spacecraft's mass distribution and CoM location, an additional conservative offset ($\Delta x, \Delta y, \Delta z = 0.4\,\text{m}, 0.4\,\text{m}, 0.1\,\text{m}$) is applied to the CoM position. This offset ensures that any unmodelled mass distribution is treated as being farther from the CoM, thereby increasing the overall inertia values. The resulting inertia matrix provides a robust basis for evaluating the torque and momentum profiles.

7.3.3. Position & Attitude Modelling

To compute the torque and momentum profiles required by the ADCS, the position and attitude of the spacecraft need to be modelled at each time step. From this, the rotation at slew events can also be modelled.

Position Modelling

The spacecraft's position in orbit is propagated assuming a circular orbit around Enceladus. The tangential velocity, v_t, is calculated using Equation 7.3:

$$v_t = \sqrt{\frac{\mu}{r}} \tag{7.3}$$

where μ is the gravitational parameter of Enceladus, and r is the orbital radius. The change in the spacecraft's true anomaly, $\Delta\theta$, over a time step Δt, is derived as:

$$\Delta\theta = v_t \cdot \frac{\Delta t}{r}. \tag{7.4}$$

The spacecraft's position at each time step is then determined iteratively, starting with a uniformly random initial true anomaly between 0 and 2π.

Attitude Modelling

The spacecraft's attitude at each time step is determined based on mission mode requirements. Each mode specifies a primary direction vector:

1. Science Mode: The nadir vector is aligned with the spacecraft's y-axis.
2. Transmission Mode: The Earth-pointing vector is aligned with the spacecraft's z-axis.
3. Orbital Correction Burns: The primary vector is randomly assigned to either the velocity vector or its opposite, based on the planned burn direction.

To fully determine the attitude, a secondary vector must be identified, with its alignment maximized. This is chosen to be z-axis alignment with the sun for minimum angle of incidence with the solar panels.

Slew Modelling and Frequency

For slew manoeuvres, the rotation required between two attitudes is computed by obtaining the rotation matrices for the old (R_{old}) and new (R_{new}) attitudes. The relative rotation matrix, R_{Δ}, is:

$$R_{\Delta} = R_{\text{new}} \cdot R_{\text{old}}^{T}. \tag{7.5}$$

The rotation angle, θ, is extracted as:

$$\cos \Delta\theta = \frac{\text{Tr}(R_{\Delta}) - 1}{2}, \tag{7.6}$$

where $\text{Tr}(R_{\Delta})$ is the trace of R_{Δ}. The angle $\Delta\theta$ is later used to compute the torque and momentum requirements during slew manoeuvres.

The overall operational lifetime mission profile is simulated for 365 days (including 265 days extendable lifetime) during which, 2 types of slew events occur:

1. Pre- and post-orbital correction burns, occurring at an average frequency of 1.73 days [49].
2. Mission mode changing slews at every transition between science and transmission orbits (Section 3.3).

At each slew event, time is allocated to model the slew, after which the model returns the spacecraft to the current required mission mode attitude.

7.3.4. Torque Profile

The torque profile of the spacecraft is determined by combining two primary contributors: disturbance torques and slew torques. Disturbance torques are external forces acting on the spacecraft, including gravity gradient torques and solar radiation pressure (SRP) torques. These torques are computed for each mission time step to ensure accurate modelling of their cumulative effects.

Gravity Gradient Torque

The gravity gradient torque, $\boldsymbol{\tau}_{gg}$, is calculated using the spacecraft's attitude and inertia matrix at each time step:

$$\boldsymbol{\tau}_{gg} = 3\frac{\mu}{r^3}\left(\mathbf{I} \cdot \hat{\mathbf{r}} \times \hat{\mathbf{r}}\right) \tag{7.7}$$

Here, μ is the gravitational parameter of Enceladus, r is the orbital radius, $\mathbf{I}$ is the inertia matrix of the spacecraft, and $\hat{\mathbf{r}}$ is the unit position vector in the body frame. The transformation of the inertial position vector to the body frame is achieved using the spacecraft's attitude matrix. This approach ensures accurate representation of gravity gradient torque in the body frame.

Solar Radiation Pressure Torque

The solar radiation pressure (SRP) torque is derived by considering the effective area exposed to sunlight, the assumed reflectivity coefficient ($C_r = 0.6$), and the assumed offset of the spacecraft's centre of pressure ($\Delta x, \Delta y, \Delta z = 0.4\,\mathrm{m}, 0.4\,\mathrm{m}, 0.15\,\mathrm{m}$). The SRP force is computed as:

$$F_{\mathsf{SRP}} = \frac{P_{\mathsf{solar}} \cdot A_{\mathsf{eff}} \cdot (1 + C_r)}{c} \tag{7.8}$$

where P_{solar} is the solar pressure at Enceladus, A_{eff} is the effective illuminated area and c is the speed of light. The resulting torque is then:

$$\boldsymbol{\tau}_{\mathsf{SRP}} = F_{\mathsf{SRP}} \cdot \boldsymbol{r}_{\mathsf{cp}} \tag{7.9}$$

where $\boldsymbol{r}_{\mathsf{cp}}$ is the vector from the centre of mass to the centre of pressure.

Slew Torques

Slew torques are generated during spacecraft reorientation manoeuvres, such as transitions between mission orbits or pre- and post-orbital correction burns. These torques are calculated based on the required rotation and inertia of the spacecraft.

$$\omega_{\mathsf{max}} = \frac{2\|\Delta\boldsymbol{\theta}\|}{t}, \quad \dot{\boldsymbol{\omega}} = \frac{\omega_{\mathsf{max}}}{t/2} = \frac{4\|\Delta\boldsymbol{\theta}\|}{t^2} \cdot \hat{\boldsymbol{\theta}} \tag{7.10}$$

where t is the slew duration, and $\hat{\boldsymbol{\theta}}$ is the unit rotation axis vector. The torque required for the slew is then:

$$\boldsymbol{\tau}(t) = \mathbf{I} \cdot \dot{\boldsymbol{\omega}} \tag{7.11}$$

7.3.5. Interpreting Torque Profile

The torque profile provides a basis for determining the maximum torque and momentum accumulation experienced by the reaction wheels. Each torque vector in the spacecraft body frame, $\boldsymbol{\tau}_{\mathsf{body}}$, is distributed among three of the reaction wheels using the transformation matrix, S, which defines the spin axis unit vectors of the pyramidal reaction wheel layout. This is mathematically expressed as:

$$\boldsymbol{\tau}_{\mathsf{wheels}} = S^{+} \cdot \boldsymbol{\tau}_{\mathsf{body}}, \tag{7.12}$$

where S^{+} is the Moore–Penrose pseudo-inverse of S.

The momentum accumulation for each wheel is then determined by integrating the torque applied over time:

$$\boldsymbol{H}_{\mathsf{wheel},i} = \boldsymbol{H}_{\mathsf{wheel},i-1} + \boldsymbol{\tau}_{\mathsf{wheels}} \cdot \Delta t \tag{7.13}$$

The momentum accumulation is subsequently utilized for computing the reaction-wheel power usage and propellant mass required to dump all momentum accumulated throughout the mission.

7.3.6. Verification and Validation

Verification and validation of the ADCS tool script were carried out to ensure the methods yielded sufficiently accurate results. A mix of checks and comparisons were used to confirm the accuracy and reliability of the design process:

1. **Visualisation**: Key data, such as torque profiles, momentum accumulation, orbit propagation, and attitude configurations—were plotted to identify any inconsistencies and ensure the results aligned with expectations. Some examples of these plots are shown in Figure 7.2.
2. **Time Step Sensitivity**: The tool was primarily used with a 30 second time step. A finer 1 second time step test showed less than 0.001% difference in outputs such as power consumption and propellant usage, confirming the 30 second time step was sufficient for accurate results without unnecessary computational complexity.
3. **Comparison**: The orbital period calculated by the tool was within 7 seconds (0.043%) of the theoretical value for a 100 km circular orbit around Enceladus, derived using the gravitational parameter. This verified minimal accuracy loss due to time step approximation.
4. **Independent Calculations**: Critical calculations, such as the inertia matrix and slew torques, were manually checked at selected time steps. The tool's outputs matched these independent calculations, confirming the implementation's correctness.
5. **Validation**: Public data on ADCS subsystems of other spacecraft is limited. Instead, the tool was applied to a custom made inertia model of the Cassini spacecraft, yielding results within the expected order of magnitude.

To illustrate the visual verification process, Figure 7.2 shows four example plots, demonstrating how the data was evaluated visually and analytically.

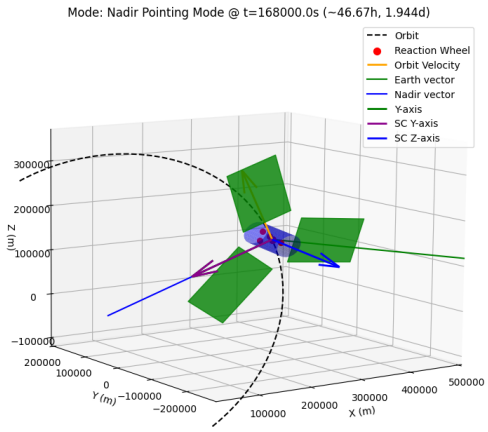

(a) Attitude configurations at each time step, verifying proper modelling of attitudes.

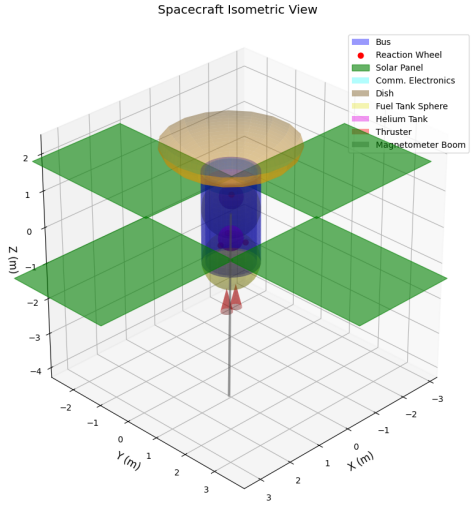

(b) Spacecraft configuration, verifying geometric representation for inertia calculations.

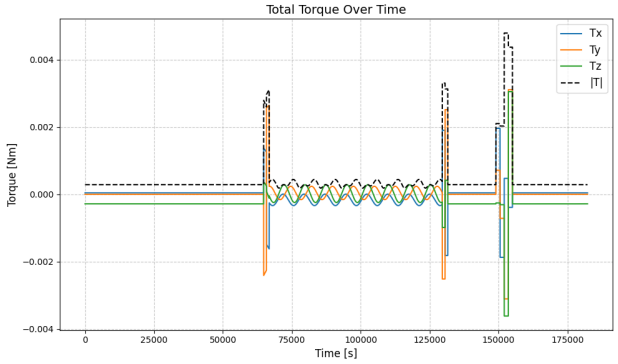

(c) Torque profile (over two operational days), verifying modelled torques per axis.

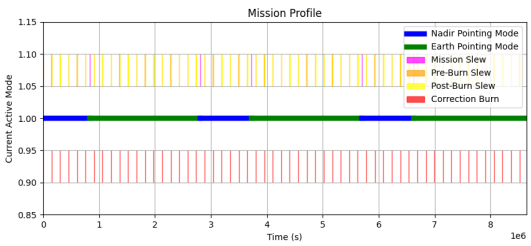

(d) Mission profile, verifying correct modelling of mission events across operational lifetime.

Figure 7.2: Verification plots, supporting in verification of simulation (input) data.

8

Propulsion

The main purpose of the propulsion subsystem is to get the orbiter to Enceladus, moreover it has to provide orbit changes and corrections. The main problem faced for designing the propulsion subsystem for ELMO is the enormous amount of ΔV it has to provide. Considering the $6.0\,\mathrm{km/s}$ required is roughly 3 times higher than similar orbiters, the propellant mass will be of high significance to the system. This causes the bi-propellant tanks (including the bi-propellant mass) to be very large and heavy, leading to challenges for the structure and ADCS subsystems to accommodate these masses and dimensions. The chapter is split up, starting with the requirements in Section 8.1. Followed by the subsystem overview in Section 8.2 and the method and calculations in Section 8.3. Lastly, Section 8.4 covers the verification and validation of the methods and outcomes and Section 8.5 shows a couple of recommendations.

8.1. Subsystem Requirements

To start the design of the propulsion subsystem, the user requirements, found in Table 3.2, which are of influence to this subsystem, have been listed in Table 8.1. This means the propulsion subsystem's combined design requirement is: 'The propulsion system shall provide $6.0\,\mathrm{km/s}$ of ΔV and shall be compatible with the Ariane 64 launch vehicle, considering the maximum payload mass and the shall fit in the payload bay'. As a propulsion subsystem is the main mass contributor (80.9% for ELMO) the propellant with the highest specific impulse, which is feasible, shall be used. As for the sizing, the bi-propellant tanks are also potentially constraining, thus their shape combined with the configuration shall ensure the spacecraft will fit.

Table 8.1: The user requirements the propulsion subsystem shall meet

ID	Description
USR-SYS-01	The spacecraft shall be compatible with the Ariane 64 launch vehicle. The launch vehicle is considered to put the spacecraft on an Earth escape trajectory. The maximum launch mass for the Ariane 64 is $9600\,\mathrm{kg}$.
USR-SYS-07	The orbiter shall be able to perform transfer flight correction manoeuvres of total size $1200\,\mathrm{m/s}$ (high-thrust option).
USR-SYS-08	The orbiter shall be able to provide for a delta-V equal or better than $4.6\,\mathrm{km/s}$ (high-thrust option) in order to achieve the desired orbit around Enceladus.
USR-SYS-09	The orbiter shall be able to perform orbit control when in mission orbit about Enceladus to the extent of $200\,\mathrm{m/s}$ or better.

8.2. Subsystem Overview

In this section an overview of the propulsion subsystem is presented. It will address the key parameters and outcomes related to the propulsion subsystem. Moreover, the made assumptions, the propellant and chosen pressurant, and their associated tanks are shown. Lastly, the whole subsystem including all components and their layout are displayed.

8.2.1. Key Parameters and Outcomes

In Table 8.2 the most important parameters and retrieved masses and ratios are presented to get a general overview of the propulsion subsystem.

Table 8.2: Important parameters and outcomes of the propulsion subsystem.

Item	Description	Value	Unit
ΔV	Delta V	6.0	km/s
I_{sp}	Specific impulse (vacuum)	321	s
$T_{Nominal}$	Nominal thrust level	425	N
a_{Max}	Maximum acceleration achievable	0.383	m/s^2
$\Delta V_{Orbiter}$	Delta V split to orbiter	3.4	km/s
$M_{Dry\ Propulsion\ Orbiter}$	Dry mass of the propulsion subsystem orbiter	248.6	kg
$M_{Dry\ Orbiter}$	Dry mass orbiter (incl. 20 % system margin)	1633	kg
$M_{Dry\ Propulsion\ Kick\ stage}$	Dry mass of the propulsion subsystem kick stage	534.3	kg
$M_{Dry\ Kick\ stage}$	Dry mass kick stage (incl. 20% system margin)	921.6	kg
$M_{Dry\ Combined}$	Dry mass combined (incl. 20% system margin)	2555	kg
$M_{Prop\ Orbiter}$	Propellant mass orbiter	3238	kg
$M_{Prop\ Kick\ stage}$	Propellant mass kick stage	7582	kg
$M_{Wet\ Orbiter}$	Wet mass Orbiter (or payload mass kick stage)	4871	kg
$M_{Wet\ Kick\ stage}$	Wet mass kick stage	8504	kg
$M_{Wet\ Combined}$	Wet mass combined (or Launch mass)	13375	kg
$(M_{Prop}\ /\ M_{Dry})_{Orbiter}$	Mass ratio propellant mass to dry mass orbiter	1.983	-
$(M_{Prop}\ /\ M_{Dry})_{Kick\ stage}$	Mass ratio propellant mass to dry mass kick stage	8.228	-
$(M_{Prop}\ /\ M_{Dry})_{Combined}$	Mass ratio propellant mass to combined dry mass	4.236	-
$(M_{Prop}\ /\ M_{Wet})_{Orbiter}$	Mass ratio propellant mass to wet mass orbiter	0.665	-
$(M_{Prop}\ /\ M_{Wet})_{Kick\ stage}$	Mass ratio propellant mass to wet mass kick stage	0.892	-
$(M_{Prop}\ /\ M_{Wet})_{Combined}$	Mass ratio propellant mass to launch mass	0.809	-

8.2.2. Main Assumptions

The main assumptions made, related to the propulsion subsystem and their impacts/mitigation strategies are outlined in this section.

Table 8.3: Assumptions made for the propulsion subsystem sizing.

Assumption	Rationale/Implications
The ideal gas law is used	Insignificant as the pressure is not substantially high and the temperture not very low
The helium expansion is isothermal	As the burns will not be substantial, the relative pressure change will be insignificantly small, thus following isothermal expansion. This enables the exact pressure the pressurant delivers to be calculable as the temperature does not change
The temperature of the propellant and pressurant is the average of the spacecraft's temperature range (7.5 °C subsection 11.1.1)	It is used in the ideal gas law to calculate the amount of moles pressurant needed which has insignicant inpact on the amount of helium mass

8.2.3. Bi-Propellant and Pressurant

From previous design choices made, the bi-propellant used is monomethylhydrazine (MMH) as fuel and the oxidiser is dinitrogentetraoxide (N_2O_4). The pressurant was also previously selected to be helium (He). In Table 8.4 the properties of the fuel and oxidiser are listed.

Table 8.4: Properties of the fuel and the oxidiser.

Fuel/Oxidiser	Density [kg/l]	Freeze Temperature [°C] (for P = 20.5 bar)	Boiling Temperature [°C] (for P = 20.5 bar)
MMH	0.866	-52.4 [12]	212.5 (Equation 8.1)
N_2O_4	1.448	-9.3 [12] [50]	100 [50]

$$Log(P_{\,Vapour}) = 9.182 - \frac{1065}{T_{Boil}} - \frac{158906}{T_{Boil}^2} \qquad P_{Vapour}\ [Pa]\ \ \&\ \ T_{Boil}\ [K] \tag{8.1}$$

Equation 8.1 [51] above is used to calculate the boiling temperature of MMH, which is reached when the vapour pressure is equal to the external pressure. In this case, the external pressure is the tank pressure, which is set at $20.5\,\mathrm{bar}$. The tank pressure will be further elaborated on in subsection 8.2.6. As stated in subsection 11.1.1, the temperature of the spacecraft ranges from $-5\,^{\circ}\mathrm{C}$ to $20\,^{\circ}\mathrm{C}$. From Table 8.4 it becomes clear the both the fuel and the oxidiser are outside of this range, which is obviously desired.In Table 8.5 the properties and used mass ratio of the bi-propellant are shown. The stochastic chemical reaction of the bi-propellant is showed in Equation 8.2.

$$4\ CH_3(NH)NH_2 + 5\ N_2O_4\ \rightarrow\ 12\ H_2O + 4\ CO_2 + 9\ N_2 \tag{8.2}$$

Table 8.5: Used O/F mass ratio and specific impulse specifications of the used bi-propellant.

Bi-Propellant	O/F Mass Ratio	O/F Volume Ratio	Theoretical Best Specific Impulse (vac) [s]	Used Engine's Specific Impulse (vac) [s]
$MMH + N_2O_4$	1.65	0.987	336	321

Lastly, in Table 8.6 the amount of helium molecules present in each pressurant system is shown in moles. Both the fuel and the oxidiser tank have their own helium tank, which it pressurises. At the start there is already a bit of helium present in the bi-propellant tanks, thus the amount of moles given in Table 8.6 are the sums of the moles of helium in the helium tank plus the moles of helium already present in the bi-propellant tank.

Table 8.6: Molar mass and the amount of moles of helium used for each propellant tank.

Pressurant	Molar Mass [g/mol]	Orbiter Fuel Tank [mol]	Orbiter Oxidiser Tank [mol]	Kick Stage Fuel Tank [mol]	Kick Stage Oxidiser Tank [mol]
Helium	4.003	1640	1620	3466	3425

8.2.4. Propulsion Subsystem Layout

In Figure 8.1 the whole propulsion subsystem is visualised, which is used for both the orbiter and the kick stage propulsion system. Figure 8.1 will be explained from right to left, following the mass

flow. Starting at the helium tanks, they encounter a split to the active path (bottom) and a backup path (top). After that there is a closed and open pyro valve for redundancy. These are designed to be used only once in case the active path has a failed valve, then the backup path needs to be used. In that case both pyro valves fire their explosives to permanently close, if previously open, or vice versa.

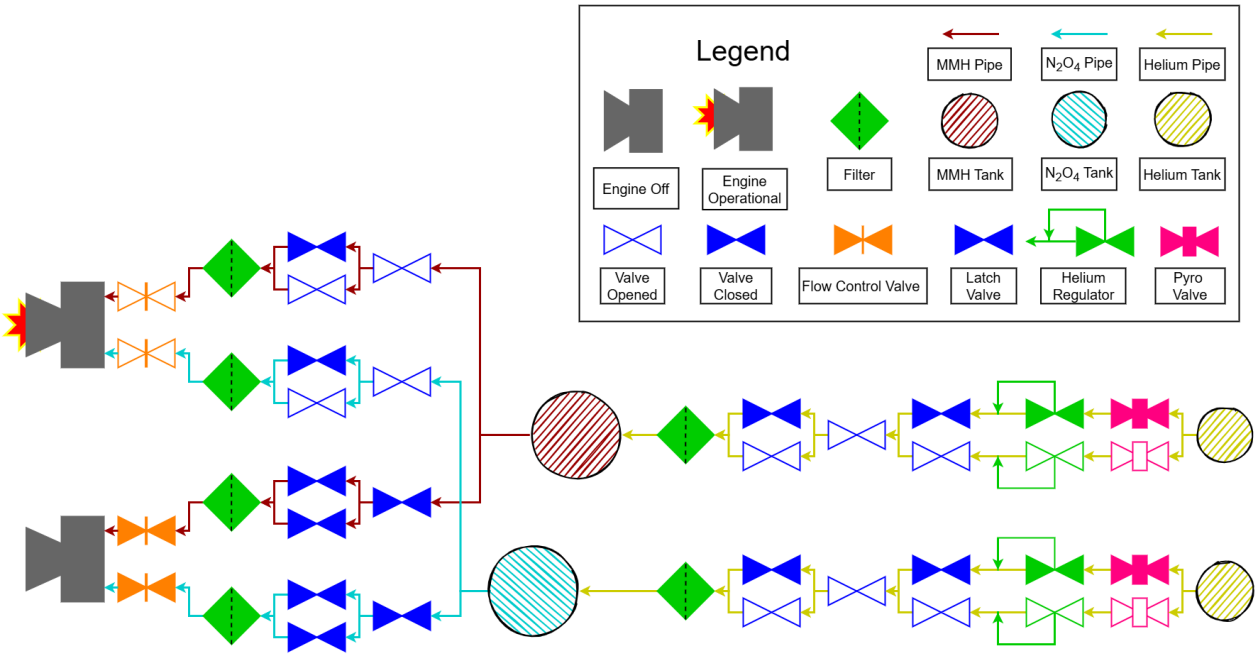

Figure 8.1: Propulsion system of the orbiter and the kick stage.

After passing the pyro valve, the helium encounters a helium regulator which regulates the amount of passing helium and reduces the pressure to $22\,\mathrm{bar}$. Next, the helium passes through a series of latch valves. These are designed to operate for 500 cycles or more. The first one (which is in series with the regulator and the pyro valve) is used as the active latch valve. In case it fails by either staying open or closed, both the pyro valves are activated and now the backup path (top) is used. Then, one of the latch valves in parallel is used for operations. If this one fails as well, their are two possibilities. Either it failed whilst being open, or it failed whilst being closed. If it fails in the open position, then the latch valve before the split takes over as the operative latch valve. If it failed in the closed position, then the latch valve in parallel takes over. This system ensures a highly redundant helium supply.

Moving on, the helium passes through a filter, which is suitable for both the helium and the bi-propellant to filter out any potential contaminations from the pipes, valves and helium tank. Then it enters the bi-propellant tank. The incoming helium assures the bi-propellant tanks to maintain their designed tank pressures. This accounts for a sufficient pressure level to flow through the second section of the piping system, finally entering the engine with the designed inlet pressure. The pipes split with the top path leading to the active engine and the bottom to the backup engine. For this reason all the latch valves leading to the backup engine are closed to ensure the least amount of propellant leakage to the backup engine while not in operation. Following the path to the active engine (top) the propellant flows through a latch valve and then encounters a split to two parallel latch valves. For operation one of the parallel latch valves is used. If this one fails and remains closed, the latch valve in parallel will take over. If it stays open, the latch valve before the split takes over, again for redundancy.

Lastly, the propellant passes through another filter, to filter out any contamination from the piping system after the bi-propellant tanks and from the bi-propellant tanks themselves. Then the propellants enter the engine via a flow control valve, which is already included in the chosen off the shelve engine. In the case one of these flow control valves fails or in the very low likelihood two of the latch valves fail, all the other valves close and operation is switched to the backup engine.

8.2.5. Mass Flow Down Propulsion Subsystem

In Table 8.7 the mass breakdown of the components used in Figure 8.1 are listed, which are used in the orbiter and also in the kick stage. In Table 8.9, a couple of key specifications of the used engine are listed, moreover a picture of the engine is shown in Figure 8.2.

Table 8.7: Component mass breakdown used in both of the propulsion subsystems.

Component	Mass [kg]	Amount	Applied Margin	Total mass [kg]	Mass %
Thruster (incl. Flow Control Valve)	4.3	2	10%	9.46	26.4
Piping	1.6	N/A	20%	1.91	5.4
Helium Regulator	1.8	4	5%	7.56	21.1
Filter	0.567	6	5%	3.57	10
Pyro Valve	0.16	4	5%	0.67	1.9
Latch Valve	0.545	22	5%	12.59	35.2
Total				**35.77**	**100**

Table 8.8: Table of the components with properties and specifications.

Component	Model/Company	Inlet Pressure Range/ MEOP [bar]	Pressure Drop [bar]	Power [W]
Thruster (incl. Flow Control Valve)	S400-15 apogee motor[1]	12.5 till 18.5	1.1	35
Helium Regulator	50X1463[2]	310	288	0
Filter	Mott[3]	-1 till 689	1.034	0
Pyro Valve	Ariane Group[4]	310	$\sim$0	$\sim$0 (TBR)
Latch Valve	Ariane Group[4]	-14 till 24.25	0.15	13.5

[1] https://www.space-propulsion.com/spacecraft-propulsion/apogee-motors/index.html
[2] https://www.moog.com/products/propulsion/space-propulsion/spacecraft-propulsion/propulsion-components/helium-regulator-pneumatic-pressure-regulator.html
[3] https://mottcorp.com/wp-content/uploads/2022/01/Mott-Propellant-Filters-Rev-0122.pdf
[4] https://www.space-propulsion.com/brochures/valves/space-propulsion-valves.pdf

Table 8.9: Table of the thruster with its properties and specifications.

Thruster	S400-15 apogee motor [a]	Unit
Specific Impulse Nominal	321	s
Thrust Range	340 - 440	N
Thrust Nominal	425	N
Mixture Ratio Nominal	1.65	-
Flow Rate Nominal	0.135	kg/s
Dimensions	0.32 x 0.67	m

[a] https://www.space-propulsion.com/spacecraft-propulsion/apogee-motors/index.html

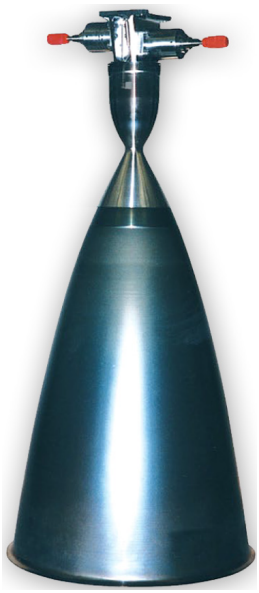

Figure 8.2: The S400-15 apogee motor.

8.2.6. Propellant Tanks

In this section the bi-propellant tanks for both the orbiter and the kick stage will be shown. To reduce the mass as much as possible, the tanks are shaped spherical, due to the lowest thickness necessary for spherical internal pressure vessels [52]. Moreover they are made form a titanium-aluminium alloy (Ti6Al4V) as this is the most widely used material for $MMH \ \& \ N_2O_4$ bi-propellant tanks [1]. This is due to the material being capable of handling reactive substances like hydrazines (MMH) as its resistant to hydrazines corrosive properties, has a very low permeability and has a high strength to mass ratio, which is highly desired in space application. To reduce the production and testing cost of the newly designed tanks it was decided to make them identical for the orbiter tanks and two identical for the kick stage. In Figure 4.2 the propellant tanks of the orbiter are shown as 'Fuel' and 'Oxidiser'.

Table 8.10: Specifications of the designed spherical bi=propellant tanks used in the orbiter and in the kick stage.

Propellant Tanks Used In:	Mass [kg]	Volume [l]	Diameter [m]
Orbiter	59.6	1600	1.46
Kick Stage	139.5	3747	1.93

8.2.7. Pressurant Tanks

Next the helium tanks for both the orbiter and the kick stage will be shown. To reduce the mass as much as possible, the tanks' shape are spherical, due to the lowest thickness necessary for spherical internal pressure vessels [52]. To reduce the mass further, the tanks are made from CFRP's, instead of Ti6Al4V. This is due to their higher allowable stress, $1200\,\mathrm{MPa}$[53] compared to $550\,\mathrm{MPa}$ [54], and lower density. This is feasible as helium is a non-reactive gas, in contrast to the used bi-propellant. However, CFRP's have a bad permeability, thus a Ti6Al4V liner inside was used to mitigate this [2]. Again to reduce the production and testing cost of the newly designed tanks it was decided to make them identical for the orbiter tanks and two identical for the kick stage. In Figure 4.2 the helium tanks of the orbiter are shown as 'Helium'. Lastly, the reason for having two helium tanks instead of one bigger one, is for configuration and ADCS benefits, by keeping the center of mass in the middle. In Table 8.11 the specifications are shown.

[1] https://www.space-propulsion.com/spacecraft-propulsion/bipropellant-tanks/
[2] https://connectivity.esa.int/projects/hehpv-helium-highpressure-vessel

Table 8.11: Specifications of the designed spherical helium tanks used in the orbiter and in the kick stage.

Helium Tanks Used In:	Mass [kg]	Volume [l]	Diameter [m]
Orbiter	23.47	116.4	0.62
Kick Stage	54.95	272.6	0.82

8.2.8. Summary Table

Lastly, in Table 8.12 the mass breakdown of the whole propulsion subsystem of both the orbiter and the kick stage are given. The category components do not get an applied margin as they are already applied in Table 8.7. Additionally, the 2% applied margin on the propellant and helium is from Sutton as it is the highest percentage residual propellant and helium [55].

Table 8.12: Mass breakdown and percentages for the Orbiter and Kick Stage.

Category	Applied Margin	Orbiter Mass [kg]	Orbiter Mass %	Kick Stage Mass [kg]	Kick Stage Mass %
Propellant Tanks	20%	142.9	4.025	334.7	4.049
Propellant	2%	3303	93.00	7734	93.58
Helium Tanks	20%	56.32	1.586	131.9	1.596
Helium	2%	13.59	0.383	28.73	0.348
Components	0%	35.77	1.007	35.77	0.433
Total	N/A	**3551**	**100**	**8265**	**100**

8.3. Method and Calculations

In this section the most important results are presented in Section 8.2.This section will elaborate on the methods used and calculations performed which lead to these results.

8.3.1. Bi-Propellant Tank Pressure

The tank pressure is retrieved from the set engine inlet pressure, while taking into account the pressure losses induced by the valves and filter the bi-propellant has to pass through. When looking at Figure 8.1, after the fuel/oxidiser tank, the bi-propellant passes through two latch valves, one filter and one flow control valve. Their combined pressure drop is $2.434\,\mathrm{bar}$, calculated using Table 8.8. This means the tank pressure has to be $2.556\,\mathrm{bar}$ higher (with a 5% margin added) than the inlet pressure of the engine. To come up with the engine inlet pressure, the inlet pressue range and other specifications of the engine are given in Table 8.8 and Table 8.9. As most of the specifications apply to the nominal values, like the specific impulse and mixture ratio, it was chosen to determine the nominal inlet pressure as this results in the most accurate specific impulse and mixture ratio values. The used method compared the thrust range to the inlet pressure range with the nominal thrust value. This is described in Equation 8.3. From this the engine inlet pressure is estimated to be $17.1\,\mathrm{bar}$. Summing these pressures lead to a tank pressure of $20.5\,\mathrm{bar}$, as there was also a 5% margin added to the engine inlet pressure to assure sufficient inlet pressure.

$$P_{Nominal} = P_{Low} + (P_{High} - P_{Low}) \cdot \frac{T_{Nominal} - T_{Low}}{T_{High} - T_{Low}} \tag{8.3}$$

8.3.2. Bi-Propellant and Helium Tank Thickness and Shape

For calculating the thickness of the bi-propellant tanks and the helium tanks Equation 8.4 was used. Here S is the allowable stress showed in subsection 8.2.7, with an added safety margin of 1.5. and

E is the joint efficiency, which was assumed to be the theoretical optimum of 1.0, as this is a space application, the manufacturer obviously will use the best welds possible. This resulted in a thickness of the orbiter bi-propellant tanks of $2.034\,\mathrm{mm}$ and helium tanks of $5.891\,\mathrm{mm}$. For the kick stage the bi-propellant tanks have a thickness of $2.701\,\mathrm{mm}$ and helium tanks of $7.823\,\mathrm{mm}$. If cylindrical tanks would have been used, the cylindrical part would be around two times as thick (see Equation 8.5), adding a lot of mass. For this reason spherical tanks were used. Lastly, the reason for not using off the shelf bi-propellant tanks, was to enable a perfect fit of the tanks in the orbiter. This saves as much unnecessary tank volume, hence mass, as possible. This was desired, as saving mass was the driving requirement during designing.To ensure they own designed tank masses are accurate, off the shelf tanks were put in the used model, which gave a correction factor for the bi-propellant tanks of 1.095 and another for the helium tanks of 2.12, this will be elaborated on in subsection 8.4.1.

$$t_{Sphere} = \frac{P_{Tank}\ R_{Internal}}{2SE - 0.2P_{Tank}} \tag{8.4}$$

$$t_{Cylinderical} = \frac{P_{Tank}\ R_{Internal}}{SE - 0.6P_{Tank}} \tag{8.5}$$

8.3.3. Amount of Helium Calculation

Using the ideal gas law and isothermal expansion from subsection 8.2.2, Equation 8.6 can be simplified. Since the pressure of the helium tank reduces during the mission, as helium flows out to keep the bi-propellant tank at the same pressure level, the start and end pressure of the helium tank differs. Moreover, the helium starts with occupying 11.8 percent of the fuel tank volume (not oxidiser as this needs another 1.32 percent of helium tank volume has to be added as volume wise their is slightly less oxidiser in the tank relative to the fuel tank) at the beginning. This is found following Brown's 3% [36] lowest required helium volume percentage at the start and ESA's helium in propellant tank's volume safety margin of 10% [11] on top of the minimum required, leading to a helium volume percentage at the start of $1.1/0.97 = 1.13 \quad \rightarrow \quad 1 - 1/1.13 = 11.8$ percent.

This means Equation 8.7 can be set up, with $P_{1\ Tank}$ meaning the pressure of the helium in the tank at the start, $V_{1\ Tank}$ the volume of the helium at the start in the tank and $V_{2\ He}$ meaning the end volume of the helium in the helium tank. Thus all parameter are corresponding to the pressure or the volume of the helium in either the propellant tank or in the helium tank. As stated before, the tank pressure is set at $20.5\,\mathrm{bar}$, moreover the pressure at the start of the helium tank is $310\,\mathrm{bar}$ and the end pressure is $27.5\,\mathrm{bar}$ (with a margin included, so actually slightly higher), as this is the lowest inlet pressure of the helium regulator (Table 8.8). Lastly, the end volume of the tank is the bi-propellant volume plus the starting helium volume in the tank. This can be simplified leading to Equation 8.8, which calculates the volume of the helium tank.

$$PV = nRT \rightarrow PV = Constant \tag{8.6}$$

$$P_{1\ Tank}\ V_{1\ Tank} + P_{1\ He}\ V_{1\ He} = P_{2\ Tank}\ V_{2\ Tank} + P_{2\ He}\ V_{2\ He} \tag{8.7}$$

$$Where \quad V_{1\ He} = V_{2\ He} \ \ and \ \ P_{1\ Tank} = P_{2\ Tank}$$

$$V_{He} = \frac{P_{Tank}\ (V_{2\ Tank} - V_{1\ Tank})}{P_{1\ He} - P_{2\ He}} \tag{8.8}$$

With the volume (and pressure) of the helium in the helium tank and the volume (and pressure) of the helium in the propellant tank known, the ideal gas law (Equation 8.6) can be used to calculate the amount of helium moles using Equation 8.9. Lastly, with the molar mass (Table 8.6) the total mass of the helium can be calculated.

$$n_{He} = \frac{P_{1\ He}\, V_{He}}{RT} + \frac{P_{Tank}\, V_{1\ He}}{RT} \tag{8.9}$$

8.4. Verification and Validation

To finalize the propulsion subsystem design, verification and validation on the models and key outputs was performed in order to make sure the the results are reliable and accurate.

8.4.1. Bi-Propellant and Helium Tank Mass Correction Factors

To make sure the model to do calculations on the own design bi-propellant and helium tanks are accurate, off the shelf tanks were put in the model to include any needed correction factors. For the bi-propellant tanks, tanks from the ariane group [3] were used, and for the helium tanks CSC [4] was used. This resulted in a correction factor of 1.043 for the bi-propellant tank and a factor of 2.017 was found. The last correction factor was expected to be so high, as in the model the Ti6Al4V liner was not included, however the off the shelf helium tank did have the liner. To be on the safe side another 5 % margin was added to the correction factors resulting in the a 1.095 correction factor for the bi-propellant tanks and a 2.118 correction factor for the helium tank. Furthermore, as they tanks are newly designed a 20 % component margin is afterwards also added. This results in the tanks certainly not being underestimated in their mass and volume.

8.4.2. Kick Stage Dry Mass

To verify whether the dry mass of the kick stage is resonable, the following relation from SMAD to estimate the dry mass of the kick stage given its bi-propellant mass is :

$M_{Dry\ Kick\ stage} = 17.5\%\ \ of\ \ M_{Prop\ Kick\ stage}$; % range is 10-25% [36].

From Table 8.2 it is found that the percentage $M_{Dry\ Kick\ stage}$ / $M_{Prop\ Kick\ stage}$ = 12.2%. This is in the 10-25% range and it makes sense it is close to the lower limit, because the kick stage is designed to be as light as possible, utilising spherical bi-propellant and helium tanks. Moreover, the structure around them and the two engine gimbals from mechanics are the only other subsystems present as the power and commanding is all done from the orbiter power and C&DH subsystems. For these reasons the kick stage dry mass to propellant mass ratio is verified to be correct as it is still in the 10-25% range.

8.4.3. Propulsion Subsystem Overview

For the propulsion subsystem overview in Figure 8.1, this was partly copied from the propulsion subsystem of Cassini [56]. This was used a verification to assure the amount of pressure drop caused by certain valves, especially after the bi-propellant tanks, were not underestimated. For this reason the piping system including the valves after the bi-propellant tanks is the same when it comes to the layout and amount of valves. The valves themselves are all off the shelve and thus gave their own accurate maximum pressure drop.

8.4.4. Mass Propulsion Subsystem Orbiter

From ADSEE I, the following formula to calculate the mass of the propulsion subsystem is Equation 8.10 [12]. Putting our propellant mass of the orbiter in this equation leads to a propulsion subsystem mass of $171\,\mathrm{kg}$. However, the orbiter's propulsion subsystem dry mass is $249\,\mathrm{kg}$. This difference of 31 % is explained by two reasons. Firstly, the formula used has a propellant mass range of [700 - 1800 kg] thus our propellant is 1.8 times as large as the maximum propellant mass of the range. This means the 6 % RSE is higher. Moreover, as stated in the chaper introduction, ELMO requires

[3] https://www.space-propulsion.com/spacecraft-propulsion/bipropellant-tanks/

[4] https://connectivity.esa.int/projects/hehpv-helium-highpressure-vessel

a very high ΔV of $6.0\,\mathrm{km/s}$, which is substantially higher than most other spacecraft, for example Cassini, which also was at Saturn had a ΔV of $2.352\,\mathrm{km/s}$. This means ELMO's bi-propellant tanks, helium tanks and helium mass is by definition way higher, leading to a significantly higher mass of the propulsion subsystem.

$$M_{Dry\ Propulsion\ Orbiter} = 0.0348 M_{Propellant} + 58.15 \quad ; \quad RSE = 6.0\% \tag{8.10}$$

8.5. Recommendations

Finally, in section multiple recommendations are given for future studies. Firstly, to make a more accurate estimation, the specific temperature of the helium and bi-propellant should be set, for in the calculation of the amount of He moles using the ideal gas law. For now it was assumed to be 7.5 deg as it is the average of the orbiter's temperature range. This would make the whole model more accurate.

Secondly, if long storable cryogenic bi-propellant tanks will ever become available, cryogenic bi-propellants, $LOX + RP - 1$ for example, causing a massive specific impulse increasing, leading to a significantly lower propellant mass. As this mission required the an enormous amount of ΔV this would be highly desired to make the spacecraft feasible to be launched from the Ariane 64, as this was one of the given launchers in the requirements. If these bi-propellant tanks could also be partly made of CFRP's, this will reduce the bi-propellant tank masses, resulting in an even lighter dry mass of the propulsion subsystem.

Lastly, a potential mass reduction could be achieved when using a pump-fed configuration, rather than a pressure-fed configuration. This will remove the helium and the helium tank masses, moreover the bi-propellant tanks are able to be set a much lower pressure, which will lower the required thickness of the tanks, thereby reducing their mass significantly. On the other hand, by adding the pumps themselves will add there mass and moreover, the power usage. It is not certain for now whether the usage of a pump-fed configuration is feasible as almost all spacecraft use a pressure-fed system. To conclude, this option could be investigated to potentially reduce the mass of the propulsion subsystem, however the following influences should be considered on the pumps: Power usage, reliability, redundancy, generated heat, compatibility with MMH as fuel and, any induced vibrations, in short it adds complexity and costs.

9
Structures

The structure forms the backbone of a spacecraft, and supports the many delicate subsystems within it. This subsystem withstands the harsh loads and vibrations experienced during launch and burns. Section 9.1 defines the requirements this subsystem must fulfil, Section 9.2 provides a general overview of the final design of the subsystem along with some estimated parameters, Section 9.3 outlines the methods used to estimate these final parameters of the design and Section 9.4 shows the verification and validation procedures used in this design.

9.1. Subsystem Requirements

Table 9.1 outlines the requirements generated that the structural subsystem is expected to satisfy. All of these requirements are derived from the launch vehicle, the Ariane 64 [57]. As shown in Section 9.2, this subsystem meets all these requirements.

Table 9.1: Requirements table for the structures subsystem.

Code	Requirement
ELM-US01-STR-01	The spacecraft shall withstand 1.8 g of lateral loads.
ELM-US01-STR-02	The spacecraft shall withstand 6 Hz of lateral vibration.
ELM-US01-STR-03	The spacecraft shall withstand -6 g to 2.5g of longitudinal loads.
ELM-US01-STR-04	The spacecraft shall withstand $20\,\mathrm{Hz}$ of longitudinal vibration.

9.2. Subsystem Overview

This subsystem functions to support all other subsystems and spacecraft elements during launch and other high-load phases. Table 9.2 outlines the main figures of the structural subsystem. As visible in the table, the upper and lower stages of the spacecraft differ greatly in their structures. It should be noted that a system mass margin of $20\,\%$ was added to this subsystem, as the entire system is not off the shelf or modified.

Table 9.2: Overview of final structure design

Characteristic	Upper stage	Lower stage
Total mass, with system margin (kg)	60.6	173.3
Load-bearing mass, no margin (kg)	38.5	109.9
Type	Truss	Shell
Material	T50/ERL1962	T50/ERL1962

The loads experienced by both stages of the structure are summarised in Table 9.3, while the stresses the structure experiences and its natural frequencies are outlined in Table 9.4. As visible in these tables, and the material properties shown in Table 9.5, it is clear that the structure meets the requirements.

Table 9.3: Loads applied on the structure of the spacecraft

Parameter	Value
Equivalent compressive load, upper stage	$-736\,000\,\mathrm{N}$
Equivalent compressive load, lower stage	$-3\,050\,000\,\mathrm{N}$
Equivalent tensile load, upper stage	$527\,000\,\mathrm{N}$
Equivalent tensile load, lower stage	$2\,480\,000\,\mathrm{N}$
Maximum bending moment, upper stage	$142\,000\,\mathrm{N\,m}$
Maximum bending moment, lower stage	$1\,010\,000\,\mathrm{N\,m}$

Table 9.4: Stresses and natural frequencies of the structure

Property	Value
Longitudinal natural frequency, upper stage	$36.2\,\mathrm{Hz}$
Longitudinal natural frequency, lower stage	$37.0\,\mathrm{Hz}$
Lateral natural frequency, upper stage	$23.1\,\mathrm{Hz}$
Lateral natural frequency, lower stage	$13.7\,\mathrm{Hz}$
Maximum compressive stress, upper stage	$-138\,\mathrm{MPa}$
Maximum compressive stress, lower stage	$-232\,\mathrm{MPa}$
Maximum tensile stress, upper stage	$99\,\mathrm{MPa}$
Maximum tensile stress, lower stage	$188\,\mathrm{MPa}$

9.3. Method and Calculations

The structural subsystem was designed in two main categories: shell and truss. Both options have been used in many spacecraft throughout time. subsection 9.3.1 determines the critical loads on the spacecraft, subsection 9.3.2 outlines the design of the shell structure, subsection 9.3.3 explains the design of the truss structure and subsection 9.3.4 expands on the material choices made.

Following Table 11-54 of SMAD, it was decided that as all structures will be tested before use, the safety factor of 1.1 on the yield stress and 1.25 on the ultimate stress will be used[58, p. 468]. As visible in subsection 9.3.4, Composite materials tend to have no reported yield stress or contain one that is close to the ultimate stress. For this reason, the limiting safety factor is 1.25 on the ultimate stress for the final selected material. Throughout the design of the shell structure, the thin wall assumption was used when calculating areas and mass moments of inertia. The difference in assumptions was later estimated to be in the order of $10^{-9}\%$.

Following the empirical data of the ATS 6, Magellan and Mars Observer spacecraft, it was estimated that the load-bearing structure is 63.5% of the structural mass. This statistic was applied to the truss and shell structures to obtain the total structural mass[59, p. 30].

Eventually, at the time of the design freeze, it was determined that the truss structure was lighter for the upper stage, while the shell was lighter for the kick stage. It was later discovered that a truss would indeed be lighter in both cases and in future design it is recommended to use a truss in both cases. Another factor to be considered is the statistical estimation used for the attachments of the subsystems, the inter-beam connections and the connection to the launch vehicle adapter. The LVA connector needs to be designed with an efficient load path to connect the $1.95\,\mathrm{m}$ diameter lower stage to the PLA6 1666 LVA with a diameter of $1.666\,\mathrm{m}$ and mass of $80\,\mathrm{kg}$ [57]. Designing these

sections in more detail provides the possibility to further reduce the mass of the structure, including the possible use of 3D printing to reduce labour costs and increase accuracy.

9.3.1. Critical Load Determination

To design a mass efficient system, the critical loading and vibrational cases must first be identified. The specified launch vehicle insinuates certain requirements that should be met by the spacecraft, as described in Section 9.1. The most constraining requirement is for compressive loads. Therefore, the main design aspect for this subsystem is the compressive loading case. As seen in Section 9.1, the launcher also requires the structure to withstand $1.8\,\mathrm{g}$. As bending loads contribute to the axial loads the spacecraft will experience, they are combined as follows [58]:

$$P_{eq} = P \pm \frac{2M}{R} \tag{9.1}$$

Where R is the radius of the spacecraft and M is the bending moment created by the lateral loads, which is obtained by multiplying the lateral load by half the length of the spacecraft.

9.3.2. Shell Structure

In the initial stages of the design, monocoque and semi-monocoque structures were compared. As the critical loading case is compression, this means that the semi-monocoque design performed significantly better. The axial natural frequency of a hollow tube is calculated using the following equation [58, p. 486]:

$$f_{ax} = 0.25\sqrt{\frac{AE}{mL}} \tag{9.2}$$

where A is the cross sectional area of the structure, and L is the length. Similarly, the lateral axial frequency can be calculated [58, p.487]:

$$f_{lat} = 0.56\sqrt{\frac{EI}{mL^3}} \tag{9.3}$$

where I is the mass moment of inertia of the cross-section. The elastic buckling stress for curved skin panels in compression is defined as follows[58, p. 478]:

$$\sigma_{cr} = \frac{k\pi^2 E}{12(1-\nu^2)}\left(\frac{t}{b}\right) \tag{9.4}$$

Where t is the skin panel thickness, b is the width of each panel (i.e. the distance between stringers), ν is Poisson's ratio and k is a geometric coefficient read off of graph 11-35[58, p. 479].

In the case of a shell structure, the possibility of integrating the sides of the fuel tanks into the load-bearing shell was considered. This option was eventually discarded, as the fuel tanks are most mass-optimized when they are made spherically, the decrease in structural mass was smaller than the increase in tank mass (when moving from spherical to cylindrical). The reason for this is that the cylindrical section of the propellant tanks are on average $4\,\mathrm{mm}$ thick (twice the thickness of the spherical sections in subsection 8.3.2) to withstand high internal pressures, while the structural shell is only $1\,\mathrm{mm}$ thick.

The final configuration of the lower stage of the spacecraft was estimated to have a length of $4.18\,\mathrm{m}$, and a diameter of $1.95\,\mathrm{m}$. These dimensions were then used for the final structure. The final shell structure, which was used in the kick stage of the spacecraft, was determined to be a $1\,\mathrm{mm}$ thick shell with 236 $1\,\mathrm{mm}$ thick, $3\,\mathrm{cm}$ long stringers.

9.3.3. Truss Structure

The truss structure contains a variable number of sides, with each side containing a rectangular skeleton and four diagonal beams running through a node in the rectangle's center. It was noticed

that for mass optimization, a square truss was considered the most mass efficient, and was therefore used. Additionally, a square truss simplifies the integration of the solar panels, as there would then be one panel per side. The loads are modelled to be introduced at the top nodes of the spacecraft, while the bottom is estimated to remain fixed. The distribution of the internal forces is then determined. Following this, the stresses within each beam can then be calculated. Figure 9.1 shows the layout of the beams within the truss structure.

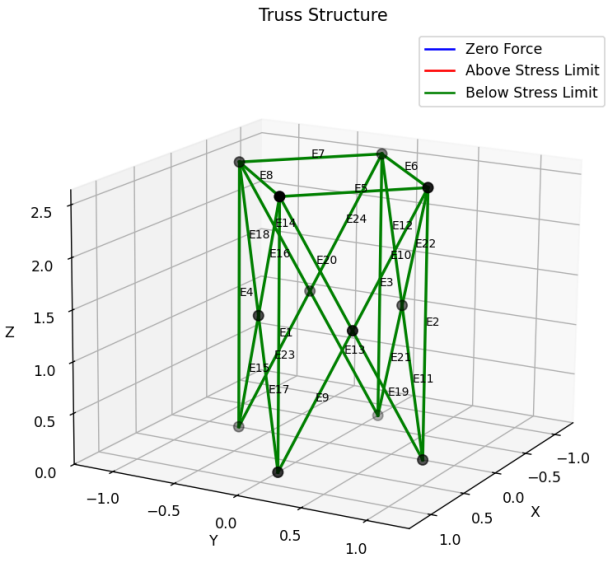

Figure 9.1: Visualisation of truss structure dimensions and elements, upper stage

As mentioned in subsection 9.3.1, the critical load to consider is compression. For simplicity and to avoid localised stress concentrations, the beams within the truss structure are modelled as hollow tubes, with a specified inner diameter and thickness. As these beams are small in nature, the thin wall assumption in Section 9.3 was not applied for the truss. To size for compressive buckling, the following equations apply[58, pp. 488-489]:

$$\varphi = \frac{1}{16}\sqrt{\frac{R}{t}} \tag{9.5}$$

$$\gamma = 1.0 - 0.901(1 - e^{-\varphi}) \tag{9.6}$$

$$\sigma_{cr} = 0.6\gamma\frac{Et}{R} \tag{9.7}$$

where E is the Young's modulus of the material used. In a similar fashion to subsection 9.3.2, the axial and lateral natural frequencies can be calculated using the same equations, though the total cross sectional area and moment of inertia are calculated differently.

The final configuration dimensions of the upper stage were a diameter of $1.51\,\mathrm{m}$ and a length of $2.64\,\mathrm{m}$. The final truss contains vertical beams of radius $4\,\mathrm{cm}$ and thickness $3\,\mathrm{mm}$, horizontal beams of radius $3\,\mathrm{cm}$ and thickness $1\,\mathrm{mm}$ and diagonal beams of radius $4\,\mathrm{mm}$ and thickness $2\,\mathrm{mm}$. Each horizontal beam has a length of $1.07\,\mathrm{m}$, each vertical beam has a length of $2.64\,\mathrm{m}$ and each diagonal beam has a length of $1.43\,\mathrm{m}$.

9.3.4. Material choice

In the initial phases of this design, AL7075 was considered, as it was the best-performing metal in terms of buckling resistance, manufacturability, minimum thickness tolerances and cost. However, as the design matured, it was evident that more mass needed to be saved in every subsystem,

including the structure. For this reason, the material T50/ERL1962 was selected. While this is not a new material, it is a tried and tested composite which was used in the MSX spacecraft [60]. Table 9.5 summarises the properties of this composite.

Table 9.5: Material properties of T50/ERL1962

Property	Value
Tensile strength	$346\,\mathrm{MPa}$[60]
Compression strength	$334\,\mathrm{MPa}$[60]
Tensile modulus	$92.8\,\mathrm{GPa}$[60]
Compression modulus	$88.3\,\mathrm{GPa}$[60]
Compression Poisson ratio	0.33[60]
Density	$1661\,\mathrm{kg/m^3}$[61]

9.4. Verification and Validation

All area and mass moment of inertia values have been verified using hand calculations. For validation of the truss structure, the MSX spacecraft was used [12, pp. 83-84]. The launch loads and total mass of the spacecraft were replaced with the MSX, and the total structural mass was estimated. This value was within 10% of the $54.4\,\mathrm{kg}$ structural mass of the MSX spacecraft. The shell structure design has been verified using the example present in SMAD, with a 1:1 convergence [58, pp. 487-494].

10
Mechanisms

At several locations on the spacecraft, mechanisms were deemed necessary. These mechanisms are described in this chapter. The chapter starts with the subsystem requirements in Section 10.1 and a subsystem overview in Section 10.2. Afterwards, each mechanism is explained in depth, starting with the Magnetometer boom in Section 10.3, Hopper deployment and kick stage separation mechanism in Section 10.4 and gimbals in Section 10.5. Finally, mechanisms not used in the spacecraft are briefly elaborated upon in Section 10.6.

10.1. Subsystem Requirements

The mechanisms mentioned are subject to the requirements in Table 10.1. These are similar to the structures requirement with two additional requirements added on top.

Table 10.1: Requirements table for Mechanisms

Code	Requirement
ELM-US01-STR-01	The spacecraft shall withstand 1.8 g of lateral loads.
ELM-US01-STR-02	The spacecraft shall withstand 6 Hz of lateral vibration.
ELM-US01-STR-03	The spacecraft shall withstand -6 g to 2.5g of longitudinal loads.
ELM-US01-STR-04	The spacecraft shall withstand 20 Hz of longitudinal vibration.
USR-PLD-04	The magnetometer sensors shall be mounted on a boom to be at least $6\,\mathrm{m}$ outboard from any other part of the spacecraft.
USR-PLD-07	The orbiter shall provide the pointing accuracy of at least 10 arcsec or better

10.2. Subsystem overview

The mechanisms subsystem consists of many different components distributed throughout the spacecraft. These components are the magnetometer boom, hopper deployment mechanism, kickstage release mechanism and thruster gimbals. Several other mechanisms were considered but were scrapped such as the antenna pointing mechanism, instrument pointing mechanism and solar array drive mechanism (SADM). The analysis and design of the mechanisms subsystem concluded in the masses shown in Table 10.2. Since these mechanisms are only activated once, it was assumed that their contribution to the power requirement is zero.

Table 10.2: Mass breakdown of mechanisms

Mechanism name	Mass without margin [kg]	margin	Mass with margin [kg]
Magnetometer boom	22.6	10%	24.86
Hopper deployment mechanism	2	20%	2.4
Thruster gimbals (orbiter)	20	10%	22
Thruster gimbals (kick stage)	20	10%	22
Kickstage separation mechanism	1	20%	1.2
Total	65.6	10%	72.46

10.3. Magnetometer Boom

ELMO will carry 2 magnetometers measuring Enceladus' and Saturn's magnetic field. To limit the interference of the spacecraft's magnetic field in the measurement, it is required that the Magnetometers are positioned at least $6\,\mathrm{m}$ from the body of the spacecraft (USR-PLD-04). The solution for this requirement is to add a magnetometer boom. The designed magnetometer will be $8\,\mathrm{m}$ long, this is longer than the required boom length to allow for a separation between magnetometers of $2\,\mathrm{m}$. This separation is required such that the two magnetometers do not interfere with each other. To fit the boom in the launch vehicle, it will be folded in 3 pieces, similar to JUICE's magnetometer boom. The stowed boom and extended boom are shown in Figure 10.3, the two magnetometers can be seen at the end of the boom.

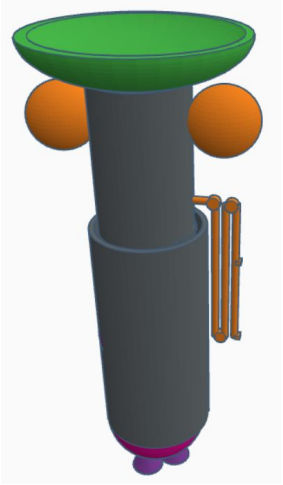

Figure 10.1: Retracted magnetometer boom

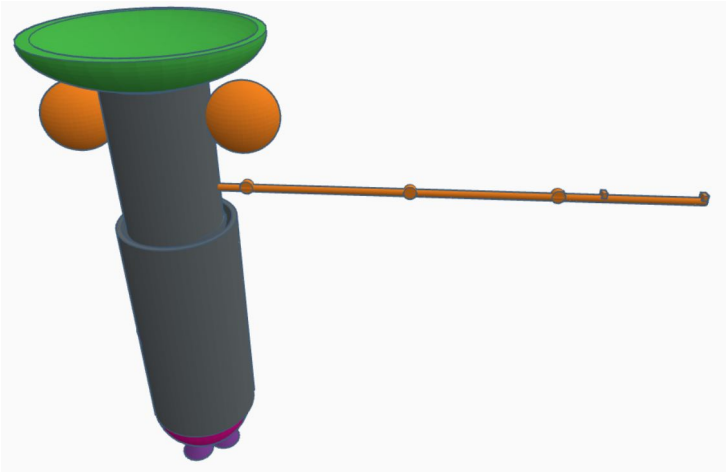

Figure 10.2: Extended magnetometer boom

Figure 10.3: Magnetometer boom in retracted and extended configurations

During a preliminary analysis, a boom mass was estimated using the thin-walled hollow circular cross-section and a solid light material such as aerospace-grade aluminium. However, due to the small loads on the magnetometer boom, the analysis concluded to use a wall thickness which was too small to be manufactured. This design choice would therefore be limited by manufacturing, setting the thickness of the magnetometer boom to $\approx 1\,\mathrm{mm}$. This leads to a design of roughly $\approx 8\,\mathrm{kg}$. Instead of using a high-strength, high-density material like a metal, the option was explored to use a low-strength, low-density material such as a honeycomb structure (approximating it like a homogenous pseudo-material). Using the new material and a solid circular cross-section, the radius of the boom was estimated for the following limiting cases:

- Stress at the base due to bending: $\sigma = \frac{MY}{I}$

- Euler column buckling of the retracted boom: $F_{cr} = \frac{\pi^2 EI}{L^2}$
- Axial compressive stress of the retracted boom : $\sigma = \frac{F}{A}$
- Axial and lateral frequency of the extended boom: $\omega_n = \sqrt{\frac{k}{m}}$

The structural analysis concluded that the limiting load is the lateral launch load of $1.8\,\mathrm{g}$, making the structure of the magnetometer boom merely $1.1\,\mathrm{kg}$ with a cross-sectional radius of $4\,\mathrm{cm}$ using the material from Tounsi [43]. However, during verification, this number was compared to JUICE's magnetometer boom mass, which was $30\,\mathrm{kg}$ for a $10.6\,\mathrm{m}$ boom [1]. Due to a large discrepancy between the calculated boom mass and Cassini's boom mass, it was decided to use a conservative number for the mass and scale Cassini's boom mass linearly with length to ELMO's boom mass. This method gives a boom mass of $22.6\,\mathrm{kg}$. Adding a 10% margin yields $24.86\,\mathrm{kg}$. Further research will need to be done to conclude whether the boom mass can be reduced to the $1.1\,\mathrm{kg}$ calculated using structural analysis.

10.4. Hopper Deployment and Kickstage Separation Mechanism

The Hoppers are constructed to have a core containing all the main components and instruments and an outside sphere-like grid protecting the internal components from impact damage. This raises a question of how to attach the hoppers to the main body of the spacecraft, as the spherical grid does not seem to be strong enough to use as an attachment, especially considering the 6 g of acceleration during launch. The proposed alternative is to use two beams connecting to the core of the hopper. This attachment method can be seen in Figure 10.4. The two beams can be modelled as 2-force members, meaning no bending stresses are present. Similarly to the Magnetometer boom, the hopper attachment beams are analysed for axial stress, Euler column buckling and frequency constraints. Compressive stress is the limiting load, requiring a cross-sectional radius of $5\,\mathrm{cm}$. However, due to the lightness of the honeycomb material, each beam is only half a kilogram. Considering ELMO uses 4 of these beams (2 per hopper), means that there are $2\,\mathrm{kg}$ of hopper deployment mechanism (+ 20% margin).

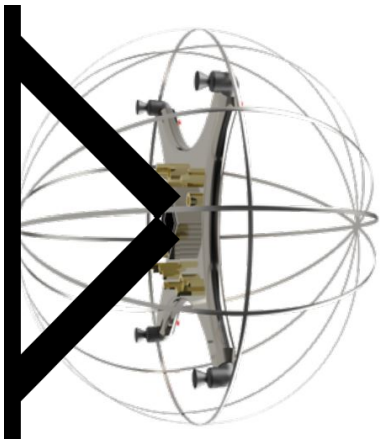

Figure 10.4: Hopper attached to the spacecraft main body

Both the kickstage and the hoppers will be separated using frangible bolts, as it is a well-established technology within the aerospace industry. The kick-stage will be separated using explosive bolts, but it was decided to not use explosives for cutting the bolts but use a mechanical actuator instead. This is to avoid damaging the instruments in the hopper with excessive vibrations from using a pyrotechnical separation method. The separation mechanism is assumed to have negligible mass and therefore estimated as $1\,\mathrm{kg}$. However, after research on separation mechanisms on other deep space mission, it was found that for a radius of $60\,\mathrm{cm}$, a separation mechanism has a mass of $3.7\,\mathrm{kg}$. Given that the radius of ELMO's separation mechanism is $1\,\mathrm{m}$, it would mean a separation mechanism mass of around $\approx 6kg$.

10.5. Gimbals

The requirement to have no single point of failure led to the design decision to have two engines on the orbiter and two engines on the kick stage. However, this means that the propulsion system will need to be able to function while one of the engines is inactive. To ensure that the thrust vector still aligns with the centre of mass of the spacecraft, a gimbal was deemed necessary. Using ADCS to offset the thrust misalignment was also considered, but this would make the ADCS much heavier. It

[1] https://www.group.sener/en/project/juices-deployable-magnetometer-boom-magboom/

was decided that adding a gimbal was the most mass and cost-effective decision. Cassini's gimbal mass was $10\,\mathrm{kg}$ per engine [62]. Using that figure in ELMO would mean a total gimbal mass of $40\,\mathrm{kg}$. With a 10% margin, this means $44\,\mathrm{kg}$ of gimbal mass.

10.6. Eliminated mechanisms

Three mechanisms were considered but scrapped: the antenna pointing mechanism (APM), instrument pointing mechanism and solar array drive mechanism (SADM). It was decided to split the mission into science phases and transmission phases. This allows the antenna to be fixed since ADCS can be used to point the antenna to Earth during the transmission phase. The chosen polar dawn-dusk orbit causes an angle of incidence of 26.7° at all times. The instrument-pointing mechanism was a possible solution to this problem, as it renders it possible to point the solar array and instruments independently. However, this option was discarded because it was difficult to ensure that the mechanism was accurate enough to satisfy the pointing knowledge requirement. Lastly, a SADM was considered, but the 4-wing design choice for the solar arrays renders would make it too complicated to use the SADM. Changing the 4-wing design to a 2-wing design would increase the solar array's length, causing other complications.

11
Thermal and Radiation

The purpose of the spacecraft's thermal and radiation control design is to ensure its components can withstand the thermal and radiation environment encountered, ensuring reliable performance of the spacecraft. This chapter shows how the design of the thermal and radiation control subsystem was performed. Section 11.1 presents how the thermal control was designed and Section 11.2 how the radiation control was designed.

11.1. Thermal Design

The following section first contains a description of the design drivers of the thermal control in subsection 11.1.1, then how the thermal model was created is presented in subsection 11.1.2 and finally it explains the baseline design in Table 11.1.2.

11.1.1. Subsystem Requirements

The spacecraft design was made using a thermal simulation utilizing two nodes, where the allowable temperature range for each node served as the design driver. This range dictated the flexibility the author had in adjusting the equilibrium temperature determined in the performed heat balance. Please refer to subsection 11.1.2 for a more in-depth explanation on the thermal control design method. The second node (solar arrays) was furthermore also constrained by the inability to apply multi-layer insulation (MLI) or coating on the solar cells, as this would interfere with the performance of the cells. Please see Table 11.1 for a more extensive description of all the design driving requirements in the thermal control design process.

Table 11.1: Thermal control system requirements

ID	Title	Description
ELM-TRC-BAT-01	Allowable temperature range batteries	Most limiting allowable temperature range is from the EPS batteries [-5,20](°C)[44].
ELM-TRC-ARR-01	Allowable temperature range solar array	Limiting allowable temperature range of the solar array is [-165,28](°C)[63].
ELM-TRC-ARR-02	Allowable coating location solar array	No coating or MLI allowed on the solar cells (side) of the array.

Subsystem Assumptions: In order to create a model that will efficiently and accurately represent the thermal control system, several assumption were made. Please see Table 11.2 for the assumptions and their justifications.

Table 11.2: Thermal control system assumptions

Assumption	Justification
The Louver can be configured to have no net radiated heat in deep space.	Louver can drastically reduce its heat radiation, making its influence negligible.
No heat conduction between nodes.	Steady state analysis is performed, a thermal equilibrium is reached for each node.
No influence of RHU's(Radioisotope heating units) on heat balance during Venus flyby.	RHU heat added is less than 10% of total heat input of heat balance.
Uniform heat distribution throughout the nodes.	Steady state conditions used for analysis of nodes.
All thermal radiation at the Venus flyby lands on the satellite dish.	Helps simplify calculations, causes overdesign.
Power consumed by temperature sensors is zero.	0.026 W consumed over all sensors combined, negligible amount.
No battery dissipation in deep space.	Battery waste heat added to heat balance is less than 4% of total heat input.
Spacecraft side is sunlit in deep space conditions.	Possible configuration of spacecraft.
Area of side of cylinder can be calculated with $A = 2 \cdot r \cdot h$.	Allows for model simplification, leads to overdesign.
The value of parameter Ka is equal to 1.	Leads to overdesign.

11.1.2. Subsystem Overview

The thermal control system was designed by creating a thermal model that consisted of heat balances of two nodes. The purpose of these heat balances was to determine the required subtraction or addition of heat to the system in order to remain at a allowable temperature equation. By determining the heat change needed, the spacecraft T&RC components could be sized. The first node represented the spacecraft bus with all its subsystems and payloads, the second node represented the solar arrays. For both nodes two thermal environments were investigated; the coldest and the hottest environment encountered for an extended period of time. After some investigation these two turned out to be the Venus flyby conditions and deep space conditions(far away from any planet/-moon), at the furthest point from the sun. It should be noted that the 2nd node wasn't examined for Venus flyby conditions as the solar arrays will be undeployed and thus cannot receive relevant amounts of heat from the sun that would influence the design. For the Venus flyby section, the spacecraft's antenna dish will be the only area directly exposed to solar illumination. The spacecraft will adopt a slight tilt in its attitude relative to the incoming solar radiation to ensure that the radiation is not focused onto the antenna itself, which could otherwise compromise its functionality and structural integrity. The antenna dish was selected primarily for its mass efficiency, as it eliminates the need to allocate significant additional mass for a dedicated heat shield. Please see subsection 11.3.2 for a more extensive reasoning of the methods validity. Solar-, albedo- and planetary radiation inputs is calculated with respectively Equation 11.1[36], Equation 11.2[36], Equation 11.3[36] thermal energy radiated out is calculated with Equation 11.4[36], also known as the Stefan-Boltzman Law.

$$q_{solar} = G \cdot \alpha \cdot A \tag{11.1}$$

$$q_{albedo} = q_{solar} \cdot a \cdot K_a \cdot \sin^2(\rho) \tag{11.2}$$

$$q_{planetary} = Q_{I_V} \cdot \varepsilon \cdot A \cdot \sin^2(\rho) \tag{11.3}$$

$$q_{radiated} = \sigma \cdot \varepsilon \cdot A \cdot T^4 \tag{11.4}$$

The final results of the heat balance calculations can be found in Table 11.3 and in Table 11.1.2 it will be shown how these results were used for the sizing of the thermal control subsystem.

Table 11.3: Heat balance outputs

Heat source	Value (W)	Additional Information
q_{in_V}	7507	Heat inputs are: direct solar radiation, albedo radiation, planetary infrared radiation
q_{out_V}	440	Radiation temperature assumed to be maximum allowable operating temperature spacecraft
Δ_{q_V}	7067	This amount of heat to be radiated away by louvers
$q_{in_{DS}}$	21	Input is solar thermal radiation, waste heat from the EPS battery
$q_{out_{DS}}$	373	Radiation temperature assumed to be minimum allowable operating temperature spacecraft
$\Delta_{q_{DS}}$	-353	This amount of heat needs to be added to the system via heaters

Table 11.4: Heat balance inputs

Sign	Value	Unit	Notes
T_{min}	268.15 [36]	K	Minimum allowable temperature, Constraint caused by EPS batteries.
T_{max}	293.15 [36]	K	Maximum allowable temperature, Constraint caused by EPS batteries.
ε_{MLI}	0.05[64]	-	(Emissivity) MLI selected for deep space conditions to retain as much heat as possible.
α_{MLI}	0.15[64]	-	(Absorptivity) MLI selected for deep space conditions to retain as much heat as possible.
ε_{GC}	0.02 [65]	-	(Gold) Coating chosen for deep space with acceptable absorptivity for Venus flyby.
α_{GC}	0.19 [65]	-	(Gold) Coating chosen for deep space with acceptable absorptivity for Venus flyby.
d_{DS}	9.5 [66]	AU	Average distance sun to Enceladus.
d_{FB}	0.72 [67]	AU	Average distance sun to Venus.
A_{FB}	9.62	m^2	Sunlit Area Spacecraft in Venus Flyby conditions.
A_{DS}	12.65	m^2	Sunlit Area Spacecraft in Deep Space Conditions.
A	42.9	m^2	Complete area spacecraft bus (radiated area).
G_{FB}	2701 [67]	$\frac{W}{m^2}$	$G = \frac{G_s}{d^2}$, $G_s = 14 \times 10^2$ W/m^2, adjusted solar flux.

Continued on next page

Sign	Value	Unit	Notes
G_{DS}	15.51 [66]	$\frac{W}{m^2}$	$G = \frac{G_s}{d^2}$, $G_s = 14 \times 10^2$ W/m^2, adjusted solar flux.
Q_{I_V}	127.07 [67]	$\frac{W}{m^2}$	Planetary infrared radiation.
ρ	0.96 [67]	Rad	$\sin(\rho) = \frac{R_V}{R_V+H}$, angular radius of Venus.
σ	5.67×10^{-8} [68]	$\frac{W}{m^2 \cdot T^4}$	Stefan-Boltzmann constant.
q_b	20 [44]	W	Waste heat battery.
a_V	0.77 [67]	-	Albedo factor; proportion of sunlight a planet's surface reflects.
K_a	1 [36]	-	No parametric equation exists for Venus; Earth's equation result approaches 1.
m_{RHU}	0.04 [69]	$\frac{kg}{-}$	Mass per RHU.
ρ_{MLI}	0.511 [70]	$\frac{kg}{m^2}$	MLI mass per square meter.
ρ_{GC}	0.0012 [71]	$\frac{kg}{m^2}$	Gold coating mass per square meter.
ρ_L	8.00 [72]	$\frac{kg}{m^2}$	Louver mass per square meter.
ρ_{alu}	2710 [73]	$\frac{kg}{m^3}$	Density of aluminum.

Baseline Design: Each subsystem component in the spacecraft will be equipped with two temperature sensors to monitor component temperatures. One of the two sensors will serve as redundancy to ensure reliability. In the event both sensors fail, temperature data from nearby components can be analyzed to detect changes in conduction caused by temperature variations in the component of interest.

During the design iterations, it was determined that a functional design could be achieved by using MLI to cover the entire spacecraft bus, with the sole exception being the satellite dish, which is coated with a cold coating. To radiate additional heat during the Venus flyby a Louver was sized and added which will radiate heat in high temperature conditions while having net zero heat exchange in any other conditions (reducing the amount of heat needed to be produced in deep space). The Louver was sized using Equation 11.5, with the Louver being placed in the eclipsed part of the spacecraft (during the Venus flyby) to maximize the efficiency of the Louver.

$$A_L = \frac{Q_{diss}}{\sigma \cdot \varepsilon \cdot T^4} \tag{11.5}$$

The spacecraft bus equipped with low emissivity MLI to minimize the heat radiated away, this is to make sure that in deep space as much heat as possible is retained in the spacecraft. Though this helps a lot there is still a significant shortage of heat in deep space, as can be seen in Table 11.3. In order to solve this problem it was decided that the radioisotope thermo-electric heater's (RHU) will be used to solve the shortage of heat in deep space conditions. The RTHs will add extra heat to the spacecraft bus which will cause the equilibrium temperature in deep space to be within the allowable temperature range. The final summary of all components used to achieve an effective thermal control system is shown in Table 11.5.

Table 11.5: Thermal control equipment list

Component	Mass (kg)	Notes
Temperature sensor	≈ 0	52 units
MLI	22	22 layers (2 layers kapton with 20 layers aluminized Mylar in between)[12], $A_{MLI} = 42\ m^2$
Louver	18	6.5 kW radiated by Louver, $A_L = 2.25\,\mathrm{m}^2$
RHU	40	819 W Thermal produced (0 W Electric needed), 1000 units
Gold coating	0.1	Applied to satellite dish and the back of the solar arrays, $A_{GC} = 106\ m^2$.

11.2. Radiation Design

In this section subsection 11.2.1 will first be explain what the most important requirements for the design were. Then the assumptions made will be explained in Table 11.7, the design method is presented in subsection 11.2.2 together with the results.

11.2.1. Subsystem Requirements

The radiation design was mainly driven by one requirement that was given at the start of the project.[2] This requirement can be divided up into a requirement for payload components, and a requirement for non-payload components, please see Table 11.6 for a more extensive description of the requirements.

Table 11.6: Radiation control system requirements

ID	Title	Description
ELM-TRC-PAY-01	Allowable payload radiation dose	Over its lifecycle, the spacecraft payload components shall be able to withstand a radiation dose of at least 10 krad[2].
ELM-TRC-PAY-02	Allowable non-payload radiation dose	Over its lifecycle, spacecraft non-payload components shall be able to withstand a radiation dose of at least 50 krad[2].

Subsystem Assumptions: While in terms of hardware the radiation control system is much less extensive and/or complex, it still requires assumptions in order to effectively use the tools used to perform the design. Please see Table 11.7 for the assumptions made and their justifications.

11.2.2. Subsystem Overview

The spacecraft subsystem and payload components have different allowable radiation doses. By using radiation vaults around the components the magnitude of radiation dose received is managed. The required thickness of the radiation vaults is determined by using a plot that is produced with the SPENVIS software. The HRC sensor misses one side of shielding due to the fact that the camera needs to be able to take pictures, which is not possible with a shield blocking it.

SPENVIS

The SPace ENVironment Information System (SPENVIS) is a web-based modelling tool developed by the European Space Agency that allows the user to analyse the radiation environment around a spacecraft and the its effects on the spacecraft systems. During several meetings with space

Table 11.7: Radiation design assumptions

Assumption	Justification
Orbiter transfer flight duration is 8 years.	Most extreme case, leads to overdesign.
The average distance of the spacecraft to the sun during its entire mission is 5.225 AU.	Expert opinion argues that this is allowed[74] [75] – only needed for proper radiation model in SPENVIS.
The spacecraft's radiation exposure equals the dose it would receive if it stayed at its average distance from the Sun throughout its lifetime.	Expert opinion argues that this is allowed – only needed for proper radiation model in SPENVIS.
The HRC sensor will be adequately shielded, with one side exposed, while maintaining the same protection level as other payload components that have no sides exposed.	Prolonged lack of solar exposure due to the HRC sensor's placement during design likely reduces radiation sufficiently to support this assumption, consultation with expert reveals option of radiation shielding in camera shutter[74].
IPR sensor does not need radiation shielding.	Functionality of sensor will be lost if it gets an extra layer of shielding around it.

radiation (modelling) experts[74][75] the following method using SPENVIS was devised.

Step 1, define orbital trajectory: The first step in modelling the radiation environment for the ELMO spacecraft is generating usable trajectory data. After deliberation with the before mentioned experts it was determined that using a singular trajectory segment is the most effective method to achieve a reliable model of the radiation environment encountered during the mission. The orbit was modelled as a near earth interplanetary orbit at a distance of 5.225 AU[66], representing the average distance of the spacecraft to the sun during its lifetime. By modelling this trajectory with a launch date of January 1, 2035 [2], useful data was generated for subsequent use in the radiation environment modelling process.

Step 2, define radiation sources: Based on expert opinions the following radiation sources were used together to create a reliable radiation environment:

- Trapped proton and electron fluxes
- Solar particle mission fluences
- Solar particle peak fluxes
- Galactic cosmic ray fluxes

Once all these sources were defined and the right models were applied to each source, the radiation environment was properly defined and ready for use. The final step was to analyse the radiation dose caused by this radiation environment at different shielding thicknesses.

Step 3: Determine ionizing dose as a function of thickness: The long-term radiation dose was calculated using the 'Ionizing Dose for Simple Geometries' tool in SPENVIS. This tool allows the user to plot shielding thickness against the radiation dose

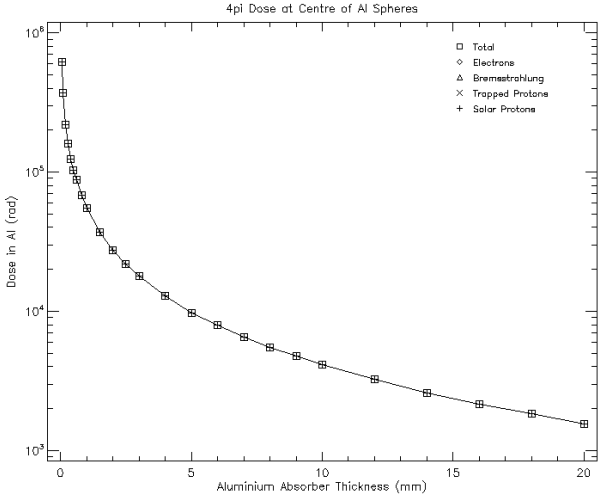

Figure 11.1: SPENVIS plot of radiation dose received for given amount of shielding.

received from the previously defined
sources along the earlier generated orbital trajectory.

Sizing radiation vaults: In the electronics bay three separate aluminium 6061 radiation vaults were created based on the allowed radiation dose and positional constraints of the components. Furthermore each payload sensor has its own radiation vault as they are not near any other components. Finally it should be noted that each radiation vault has one side without aluminium plating, this is the side that connects the vault to the spacecraft, thus no radiation shielding is needed here. For the HRC sensor the side where the camera expands additionally also doesn't have shielding. This leads to the following design:

Vault	Contents	Dimensions (m)	Thickness (m)	Mass (kg)
Main payload vault	HRC-, IPR-, TAM electronics, TAA, LA	0.41x0.272x0.55	0.005	10.21
Subsystem vault	EPS & ADCS	0.395x0.18x0.30	0.001	1.00
Redundancy ADCS vault	ADCS redundancy unit	0.17x0.17x0.07	0.001	0.30
HRC sensor vault	HRC sensor	0.515x0.30x0.26	0.005	22.09
TAM sensor vault	TAM sensor	0.11x0.07x0.05	0.005	4.74

Table 11.8: Table with data on dimensions, thicknesses, and masses of the aluminium 6061 spacecraft radiation vaults.

11.3. Verification and Validation

To finalize the design verification and validation on the T&RC design method was performed in order to make sure the the results are reliable and accurate. subsection 11.3.1 presents the verification and subsection 11.3.2 the validation.

11.3.1. Verification

Several methods of verification were performed: A unit check on all equations to make sure that their units are consistent with regards to each other. Furthermore a logic check was performed where the results reviewed to see if they logically make sense (no negative mass or area, excess of heat at Venus, lack of heat in deeps space, area of Louver w.r.t. spacecraft bus area reasonable). Finally to round off the calculations of the model were double-checked by doing hand calculations, during this process 2 mistakes were found. Firstly, the input area for the area that radiated heat in deep space was an old value of $54.05\,\mathrm{m}^2$ whereas the correct value to be used is $42.9\,\mathrm{m}^2$ this mistake was caused by the thermal control model not using the area of a new iteration. Due to this mistake the RTHs are 9 kg heavier in the final design than it could be without mistakes. The second mistake is a multiplication syntax error in the radiation model, causing 2 vaults for the payload sensors to be overdesigned, causing the radiation design to be 21 kg heavier in the final design than it could be without mistakes. Because the mistakes were found after the model freeze, the model could not be changed anymore and instead the error was calculated for future continued iterations of the model/design'. It should be noted that the amount of RTHs (1000 with error, 776 without) feels quite high, future iterations of the design process should put it in high priority to find a more effective design to deal with the extreme changes in thermal conditions; preventing such excessive RHU requirements.

11.3.2. Validation

Validation was performed by examining missions with similar properties (in terms of trajectory, lifetime and T&RC design) to ELMO and comparing values for the designs.

MLI: The first thermal control system component examined in the design of the ELMO spacecraft was the sizing of the Multi-Layer Insulation (MLI). The ELMO spacecraft design incorporates $42\,\mathrm{m}^2$ of MLI with a total mass of $22\,\mathrm{kg}$. In comparison, research shows that the JUICE mission to Jupiter uses

$100\,\mathrm{kg}$ of MLI to cover $45\,\mathrm{m}^2$.[76] A possible explanation for this disparity in mass is that the ELMO spacecraft's MLI configuration may not be adequately sized in terms of layers. Further research is recommended to determine the appropriate number of MLI layers needed for an optimal design, as it currently seems like not enough layers are used (based on the mass disparity). The MLI size in terms of area can be reasonably validated, as the surface areas of ELMO and JUICE are very similar, suggesting that an adequate surface was covered with MLI.

Louver: For the Louver, the JUNO spacecraft design was examined to compare the Louver designs of JUNO and ELMO. The analysis revealed that JUNO uses four[1] Louvers.[77] Although no exact data was available, information derived from the manufacturer's datasheets suggests that the four Louvers have a combined surface area of approximately $0.64\,\mathrm{m}^2$ and a mass of $4.8\,\mathrm{kg}$. When compared to ELMO's Louvers, it was found that ELMO's Louver has about four times the area and mass of JUNO's Louver. This comparison confirms that the appropriate mass-to-area ratio was applied and validates that the design is within the correct order of magnitude, ruling out significant errors. A likely reason for the smaller Louver area in JUNO is the decreased MLI used in the design, this will be discussed in more deph in the next paragraph.

Heater: From investigating old missions it was found that Cassini used 117 RTHs[2] over all its systems, which approximately is a tenth (or a sixth if the error is fixed) of the design of ELMO in terms of the amount of RTHs used. Though no conclusive conclusion can be made it is reasoned that due to the decreased amount of MLI used in ELMO in terms of mass, the size of the Louver and heaters needs to increase in order to make up for the more extreme thermal cycles encountered(more internal heat needs to be dissipated and more internal heat needs to be generated at the two extremes - Venus flyby and deep space) in the spacecraft trajectory.

Heat shield configuration: By examining old missions it was found that ELMO would not be the first mission to use the antenna as a heat shield. Among other missions two notable missions are JUNO[78] and BepiColombo[79], which both used heat shields near the sun, JUNO even used its HGA as a heat shield, just like ELMO. This demonstrates that the method of heat shielding using an antenna is feasible, providing evidence to support its validity.

[1] https://www.sncorp.com/news-archive/sierra-nevada-corporation-helps-juno-keep-cool-and-science-on/
[2] https://www.energy.gov/ne/timeline-rtg-and-rhu-space-missions

12
Command and Data Handling

The Command and Data Handling subsystem (C&DH) acts as the brain of the spacecraft, coordinating all onboard activities and ensuring the proper execution of all spacecraft functions. As this report is a study into the feasibility of the ELMO spacecraft, this chapter focuses on high-level system design and key mission considerations, while omitting in-depth analysis of aspects such as software architecture and lower-level implementation details.

12.1. Subsystem Requirements

The C&DH subsystem is driven by the requirements found in Table 12.1.

Table 12.1: Requirements driving C&DH design

Requirement ID	Description
ELM-US02-RRS-02a	Single-point failures shall be avoided in the spacecraft design.
USR-SYS-05	The spacecraft shall be able to withstand a radiation dose of at least 50 krad over its lifetime.

12.2. Subsystem Overview

Besides acting as the brain of the spacecraft, it is critical that the C&DH subsystem is capable of storing and transporting the high amounts of data produced by the onboard instruments. The data buses shall make use of MIL-STD-1553, a standard originally produced by the US military, but later adopted by NASA and ESA due to its robust and fault tolerant design [80]. The standard has been used on numerous space missions such as BepiColombo, Galileo, and the International Space Station [81]. In order to ensure robustness, MIL-STD-1553 has a fixed data rate of $1\,\mathrm{Mbps}$. However, both the HRC and IPR produce higher data rates. For this reason, several high speed data links directly connect the storage elements with those payload instruments. Similarly, the storage element also has a high speed data link connection to the HGA transmitter, in order to reduce processing load on the computer during transmission to Earth ground systems [82]. The high speed data link shall be done using the SpaceWire, developed by ESA, and capable of handling up to $200\,\mathrm{Mbps}$ [83]. SpaceWire has been used on many missions, notably BepiColombo, SWIFT, and the James Webb Telescope [84].

During critical operations such as orbital insertion or transfer manoeuvres, the C&DH subsystem must be fail-operational, meaning that operations may be continued in the event of a computer failure, also known as hot redundancy [85]. Therefore, the On Board Computer (OBC), as well as the RAM and storage, will be doubly redundant systems, including redundant standard and high speed data links, in order to ensure no common failure points. The redundant OBC shall actively shadow the nominal OBC, preserving continuous synchronization to enable rapid takeover in the event of an anomaly. This is standard practice for science missions [82].

The block handling diagram in figure 12.1 highlights how data is handled within the spacecraft.

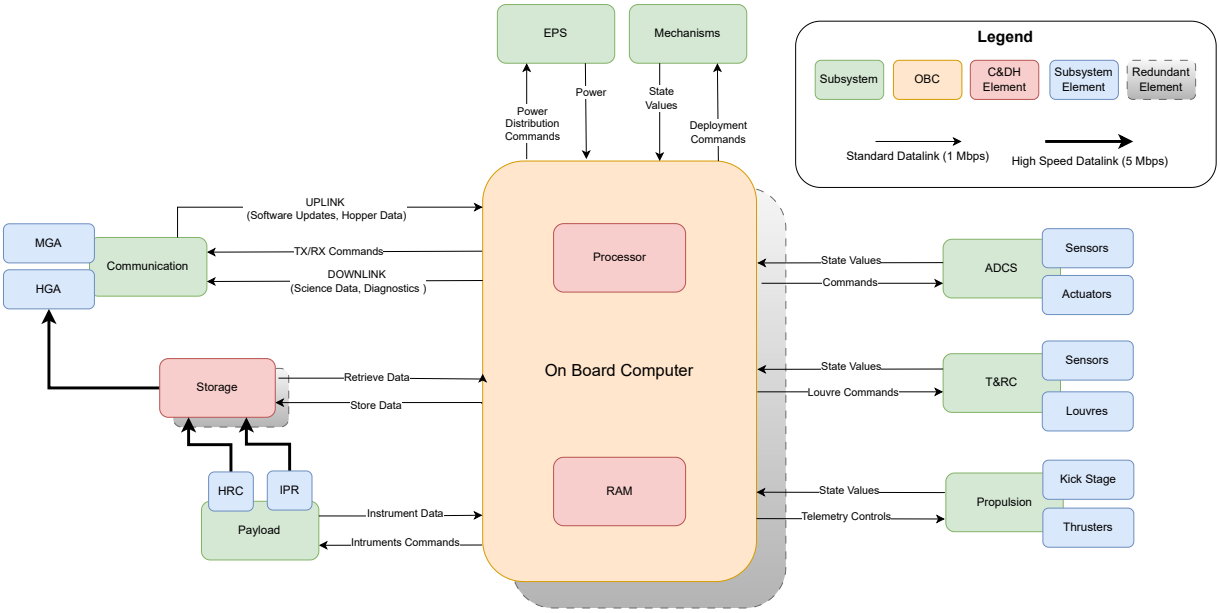

Figure 12.1: Data handling block diagram. Elements not included are beyond the scope of this study.

In subsection 3.3.2, it is stated that each science portion of a batch produces a total of $700.35\,\mathrm{Gbit}$, or equivalently $87.54\,\mathrm{GB}$. This serves as the basis for the data storage required by the subsystem. On top of this data, there should also be storage allocated for software data, diagnostic reports, and other miscellaneous data. These would take up significantly less space than the scientific data itself. Upon successful transmission of all raw scientific data to Earth, the data can be deleted from onboard storage as it is no longer required.

12.3. Hardware

For this study, the C&DH Subsystem Architecture will be simplified into 3 main elements: On Board Computer (OBC), RAM, and storage. An OBC was chosen rather than a lone central processing unit (CPU) in order to provide a more comprehensive estimation for the power required by the subsystem.

On Board Computer

The architecture for the OBC was chosen to be RAD750® 6U CompactPCI single-board computer produced by BAE Systems. The single board computer comes with a RAD750 processor, which has been extensively utilised across numerous space missions, demonstrating its reliability and effectiveness in deep space environments. The processor was notably used on both the Clipper and JUNO missions [86].

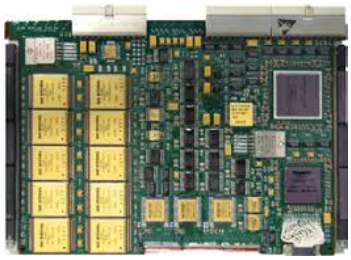

Figure 12.2: RAD750® 6UCompactPCI Single-Board Computer produced by BAE Systems.

The RAD750® 6U CompactPCI single-board computer is built around the robust RAD750 microprocessor, providing necessary onboard computing while ensuring integration with other essential C&DH hardware. By including the OBC rather than the processor alone, a more comprehensive power estimation for C&DH can be made. The RAD750® 6U CompactPCI has a mass of $1.22\,\mathrm{kg}$, and is specified for a total radiation dose of $>100\,\mathrm{krad}$. In terms of memory, the single-board computer has $48\,\mathrm{MB}$ of SRAM, as well as $4\,\mathrm{MB}$ of EEPROM. The following data were taken from BAE Systems RAD750® 6U CompactPCI datasheet [87]. The RAD750® 6U CompactPCI single-board computer was used on the Lunar Reconnaissance Orbiter (LRO) in 2009 [88]. An analysis by BAE Systems

in conjunction with the NASA Goddard Space Flight Center found that the single-board computer in its standard configuration has a power consumption of $20\,\mathrm{W}$ [89].

RAM

For the RAM architecture, the Monolithic 64M radiation-hardened SRAM, produced by BAE Systems, was chosen. The SRAM is capable of providing $64\,\mathrm{Mbit}$ of RAM for the OBC. It has a radiation tolerance of >$100\,\mathrm{krad}$ [90]. Its power consumption is roughly $1\,\mathrm{W}$ during nominal activities. The mass of the SRAM is negligible. Since the spacecraft is not required to perform significant amounts of data processing, it is assumed that a single SRAM is sufficient, but this should be evaluated in further design studies.

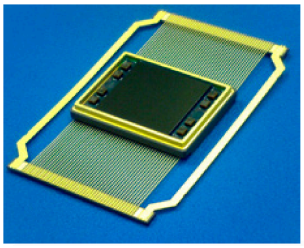

Figure 12.3: Monolithic 64M Radiation-Hardened SRAM

Storage

The 440 GB 3U VPX Rad-Tolerant SSDR, produced by Mercury, is capable of providing sufficient storage for the spacecraft. Given the $87.54\,\mathrm{GB}$ acquired per batch, the SSDR is more than capable of storing such data, as well as all other necessary data. There are also $480\,\mathrm{GB}$ and $4.5\,\mathrm{TB}$ variants that could be utilised if needed. The SSDR is capable of reading and writing data at speeds of over $200\,\mathrm{Mbps}$. It is also designed for a radiation dose of >$100\,\mathrm{krad}$. The SSDR has a mass of $0.62\,\mathrm{kg}$ and a power consumption of $7\,\mathrm{W}$ in idle conditions, which it shall be in for the majority of the mission duration. All data was taken from the 440 GB 3U VPX Rad-Tolerant SSDR datasheet [91].

12.4. Power and Mass Estimations

It can be seen from Section 12.3 that the mass of the aforementioned hardware elements, as well as their redundancies is $3.68\,\mathrm{kg}$. However, this does not account for either the cable harness mass, any supporting structures, or radiation reducing structures. For this reason, the level 0 estimation was used as a proxy for the mass of the C&DH subsystem. The level 0 estimation for the C&DH subsystem mass is $45.1\,\mathrm{kg}$. This is common practice for early phase studies at ESA [42]. As for power, Table 12.2 shows the calculations for total power estimates including margins. It can be seen that when including a 5% margin for power, the C&DH total power consumption is $58.8\,\mathrm{W}$.

Table 12.2: C&DH hardware elements power consumption calculations. A 5% margin is added to the total as the elements are considered to be off the shelf components.

	Power	Redundancy	Total Power
RAD750® 6U CompactPCI	$20\,\mathrm{W}$	2x	$40\,\mathrm{W}$
Monolithic 64M radiation-hardened SRAM	$1\,\mathrm{W}$	2x	$2\,\mathrm{W}$
440 GB 3U VPX Rad-Tolerant SSDR	$7\,\mathrm{W}$	2x	$14\,\mathrm{W}$
Total Power (+5% Margin)	-	-	$58.8\,\mathrm{W}$

13

Sustainable Development Strategy and End of Life Plan

This chapter details the way the team has ensured that sustainability has been considered in ELMO's current design. A sustainability trade-off criterion was established in the general trade-off method. Additionally, as ELMO's end of life is primarily constrained by sustainability concerns, this chapter discusses them. Finally, specific design options relating to sustainability and the decision process behind their implementation are mentioned.

13.1. Sustainability Trade-off Criterion

Sustainability is a difficult criterion to assess objectively since sustainability has such a large scope and encompasses different considerations which are impossible to compare quantitatively. It was decided that the sustainability scores of design would qualitatively be based on 4 categories that are described in this section.

Space Debris

This is the only sustainability category directly taken from the user requirements of this feasibility study, namely, SYS-TRT-01 states that the design should comply with the Outer Space Treaty Guidelines on Space Debris [92]. This clause of the Outer Space Treaty is generally meant to limit the debris in Earth's orbit, as such it is unclear to what extent the OST applies to deep space missions like ELMO. The treaty had to be subjectively interpreted and it was decided the requirement would be met as long as no human-made object is left in orbit of any celestial body after EOL except when the following 2 conditions being met: the spacecraft or stage is intact and not at risk of breaking up from collisions or otherwise, and that the spacecraft is in a stable Saturn orbit or has escaped Saturn's sphere of influence. The first of these conditions is derived from guideline 1 of the OST [92] and the second one is based on other missions having left spacecraft stages in stable orbits such as BepiColombo [93]. In design options trade-offs, options that increase the risk of debris being left in space were given a lower score.

Biological Contamination

Enceladus is a protected body due to its potential to harbour life and international law requires spacecraft visiting it to minimise the risk of contaminating its subsurface oceans with microorganisms originating from Earth [94]. The reasons and implications of this are explored in subsection 13.2.1. Design options which increase the risk of contaminating Enceladus were given lower sustainability scores.

Carbon Footprint

Greenhouse gases are responsible for climate change on Earth and their sources in engineering should be limited wherever possible. Estimating the carbon footprint of specific components is very difficult without a complex life cycle analysis so this category does not always apply.

Environmental Risk in Case of Launch Failure

Spacecraft and their launchers often contain highly dangerous materials which can pose major risks in case of launch failures. A notable example is the Nedelin disaster where a hypergolic fuelled soviet

missile exploded during launch in 1960, killing over 90 people [95]. Options such as the inclusion of toxic or radioactive materials will negatively impact the sustainability score of design options.

13.2. End of Life

In all space missions visiting protected environments such as Enceladus or Europa, sustainability and more specifically planetary protection are the biggest drivers of the EOL design of the mission. It was explicitly requested by the customer during this study that EOL should not be considered in ELMO's design. This request was followed, but future iterations of ELMO will need to consider EOL more carefully. This section will provide the EOL options that were studied as recommendations for future design phases. Firstly, the importance of protecting Enceladus must be stated.

13.2.1. COSPAR & Planetary Protection

Alongside guidelines on space debris, the Outer Space Treaty discussed earlier also states in article IX that signatories shall "conduct exploration of [the moon and other celestial bodies] so as to avoid their harmful contamination" [92]. The OST does not provide technical engineering guidelines, so space agencies have all adopted the Committee for Space Research's (COSPAR) guidelines for planetary protection [96]. COSPAR's Planetary Protection Policy (PPP) has become de facto international law and must be followed by every mission launched by space agencies. COSPAR lists Enceladus as its most protected celestial body alongside Europa and Mars due to these bodies' interest in the study of extraterrestrial life [97]. Enceladus has a salty subsurface ocean warm enough to potentially harbour life [98] and is geologically active enough for the exchange of material between the surface and ocean to happen regularly through its tiger stripes and cryovolcanoes [99].

The EOL plans for Cassini, Juice, and Europa Clipper were all designed to minimise the risk of contaminating Enceladus or Europa [6][100][101]. For a mission like ELMO which will get so close to such a protected planet, a sensible EOL plan in accordance with the PPP should be considered as one of the most key parts of mission design.

13.2.2. Orbiter Stage EOL Design Options

ELMO is in a particularly difficult position for its EOL. Unlike Cassini which had a highly elliptical trajectory around Saturn during its entire science phase, ELMO will orbit a moon directly, meaning it will require much more energy to travel to anywhere other than Enceladus once it has arrived. The ΔV demands of various EOL scenarios have been estimated with Hohman transfer calculations and the results are displayed in Table 13.1.

Table 13.1: ΔV estimates per EOL option.

EOL Option	Delta V (m/s)	EOL Option	Delta V (m/s)
High Saturn parking orbit	6800	Saturn aerobrake	4500
Low Saturn parking orbit	4600	Direct impact into Saturn	4700
Titan trojan orbit	6200	Bi-elliptic Saturn impact	4700
Direct Saturn escape	17000	Impact into Tethys	550
Titan assisted Saturn escape	3800	Impact into Mimas	850
Impact Enceladus	40	Enceladus soft landing	200

The only options with a ΔV requirement even worthy of consideration are impacting Enceladus, soft landing on Enceladus, Impacting Tethys, and impacting Mimas. Both Mimas and Tethys have lower protection categories than Enceladus. Impacting Mimas can be rejected since impacting Tethys has the same advantages for less ΔV. Impacting Enceladus can also be rejected as it wouldn't comply with the PPP. This leaves the only viable options as soft landing on Enceladus and Impacting into

Tethys.

Performing a soft landing on Enceladus with a system primarily designed as an orbiter would pose major design challenges. The propulsion and ADC subsystems would have to be designed for very high thrust and pointing accuracy. Landing systems typically have much lower success rates than orbiting systems [36], and as the PPP states that the chance of impacting Enceladus must be shown to be less than 1 in 10,000, it would be extremely unlikely that ELMO would be able to meet this reliability requirement. Furthermore, while soft landing on Enceladus would avoid spreading debris across its surface, ELMO would still make direct contact with its surface and this might be considered too high of a risk by COSPAR for ELMO to be allowed to fly.

This study found that the only viable EOL option for ELMO would be to transfer to Tethys, the nearest moon to Enceladus which has a much lower protection classification [97]. This option also has the most historical precedent; Juice and Europa Clipper will both spend large portions of their missions studying Europa, but both probes have chosen to perform EOL by crashing into Ganymede which like Tethys is less protected than Europa and Enceladus [101][100].

13.2.3. Kick Stage EOL Design Options

Since it was decided ELMO should have a kick stage, a separate EOL plan should be considered for this stage to avoid it crashing into Enceladus after is detached from the orbiter stage. Several design options for this have been identified which minimise the additional need for ΔV since the kick stage will be detached before ELMO arrives at Enceladus.

Kick stage is left in interplanetary space

If the split in ΔV between the kick stage and orbiter allows for the kick stage to be detached in interplanetary space, the kick stage can be left to drift in a heliocentric orbit where it poses no risk to Enceladus.

Kick stage in separated in Saturn impact trajectory

The spacecraft may place itself in a Saturn impact trajectory before detaching the kick stage so that it does not need to perform any additional manoeuvres once detached. The orbiter would then correct its course to avoid impact.

Kick stage autonomously performs EOL

If the kick stage is equipped with independent C&DH, ADC, and communications subsystems, it would be able to perform an independent EOL manoeuvre after detaching. This options would be the most demanding and is not considered favourable.

Kick stage is pushed into impact trajectory by solid rocket motors

Small solid rocket motors could be attached to the kick stage and set to activate upon separation from the orbiter. If the separation is aimed correctly and performed at Saturn apoapsis while in an elliptical orbit, the kick stage would be propelled into a Saturn impact. The solid rocket motors should be placed at a small angle so that the kick stage is spin-stabilised during this burn. This option would not require the kick stage to have autonomous subsystems like the previous option.

13.3. Design Options Pertaining to Sustainability

The two design options selected during this study which related to sustainability the most were the choice of the power source and propellant. The justification for choices made are briefly discussed in this section.

RTG vs. PV

RTGs are considered a less sustainable design option than solar panels. The first reason for this is that RTGs require a lot of energy to manufacture and produce nuclear waste in this process.

Secondly, many members of the public are concerned by the possibility of nuclear contamination of populated areas in case of a launch failure of a spacecraft equipped with RTGs. A notable example of this is a lawsuit that nearly delayed the Cassini mission over its inclusion of RTGs [102][103]. Ultimately, a solar array configuration was chosen for ELMO for various reasons, sustainability being one of them.

Hypergolic vs. non-toxic propellants

Using highly toxic hydrazine was considered non-optimal from a sustainability standpoint due to its significant health and environmental risks. An alternative propellant based on kerosene and hydrogen peroxide was proposed as a less toxic alternative. This option was not considered significantly more sustainable since kerosene itself is still a highly environmentally damaging hydrocarbon (however much less so than hydrazine). This option was rejected due to its low specific impulse and TRL. In Section 14.3, it was found that the increased mass from adopting the lower specific impulse propellant would likely decrease the overall sustainability of the spacecraft despite the more sustainable propellant choice.

14
Sensitivity Analysis

In this chapter the sensitivity analysis is presented. The sensitivity analysis focusses on some interesting and probable changes in system parameters to investigate the sensitivity of the design. Section 14.1 starts of with the sensitivity to changes in ΔV in the orbiter and kick stage. This is followed by Section 14.2, where changes in the payload are investigated. Lastly Section 14.3 finishes this chapter with some additional analyses.

14.1. ΔV Analyses

In this section the systems sensitivity to changes in the ΔV (Delta-V) parameters is investigated. As mentioned in Section 13.2, no End Of Life (EOL) plan has been taken into account yet. As explained in this section it is likely EOL will be part of the design in the future of this spacecraft design. The results of the analysis can be found in Table 14.1.

Table 14.1: Impact of ΔV Split and Changes on System Parameters

Parameter	ΔV **Redistribution to Kick Stage**	ΔV **Redistribution to Orbiter**	**Change in Total** ΔV **Budget (Decrease)**	**Change in Total** ΔV **Budget (Increase)**
Change in Value	$1000\,\mathrm{m/s}$	$1000\,\mathrm{m/s}$	$-600\,\mathrm{m/s}$	$600\,\mathrm{m/s}$
Effect on Dry Mass	$36\,\mathrm{kg}$	$42\,\mathrm{kg}$	$-260\,\mathrm{kg}$	$226\,\mathrm{kg}$
Effect on System Wet Mass	+3.4%	+4.1%	-22%	25%
Effect on System	Less effective ΔV split resulting in higher mass.	Less effective ΔV split resulting in higher mass.	Large mass reduction.	Large mass increase.

The first two sensitivity analyses focus on changing the distribution of ΔV over the orbiter and the kick stage. These analyses are conducted to measure the impact of less-optimal distributions which could be necessary to accommodate EOL schemes. The results of these show that large changes in this distribution result in significantly less efficient use of the kick stage design, hence the increased mass. The third and fourth analyses focus on changing the total ΔV requirement to showcase the effects of more optimal orbital manoeuvring in the first case , and accommodating for the orbiter EOL scheme as mentioned in Section 13.2 for the latter. Starting from $6000\,\mathrm{m/s}$, these analyses were done for a spacecraft with a total ΔV of $5400\,\mathrm{m/s}$ and $6600\,\mathrm{m/s}$ respectively. Given the large alterations of the ΔV, it is expected the mass will fluctuate significantly, although the $22\,\%$ decrease in wet mass is not sufficient to comply with the $9600\,\mathrm{kg}$ maximum mass requirement USR-SYS-01. Although the dry mass change in the system with lower total ΔV is larger than the other case, the overall change in system mass is larger in the latter. Considering the propellant mass scales exponentially with ΔV, this is expected.

14.2. Payload Analyses

In this section the sensitivity to alterations in the payload and science requirements are explored, the results of which can be found in Table 14.2. These alterations have been selected since the payload description mentions future payload redesign studies are on the way with as goal lowering their mass and power [2]. The reduction in payload mass cascaded to a dry mass reduction upwards of 5 times the initial reduction. This enormous mass reduction illustrates very well that fluctuations in mass have a compounding effect for the entire system. Note that this compounding effect is, to some extent, present in all dry mass reductions. One more example is of this effect is found in the reduction of payload power. This reduction lowered the mass, of the EPS system by $8.6\,\mathrm{kg}$, compounding to a total of $21\,\mathrm{kg}$ dry mass. Note that the compounding factor is not linear, as fluctuations in the output of many subsystems occur in discrete steps to some extent.

The sensitivity analysis on scientific data collection time is also investigated to simulate changes in the very large data rate, as reported in Chapter 5. Since using the current design the required power during scientific operations is more demanding as mentioned in Chapter 6, a decrease in scientific operations would not affect the system unless operational redesign was conducted[1][2], only an increase was investigated. This amplified the data rate which results in higher power requirements for the communications subsystem as explained in Chapter 5. To accommodate for this power increase, the mass of the EPS grew, causing other subsystems to increase in mass. This accumulated in $39\,\mathrm{kg}$ extra dry mass for the $13\,\mathrm{W}$ increase in maximum power. Note that the required power of the communications subsystem increased by about $35\,\mathrm{W}$, however most of this increment has been mitigated by the higher power demands of the scientific operations, the EPS initially was designed for.

Table 14.2: Impact of Changes on Scientific Data Collection, Payload Mass, and Payload Power

Parameter	Scientific Data Collection Increase	Reduce Payload Mass by $20\,\mathrm{kg}$	Reduce Payload Power by 20%
Change in Value	From 15% to 20%	$20\,\mathrm{kg}$	20%
Effect on Dry Mass	$39\,\mathrm{kg}$	$-114\,\mathrm{kg}$	$-21\,\mathrm{kg}$
Effect on System Wet Mass	+1.7%	-4.3%	-1%
Effect on System Power	$13\,\mathrm{W}$	N/A	$-11\,\mathrm{W}$
Effect on System	Slight mass increase.	Great mass reduction, shows importance of mass savings.	Small mass reduction.

14.3. Additional Analyses

In this section some additional sensitivity analyses have been addressed. The Photo Voltaic (PV) efficiency reductions analysis stems from the opaqueness of Saturn's E-ring the targeted moon Enceladus is located in. Since the effects this ring could have need further investigation, a $10\,\%$ reduction was selected as an upper bound for this analysis. The results of this, and the other analyses in this section can be found in Table 14.3.

[1] This is referring to altering the distribution of science orbits and transmission orbits. These orbits are explained in Chapter 3

[2] This also renders sensitivity analysis of a higher orbital altitude useless, as this would also lower the data rate by increasing the camera's pixel-size within required bounds, leading to no immediate effects on the system.

To investigate the possibility of more sustainable, non-toxic propellant an investigation was done using a different fuel, with most notably a much lower specific impulse of $232\,\mathrm{s}$[104] in comparison to the $321\,\mathrm{s}$ of the current propellant as stated in Chapter 8. Given the large ΔV requirement, this results in more than a doubling in total system mass, rendering this option unviable. The instrument pointing mechanism was investigated to optimize the angle of incidence of the PV panels with respect to the sun during scientific operations. This option would increase effective PV area at the cost of a mechanism. Since an estimation of such an mechanism needs further investigation before a formal trade-off, as described in Section 4.3, could be conducted it was included in this analysis.

Table 14.3: Impact of Changes on Other System Parameters

Parameter	PV Efficiency Reduction	Non-Toxic, Green Propellant	Instrument Pointing Mechanism
Change in Value	$10\,\%$	New specific impulse: $232\,\mathrm{s}$ [104]	0° angle of incidence with solar panels
Effect on Dry Mass	$80\,\mathrm{kg}$	$994\,\mathrm{kg}$	$-27\,\mathrm{kg}$
Effect on System Wet Mass	+3.5%	+133%	-1.7%
Effect on System Power	N/A	N/A	Unknown
Effect on System	EPS mass increase has large snowball effect.	Enormous increase in wet mass.	Saves mass, adds cost, lowers reliability.

The conducted analyses illustrate the impact of possible changes on the spacecraft design. These can be used as a reference when investigating changes to the current system. Considering the requirements for maximum spacecraft mass and cost have not been met, as outlined in Chapter 4 and Chapter 17 respectively, the analyses on payload mass, power, and total ΔV reduction show promising results[3].

[3] In current models cost has been estimated using mass, thus mass reductions will directly improve the cost, as described in Chapter 17.

15
Further Mission Development

Mission development including assembly, integration, and validation (AIV), and mission development phases are an important component to analyse when assessing the feasibility of a mission like ELMO. With ELMO being required to launch in 2035, the time for this mission to develop to full launch readiness is particularly low. This chapter will outline the critical factors involved with further developments of ELMO beyond this study.

The first subsection estimates the mission phase timeline so that ELMO may launch in 2035 using the timelines of similar deep space missions. The second subsection proposes an alternative timeline and its advantages. The third subsection highlights the logistical considerations for ELMO's assembly, launch and operations based on Cassini's own operational history. Finally, the final subsection discusses the current testing philosophy and the tests ELMO and its qualification models will need to undergo.

15.1. 2035 Launch Timeline

The primary constraint of the mission timeline estimation is system requirement SYS-DEV-01 which states that the spacecraft shall be flight ready by 2035. This leaves almost exactly a decade from the writing of this report for ELMO to be developed to flight readiness. It is also not a reasonable assumption that this mission will begin proper development as of the end of this feasibility study; as discussed in Chapter 4 and Chapter 19, several customer requirements have not been met by the design. The ELMO mission will likely need to undergo several iterations to redefine the mission, requirements, and feasibility of the spacecraft. It will be assumed that ELMO can only be accepted by ESA starting in 2027 to allow for 2 more years of iterations. This leaves an overall mission timeline budget of only 8 years.

To divide this time budget, several other missions with known timelines have been analysed and presented in Table 15.1. The mission phases discussed in this report will be in accordance with ESA's mission lifetime cycle defined as follows. Phase 0: mission analysis and identification, phase A: feasibility, phase B: preliminary definition, phase C: detailed definition, phase D: qualification and production, phase E: utilisation, phase F: disposal[1].

Table 15.1: Start of mission phases for various missions, rough estimate for Cassini.

Phase	**Europa Clipper** [100]	**Juice** [101]	**Venus Express** [105]	**Cassini** [106]
Phase 0	2013	2008	2001	1989
Phase A	2015	2010	2002	1989
Phase B	2017	2010	2003	1990
Phase C	2019	2015	2004	1990
Phase D	2022	2020	2005	1996
Phase E	2024	2023	2005	1996

[1]Since end of life has not been implemented in this design phase, phase F will be excluded from this chapter.

Phases 0 and A are generally shorter and are the least expensive phases (especially phase 0) so missions will generally only move to further phases when the mission design has been sufficiently optimised[36]. It can be seen in the examples that phases B and C are generally the longest, and that phase D can be relatively short. It should be noted that both Europa Clipper and Juice were delayed in phase D by the COVID-19 pandemic [101][100]. It should be noted that phase C typically overlaps with phase D as design changes are often made as a result of testing [42]. It should be noted that more recent missions such as Europa Clipper and Juice take at least a decade to develop and a mission like ELMO should take at least this long. The timeline of Cassini is shorter likely as a result of the larger budgets of space agencies at the time and different development philosophies [106]. The Venus Express timeline is especially short primarily as a result of a large portion of the spacecraft being based on Mars Express [105].

With 8 years to develop ELMO, the timeline will have to be rather compressed. A proposed timeline with phase timeframes based on Table 15.1 is given in a gantt chart format below.

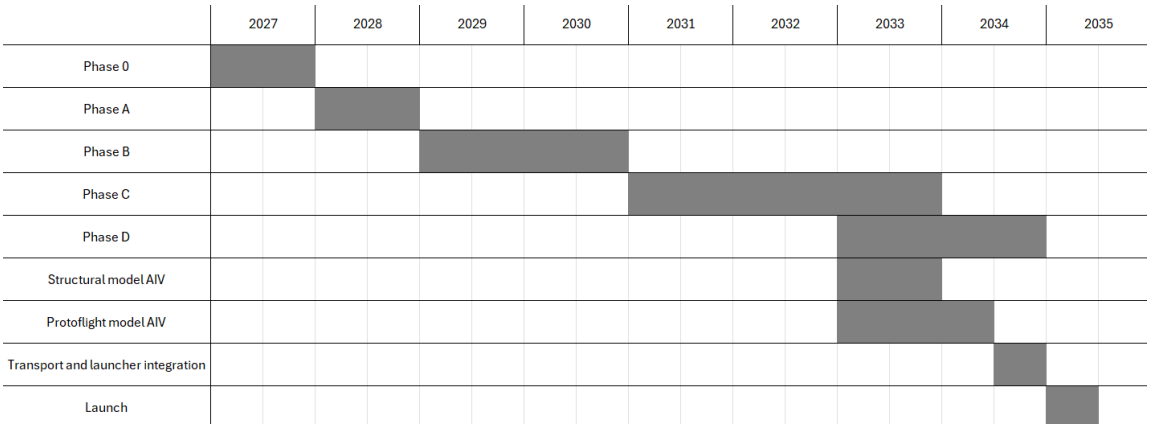

Figure 15.1: ELMO 3035 launch development timeline.

This timeline makes a number of concessions to the time restrictions. Firstly, each phase is shorter than it should be. Phases B and C only have a collective 5 years including overlap with Phase D. Phase D only has two years which results in the protoflight model needing to be produced at the same time as the structural model. Ideally, testing models should be produced subsequently or their production times should be staggered so that any design changes needing to be made as a result of testing can be applied to future models. The length of time to produce the structural model is based on Rosetta which took 8 months for assembly of the structural model alone [107]. Fully assembling and testing the structural model in a year is optimistic. The protoflight model must be made at the same time and is only allowed 1.5 years for AIV. Finally, transport and launcher integration can be expected to take several months [108]. The transport and logistics is discussed further in Section 15.3 and the testing phase is detailed in Section 15.4.

It should be noted that the kick stage will likely be developed independently from the orbiter stage. The kick stage will likely be developed in parallel by the same contractor. In future studies, these two elements should have separate timelines.

15.2. Alternative Timeline

Due to the need for more pre-phase A iterations and the short timeline, launching in 2035 is considered unfeasible by the design team. This subsection will present an alternative extended timeline and the advantages it would present.

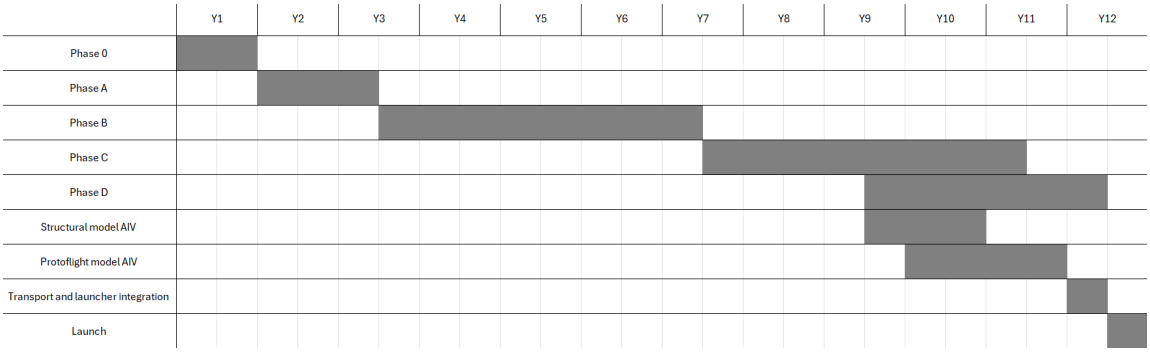

Figure 15.2: Alternative feasible ELMO timeline.

The most immediate advantage of the proposed alternative timeline is the increased length of every design phase which reduces the risk of any part of the project running over schedule. Additionally, more time has been allocated to the testing of both models and the assembly of the protoflight model has been placed half a year after the assembly of the structural model, this allows for design changes to be implemented into the protoflight model while it is at an early phase of production. Overall, this extended timeline allows for 12 years of development which is much more similar to missions such as JUICE and Europa Clipper.

In addition to extending the timeline, it is recommended that the launch is delayed to at least 2050. Delaying the timeline would also aid in resolving several major issues identified during the design of the spacecraft, notably, the readiness of key technologies, the availability of RTGs, increased solar power, and the lighting on the dark pole of Enceladus.

Starting the official development later would allow for several important technologies currently in development to be implemented. Cryogenic technologies were rejected as a design option for the propulsion subsystem earlier in this design phase due to the low technology readiness level of zero boiloff storage solutions, but these technologies are being actively developed as a part of NASA's Artemis programme [109]. Using cryogenic propellants such as LH2-LOX could increase the specific impulse of the propulsion subsystem thereby massively reducing launch mass. Rapid developments in photovoltaic technology could also allow for a better-optimised solar array for ELMO.

It was determined for the design of the EPS that having RTGs would be more beneficial for its lower mass but the option was rejected for its high cost and low availability since most RTGs currently in production are reserved for other spacecraft. Delaying the development of ELMO would significantly increase the availability for RTGs and make them a preferable option for the EPS.

In Section 3.5, it was found that if the launch was delayed by 15 years, Saturn would be 1 astronomical unit closer to the sun by the time ELMO arrives providing 20% more power to the solar array which would allow it to be designed to be much smaller and thus lighter, snowballing in a large reduction in mass.

Finally, as is discussed further in Section 3.8 the south pole of Enceladus will be in a decades-long polar night by the time ELMO arrives at its destination if it were to launch in 2035. Assuming the same trajectory to Saturn is taken, launching in 2050 would allow ELMO to arrive at a time when the south pole is receiving sunlight thus allowing for photography of its cryovolcanoes of interest.

15.3. Logistics & Operations

The logistical and operational considerations of a mission such as ELMO are highly different for the pre and post-launch phases. These are discussed separately in this section.

Logistics and operations vary a lot between space missions, as ELMO is meant to be a European

mission, and there are too many unknowns at this early phase of development to describe a comprehensive logistical plan for ELMO, this section will base itself primarily on the development of ESA's Juice, and it should be interpreted that ELMO's logistics and operations will be similar.

The post-launch operations will be based primarily on Cassini which is the the most similar spacecraft to ELMO. The trajectory will be assumed to be identical until Saturn approach, after which assumptions must be made on the transfer flight to Enceladus.

15.3.1. Pre-Launch

The logistical implications of space missions are minor prior to phase C as the physical assembly of components will not have begun. For the pre-launch phases, each subsequent phase will typically see the project growing larger in scope and will be significantly more expensive than the last.

Phase 0 is to a large degree the most decentralised development phase. Phase 0 studies are conducted by space agencies such as ESA but numerous non-profit and educational institutions may investigate different types of missions often with the goal of encouraging discussion of specific scientific objectives within the scientific community, this report being an example of such a study being conducted at TU Delft. Phase A is conducted a lot more formally; at ESA they are conducted by assigning several independent teams of engineers to assess the feasibility of a mission based on preliminary requirements, multiple teams are assigned the same task to ensure that several unique designs are explored [42]. Juice's phase A was conducted at ESTEC in less than a year, by the end of both phases 0 and A, the results are typically presented at ESA's Paris headquarters to determine whether the mission is allowed to develop further [101]. If collaborations with other space agencies are considered it will typically be agreed upon in phase 0 or A on which aspects of the mission each agency is to work on. Before Juice's phase A, the project was originally a collaboration between ESA and NASA titled Europa Jupiter System Mission - Laplace, where ESA was responsible for the Laplace (or Jupiter Ganymede Orbiter) spacecraft which would have orbited Ganymede and NASA was responsible for a Europa orbiter, however NASA withdrew from the project due to budgetary constraints and EJSM-Laplace was developed into Juice [101].

The primary objectives of phase B are to establish the final list of requirements and select the primary industrial contractor. At the start of phase B, ESA selects two industrial contractors to perform a competitive phase B1. The contractors independently define the mission, requirements, and preliminary design. By the end of phase B1 ESA assesses the proposals of both contractors and one of the two is selected to be responsible for designing and assembling the final spacecraft [101]. The contractor typically has control of their own operations. The two contractors selected for Juice were Airbus (Astrium) and Thales Alenia Space, and Airbus was selected as the primary contractor in July 2015 [101]. Since this phase has two industrial contractors working simultaneously, the selection of a contractor is a costly process.

Phases C and D are extremely demanding in terms of logistics and operations. Airbus states that 80 partners in 23 countries accounting for over 2000 personnel were involved in the making of Juice [110]. While ESA is not in direct control over the contractor's operations, they are still of concern to ESA to ensure a smooth assembly process and final delivery of the spacecraft from the contractor's facility to ESTEC. Airbus assembled Juice in their Toulouse headquarters, after which it was transported to ESTEC for testing [101]. The exact logistics of this transportation are not publicly known though spacecraft have been transported through various means previously including by truck, ship, and air [110][108]. The testing is detailed further in Section 15.4.

After testing was completed as ESTEC, Juice finalised integration in Toulouse, after which it was transported via Antonov aircraft to Europe's Spaceport in French Guyana in February 2023, 2 months before its launch [110]. Considering ELMO's current extremely high launch mass, it may be unviable to transport it by air, in which case it would likely be transported on a naval vessel. The James Webb Space Telescope was transported on board a French Navy vessel from California to French Guyana

in October 2021 [108]. During transport, JWST was kept in a mobile clean room to reduce particulate contamination as much as possible of its optical components. The transport of spacecraft especially by ship is often kept secret before the trip takes place to reduce the risks of piracy [108].

Finally, a note on clean rooms. Despite planetary protection not having been made a requirement for ELMO, the spacecraft would still need to be assembled and tested in clean room environments as the contaminations of particles and humidity pose a significant risk to highly sensitive components on a scientific spacecraft [111].

15.3.2. Post-Launch

After the launch of a spacecraft, there are far fewer logistical implications present since there is no longer a need to transport many spacecraft components for assembly. Operations of mission however remain highly significant, and different periods of the mission will require a large labour force.

The primary logistical aspect of the post-launch phase of the mission will be the storage of the qualification models used for testing. When qualification models are used for testing a spacecraft, they are stored in a clean room environment once the spacecraft has launched until the end of the mission so that in case unforeseen circumstances beset the spacecraft, additional testing may be performed to aid in finding a solution [111]. Since these models are already assembled and don't always need to be used, they will rarely need to be transported from one facility to the next.

The ground segment operations of Juice will be used as a reference for ELMO's potential operations. Juice's ground segment is managed by ESA and is divided into 2 distinct components, the Mission Operation Centre (MOC) and the Science Operation Centre (SOC) (collectively referred to as the Science Ground Segment (SGS)), which alongside the Principal Investigator (PI) instrument teams, implements the mission's science and flight operations guided by a predetermined Science Management Plan. The spacecraft operates through an offline monitoring and control approach where a pre-scheduled timeline of operations is uploaded to the spacecraft by the MOC, during science operations, this happens daily but no routine science operations are planned during the cruise phase except for Earth and Venus flybys. The high-level science activities are designed by the Science Working Team and divided into uplink and downlink activities. Uplink activities consist of establishing and transmitting the instrument operations timeline to Juice, the SOC and PI teams create this timeline from science operations requests from teams responsible for the instruments, and finally, the timeline is uploaded to the spacecraft by the MOC. For non-routine operations, the SOC assists instrument teams in making science operations requests. The planning of science operations takes place in 3 steps, Long Term Planning is done is 6-month intervals and focuses on top-level mission planning, Medium Term Planning plans in monthly intervals to finalise instrument pointing and validate instrument modes with updated spacecraft resources, and short-term planning is conducted weekly to finalise instrument commands. Downlink activities consist of data handling and archiving. The MOC supervises the retrieval of telemetry data to verify the status of the spacecraft while the SOC processes telemetry data and distributes raw instrument data to instrument teams[2].

This process happening throughout the entire science phase of the mission requires extensive coordination between several departments, each of which has many different teams to ensure 24/7 availability so that any situation may be appropriately responded to. These teams must also coordinate with ground segment antennas which are located all across the globe to ensure steady communication with the spacecraft as the Earth rotates.

In the current stage of design, it was assumed that ELMO would take an identical trajectory to Cassini. The following table provides an approximate timeline of ELMO's post-launch activities and the opera-

[2]Ground segment operations information from https://www.eoportal.org/satellite-missions/juice

tional demands of each event[3]. Some assumptions are made such as ELMO performing a year-long moon tour to reach Enceladus (half the time for Juice to orbit Ganymede [101]) and that ELMO will be extended by one year with a lower operational budget as was the case for Cassini [106].

Table 15.2: ELMO post-launch timeline and ground segment operational demands.

Elapsed Mission Time	Event Description	Event Duration	Operational Demand
Mission Start	Launch	Hours	Extremely high
Hours	Initial spacecraft telemetry	Hours	High
Hours-Days	First hibernation phase	0.5 Years	Low
0.5 Years	First Venus flyby, most demanding thermal environment	Days	High
0.5 Years	Second hibernation phase	0.7 Years	Low
1.2 Years	Correction burn at aphelion	Hours	High
1.2 Years	Third hibernation phase	0.4 Years	Low
1.6 Years	Second Venus flyby	Days	High
1.6 Years	Fourth hibernation phase	0.2 Years	Low
1.8 Years	Earth Flyby	Days	High
1.8 Years	Fifth hibernation phase	1.4 Years	Low
2.2 Years	Jupiter Flyby	Days	High
2.2 Years	Sixth and final hibernation phase	4.3 Years	Low
6.5 Years	Saturn approach	Months	High
6.7 Years	Saturn capture	Hours	Extremely high
6.7 Years	Saturn moon tour to gravity assist to Enceladus	1 Year	High
7.7 Years	Enceladus capture	Hours	High
7.7 Years	Hoppers released	Hours	Extremely high
7.7 Years	Routine science begins at Enceladus	100 Days	Extremely high
8 Years	Mission extended	1 Year	Medium
9 Years	End of life	Days	High

15.4. Testing Plan

During phase D, ELMO will need to be tested at several levels of assembly to verify its flight readiness. The testing philosophy employed in this study follows ESA's ECSS-E-ST-10-03C Rev.1 [111]. The first half of this subsection will discuss testing of the individual subsystems which as per the ECSS standards should focus on performance testing (ability to meet design requirements) whereas the second half of this subsection will discuss system testing which should focus on environmental testing. In general, the organisation of a test should be divided into 3 blocks, the Test Readiness Review which is to be held before the test, the Post Test Review which formally declares the completion of

[3]Cassini timeline from https://science.nasa.gov/mission/cassini/the-journey/timeline/

the test and releases the test item from the testing facility, and the Test Review Board which reviews the test results and assesses whether the test objectives have been met. It should be assumed that all tests listed in this section follow this procedure.

15.4.1. Subsystem Testing

Testing at a component and subsystem level is not standardised and tests must be designed bespoke to individual subsystems. Since most of the components used in spacecraft design (including the design presented in this report) are already space-qualified, environmental testing is typically not done on a subsystem level [111]. The following tables display testing plans devised by each respective subsystem engineer to performance test their subsystem and verify that they meet their design requirements. When a particular type of facility is required for a test, it will be mentioned. Tests without listed facilities are assumed not to have stringent facility requirements. It should be noted that safety margins are generally not applied at this level of testing due to several reasons. Margins are already applied to the design of the subsystem and the requirements it was designed for, if another margin is applied to the test condition the subsystem will not be able to meet the requirements it was designed for. Furthermore, testing spacecraft components beyond what they are certified for can cause major risks to personnel around the testing environment and may cause the tested components to fail earlier than expected during mission operations.

Table 15.3: Comprehensive Testing Plan for Spacecraft Subsystems

Test ID	Test Method	Test Objective	Testing Facility
Communications Subsystem			
TST-COM-01	Compare antenna gain against reference antenna	Verify antenna gain	Anechoic chamber
TST-COM-02	Rotate antenna and measure radiated power at various angles	Verify antenna radiation pattern	Anechoic chamber
TST-COM-03	Measure impedance with impedance analyser	Verify impedance and signal loss	Anechoic chamber
TST-COM-04	Run antenna at different frequencies and power levels	Verify performance over operational bandwidth range	Anechoic chamber
TST-COM-05	Input a known data stream to the encoder and get output from decoder	Verify transmission integrity with chosen modulation and components	Anechoic chamber
Electrical Power Subsystem			
TST-EPS-01	Reverse current in solar cells and visually inspect uniformity of produced glow	Verify integrity of solar cells	-
TST-EPS-02	Analyse solar array output when placed in a solar simulator	Verify solar array power, voltage, and current	ESTEC solar simulator
TST-EPS-03	Deploy solar array in specialised support structure to simulate microgravity	Verify proper solar array deployment	Microgravity support harness
TST-EPS-04	Charge and discharge battery for multiple cycles while monitoring performance	Verify battery capacity	-
Attitude Determination and Control Subsystem			

Test ID	Test Method	Test Objective	Testing Facility
TST-ADC-01	Stress test ADCS software by introducing errors, faulty sensor measurements, and null values	Verify robustness of ADCS software	-
TST-ADC-02	Monitor power usage of reaction wheels at different RPMs	Verify power curves of reaction wheels	-
TST-ADC-03	Calibrate star trackers and sun sensors in simulated lighting conditions	Verify accuracy of ADCS sensors	Constellation simulator
TST-ADC-04	Analyse inertial measurement unit outputs when subjected to controlled rotations and accelerations	Verify accuracy of IMU	-
Propulsion Subsystem			
TST-PRP-01	Hot fire the engine while monitoring thrust and propellant consumption	Verify engine thrust performance	Hot fire testing facility
TST-PRP-02	Pressurise tanks and valves to design specifications	Verify tank and valve integrity	-
TST-PRP-03	Open and close valves for multiple cycles	Verify function and durability of valves	-
TST-PRP-04	Monitor flow rate through pipes at various pressures	Verify fluid flow rate	-
Structures Subsystem			
TST-STR-01	Perform coupon testing at various temperatures on structural materials	Verify material properties	Coupon testing lab
TST-STR-02	Apply static loads on assembled structure with simulated weights	Verify static stability of the structure	-
TST-STR-03	Vibrate structure with simulated weights to design specifications[4]	Verify dynamic stability of the structure	Hydraulic shaker
Mechanisms Subsystem			
TST-MEC-01	Vibrate magnetometer boom and hopper attachment to design specifications	Verify dynamic stability of mechanisms	Hydraulic shaker
TST-MEC-02	Deploy magnetometer boom in simulated microgravity	Verify proper magnetometer deployment	Microgravity support harness
TST-MEC-03	Activate kick stage and hopper deployment frangible bolts (see footnote)[5]	Verify proper separation of kick stage and hoppers	Pyrotechnic testing facility
TST-MEC-04	Test SA deployment after extended duration of thermal cycling and exposure to radiation	Verify delayed SA deployment in mission conditions after	ESA Large Space Simulator
Thermal and Radiation Control Subsystem			

[4] While vibrations are generally considered an environmental test and performed at a system level, this subsystem was specifically designed for the vibration loads at a subsystem level.

[5] Frangible bolts use pyrotechnic charges to sever structural connections by force, as such, the bolts that will be installed into ELMO obviously cannot be tested beforehand. In this case, they would be ordered in a large batch and many tests would be performed to ensure that the bolts are reliable enough to be mounted on ELMO without being tested.

Test ID	Test Method	Test Objective	Testing Facility
TST-TRC-01	Monitor temperature of spacecraft mockup with MLI in thermal vacuum chamber with sun simulator set to Venus conditions	Verify MLI insulation performance	ESA Large Space Simulator
TST-TRC-02	Monitor radiative power of louvers at different temperatures in a vacuum	Verify louver performance	Thermal vacuum chamber
TST-TRC-03	Subject spacecraft mockup to temperature environments way more extreme than what is expected during the mission. Determine the failure mode and stress resistance of the spacecraft. [6]	Investigate weak points in thermal design, determine resilience spacecraft	Thermal vacuum chamber
Command and Data Handling Subsystem			
TST-CDH-01	Monitor outputs as computer is given commands with known outputs	Verify C&DH functions	-
TST-CDH-02	Monitor outputs and their order as computer is rapidly given many commands with known outputs	Verify C&DH robustness	-

15.4.2. System Testing

The ECSS standards are much more explicit about system-level testing. Test types, levels, durations, number of cycles, and order are provided for the environmental testing for different testing philosophies. The choice of testing philosophy is a tradeoff between certainty level and funding. The two main philosophies are qualification testing and protoflight testing.

Qualification testing implies the assembly of an additional spacecraft called the qualification model. This model is identical to the flight model with the exception that the expensive payload is usually replaced with dummies that simulate their interfaces. The testing of the qualification model is called qualification testing. These tests are only performed up to the levels that the spacecraft will encounter with a safety margin applied but the safety margin should never be so high that any spacecraft component will exceed the loads it is certified for. Testing on qualification models is usually done for long durations and for several cycles to increase the certainty of proper spacecraft functions. Even when qualification testing is done, testing must also be done on the flight model, this is called acceptance testing. Acceptance testing is performed to the same levels as qualification testing but for shorter durations and fewer cycles to avoid unnecessarily wearing out the spacecraft. Once the spacecraft launches, the qualification model is kept in storage for further testing if the need ever arises. Testing a full qualification model provides the most certainty that a spacecraft will not fail, but due to the need to assemble another spacecraft to the same specifications and the additional testing involved, it is a very expensive option.

Protoflight testing is a very different approach that sacrifices certainty for faster development times and a less costly testing phase. In protoflight testing, only a single spacecraft is assembled called the protoflight model. This is the same as the flight model. To compensate for the lack of a qualification model to perform extensive testing on, protoflight testing is performed at a higher level than qualification testing but for very short periods and only a single cycle to minimise the damage the

[6] Radiation is typically not verified with testing [74].

spacecraft might incur from testing.

In both testing approaches, structural models consisting of usually just the structures, thermal, and mechanisms subsystems are often used to perform lower-level testing while the qualification or protoflight models are still being assembled. This allows for design changes to be made to the complete models based on the conclusions of the structural model testing.

Historically, flagship missions such as ELMO have employed full qualification models to maximise mission success likelihood. This was the case for previous ESA missions such as Rosetta which employed a structural model, qualification model, and protoflight model [107]. Rosetta was part of ESA's Horizon 2000 programme which was better funded than the missions arising from ESA's newer Cosmic Vision programme [42]. As a result of reduced funding and decreased public interest in space exploration, the industry has shifted away from extensive testing and a protoflight testing approach is now more common. This was the case for Juice which used 2 simplified models for testing, the Thermal Development Model for thermal testing and the Engineering Model used to test the integration of the harness, software, and mechanical and electronic interfaces [76][101].

Considering ELMO's massively over-budget cost estimation Section 17.4, full qualification testing is out of the question due to the enormous cost that building and testing a second spacecraft would add. Considering current industry trends and more realistic requirements, ELMO would most likely use a protoflight testing approach with additional tests done on lower-level structural models, similar to Juice.

ELMO's protoflight model will need to undergo a testing phase detailed in ECSS-E-ST-10-03C starting on page 61. The details of these tests will not be provided in this report to avoid burdening this report with unnecessary tables, however, the order of the tests is provided in Figure 15.3. The order of environmental testing must be done to match the order the environmental conditions will be encountered during the mission.

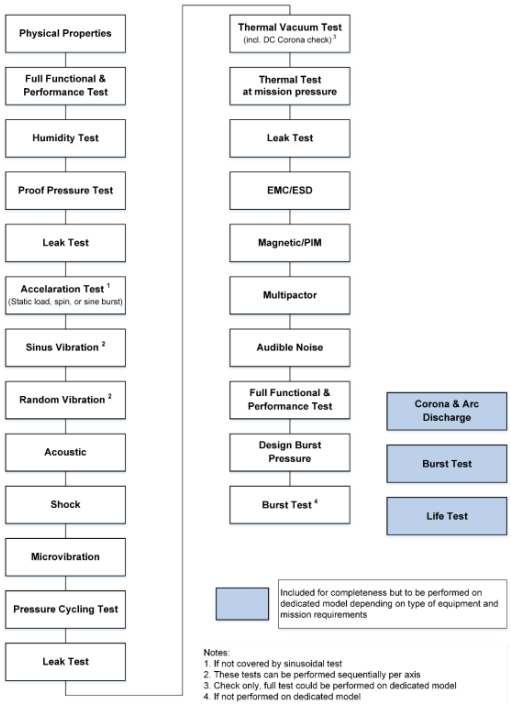

Figure 15.3: Order of environmental tests at system level [111].

16
Reliability, Safety, and Risk

Reliability, Safety, and Risk are highly related, and are crucial considerations for the design of any spacecraft. This chapter starts with the requirements in Section 16.1, after which the reliability is discussed in Section 16.2, followed by safety considerations in Section 16.3. The chapter ends with the risk management in Section 16.4.

16.1. Requirements

The requirements related to risk management, reliability, and safety requirements that have been determined for the ELMO mission are shown in Table 16.1.

Table 16.1: Risk management, reliability and safety requirements.

ID	Description
USR-SYS-02	The orbiter reliability (including payload) shall be equal or better than 0.75 for EoM.
USR-SYS-06	The orbiter (including payload) shall cost equal or less than $750\,\mathrm{M\$}$ (FY2025).
USR-MIS-01	The orbiter shall be delivered ready for launch in 2035.
USR-MIS-02	The orbiter transfer flight duration shall be a maximum of 8 years.
USR-MIS-05	The orbiter operational life in mission orbit (science life): ≥ 100 days.
USR-MIS-06	A safety policy in accordance with ECCS-Q-ST-40C shall be established that aims to eliminate hazards associated with the manufacturing, operation (including end of life) as well as personnel, other property, and the environment.
USR-MIS-07	The orbiter shall comply with the Space Debris Guidelines of the Committee on the Peaceful Uses of Outer Space.
ELM-US02-RRS-01	The bus reliability of the ELMO mission shall be equal or better than 0.87 over a period of 8 years and 100 days.
ELM-US02-RRS-02a	Single-point failures shall be avoided in the spacecraft design.
ELM-US02-RRS-02b	Retention of single-point failures in the design shall be declared with rationale.

16.2. Reliability

Reliability is a key consideration in the design of any spacecraft, especially when it is set to travel a distance of $10\,\mathrm{AU}$, making any long-term maintenance impossible.

16.2.1. Required Bus Reliability

Using the user requirement on the end-of-mission (EoM) reliability for the total spacecraft, USR-SYS-02, the EoM reliability for the bus can be determined. The bus reliability takes into account the reliability of the complete system, excluding the payload.

The assumptions for the calculation of the bus reliability are shown in Table 16.2:

Table 16.2: Assumptions for determination of the bus reliability.

Assumption	Justification
Payload turned off for full duration of transfer flight	Apart from health checks, this is true
Transfer flight takes the maximum 8 years	Most constraining
Hoppers are deployed at day 0 of operations	Most constraining
Hoppers are assumed to be on for the full duration of operations	Most constraining
Failure of any of the hoppers or payload instruments is considered failure of the payload	Most constraining
Failure rates of payload when turned off is equal to 1/10 of failure rate when turned on	This assumption comes from [2]

Table 16.3: Failure rates and duty cycle of hoppers and payload instruments.

Instrument	Quantity	Failure Rate when ON [failure/day]	Duty cycle during operational life
Hopper	2	1.9×10^{-4}	1
Ice Penetrating Radar	1	8.0×10^{-5}	0.015
Tri-axis magnetometer	1	8.0×10^{-5}	0.3
Tri-axis accelerometer	1	2.7×10^{-7}	0.3
Laser Altimeter	1	4.8×10^{-5}	0.15
HRC	1	2.4×10^{-5}	0.15

Table 16.3 shows the failure rate of the hoppers and payload instruments [2] as well as their duty cycle during operations (see subsection 3.3.1). With this data, the reliability of the payload over the 8 years and 100 days nominal mission duration can be calculated. This is done by using Equation 16.1 for the reliability of a system, where failure of any of the components means failure of the system [12]:

$$R = \prod_{i}^{n} e^{(-\lambda_{equipment_i} \cdot t)} \tag{16.1}$$

Where $\lambda_{equipment}$ for each hopper or instrument can be determined by Equation 16.2 [112]:

$$\lambda_{equipment} = \alpha \cdot \lambda_{ON} + (1 - \alpha) \cdot \lambda_{OFF} \tag{16.2}$$

where α is the fraction that the component is active for the total nominal mission duration of 8 years and 100 days. The reliability of the payload for nominal mission duration is found to be 0.87. The required bus reliability can be found by considering the spacecraft a system that fails if either the bus or the payload fails of which the reliability shall be 0.75. The required bus reliability at the end of the nominal mission time is thus found by dividing the total reliability by the payload reliability, which equals 0.87 (ELM-US02-RRS-01).

16.2.2. Designing for Reliability

Quantitatively determining the bus reliability is difficult, since reliability data on components of the spacecraft is often not readily available. This means no definitive value can be given for the reliability of the spacecraft. Incidentally, the historical bus reliability for deep space spacecraft from 1991 to

2023 was found to be 0.87 at design life [113]. This makes a good case for the feasibility of the required bus reliability.

To design for the required reliability, requirements ELM-US02-RRS-02a and ELM-US02-RRS-02b have been formulated. The SPF, along with rationale are shown in Table 16.4.

Table 16.4: Single point failures and their rationale.

SPF	Rationale
Payload Instruments	Failure of an instrument does not result in failure of spacecraft. Considering this, identical instruments would make the spacecraft too massive.
Structure	Structure is tested extensively to ensure expected behaviour. Adding an extra structure would cause a large mass increase.
HGA antenna dish	Probability of antenna dish failure is low. An extra identical dish is a large increase in mass.
Helium tanks	Probability of failure is low. A safety factor of 1.5 is used in the design. Extra tanks would make the spacecraft too massive.
Propellant tanks	Probability of failure is low. A safety factor of 1.5 is used in the design. Extra tanks would make the spacecraft too massive.
IMU	The IMU has built in redundancy.

The reliability strategy of ELMO is shown in Table 16.5, with a column that considers similarity to Cassini based on [114] [115], Europa Clipper based on [116] and JUICE based on [117]. The table also shows the mass penalty taken for the redundancy in terms of dry mass. The total dry mass penalty caused by the redundancy is $68.4\,\mathrm{kg}$.

Table 16.5: Reliability strategy ELMO.

Domain	Components	ELMO	Same approach as	Dry mass penalty (incl. contingency) [kg]
General	Safe mode	Fail operational during critical phases in transfer flight	Europa Clipper, JUICE	N/A
Propulsion	Thrusters	2 main gimballing main engines per stage	Cassini	9.5
	Pressure regulator	2 pressure regulators in series with a valve and those sets in parallel per helium tank	Cassini	7.6
	Valves	Series and parallel valve scheme for redundancy	Europa Clipper	23.5
ADCS	Thrusters	2 sets of 12		3.7
	Flight computers	No COTS flight computer was found, the flight computer is included by an extra percentage on the subsystem for both mass and power, if it is possible in these margins	Cassini, (if double computer is used)	N/A
	Trackers	4 star trackers, 2 sun sensors	Unknown	0.2
	IMU	1 IMU with built-in redundancy	Unknown	-
	Reaction wheels	Pyramid scheme	Cassini, Europa Clipper, JUICE	5.5
C&DH	Data Processing Unit	Double Data Processing Unit	Cassini, Europa Clipper	1.2
	Solid State Drive	2 SSDs. Include software copies in case any of the other systems are corrupted	Unknown	0.6

	RAM	2 RAM sticks	Unknown	Negligible
	Data buses	Double buses	Cassini, JUICE	Part of harness
	Software	Further studies into software design is needed	N/A	N/A
Communications	Transponders	2 transceivers Ka & X band. 2 transceivers S band. All cross strapped with respective	Cassini, but for more bands	5.3
	Amplifier	2 amplifiers Ka, 2 X, 2 S	Cassini	5.5
	Antennas	1 HGA, 1 MGA	No exact match	-
Thermal & Radiation	Sensors	2 sensors for: each payload instrument (excl. hoppers), each ADCS tracker, the IMU, each reaction wheel, each transponder, each amplifier. 52 sensors in total	Europa Clipper	negligible
	Rad shielding	General vault (EPS & ADCS), Payload vault, reaction wheel vault, 2 extra payload sensor vaults, IPR has no vault	No exact match, Europa Clipper uses vault	N/A
	Passive or active	Passive: MLI and radiators	No match	N/A
EPS	SA	4 wings, all with connection to PMU	Studies into deployment are needed	N/A
	PMU	Double PMU	Europa Clipper has only double PMU for propulsion	2.6
	Batteries	Double Battery	Unknown	3.2
Mechanisms	Kickstage separation	Double the amount of explosive bolts	N/A	negligible
	Magnetometer Boom	Folded	JUICE	N/A

16.2.3. Conclusion and Recommendations

These three spacecraft have been designed for the harsh conditions of interplanetary spaceflight and in the case of Cassini, have proven reliability. By using identical, similar, or in some cases even higher redundancy than these spacecraft it can be said, with reasonable certainty, that ELMO meets the requirement of a bus reliability of 0.87 by the end of the nominal mission.

For a more quantitative and certain estimation of the reliability, theoretical reliability data, as well as actual data of individual components on orbit without failure needs to be combined into a bus reliability value, as is done for the Myriad platform in [112]. This is recommended for further studies.

Other recommendations are:

1. Further definition of the redundancy of components considering hot, cold and warm redundancy.
2. Further definition of the fail-operational mode of ELMO during critical phases.
3. Extensive testing of delayed solar array deployment (see Section 15.4). Already when considering nominal deployment, solar array deployment drives infant mortality of spacecraft [118]. In the case of ELMO, the solar array deployment mechanism will experience changing thermal conditions and damage accumulation from the harsh space environment before deployment.
4. Studies into the effect of micrometeorites on the system. This has not been accounted for in the design at this point.
5. Studies into the effect of particles from the E-ring of Saturn on the system.

6. Studies into space and time partitioning of software. Both Cassini [114] and Europa Clipper [116] use this in some form.
7. Studies into the radiation resistance of the IPR. The IPR has no radiation protection and sits outside of the spacecraft body.

16.3. Safety

According to ECSS-Q-ST-40C [119], 'The objective of safety assurance is to ensure that all safety risks associated with the design, development, production, and operations of a space product are adequately identified, assessed, minimized, controlled, and finally accepted through the implementation of a safety assurance programme.' Safety assurance concerns a number of principles. One principle is safety engineering, the identification and mitigation of risks. This is done in Section 16.4. Another principle is safety analysis and verification, which can be accomplished by rigorous testing. The testing campaign is discussed in Chapter 15. For operational safety, for example handling of hydrazine, the principles set by ESA are followed. The last principle of safety for spacecraft is the consideration of disposal. Disposal of ELMO is considered in Chapter 13, but the ΔV required for disposal is not incorporated in the design. However, in the sensitivity analysis performed in Chapter 14, the effect of extra ΔV on the spacecraft design is assessed.

16.4. Risk Management

Risk management is a structured and systematic decision-making process that effectively identifies, evaluates, plans, monitors, mitigates, communicates, and documents risks to improve the probability of successfully achieving the mission objectives. The risk management outlined in this section follows the ECSS-M-ST-80C standards [120].

16.4.1. Success Criteria

The first step of the risk management process is the definition of the success criteria of the project, which are shown in Table 16.6.

Table 16.6: Success criteria for the ELMO spacecraft.

Domain	Success Criteria
Science + Technical	SCI01. The mission accomplishes the key science goals. TEC01. The spacecraft operates successfully over the mission lifetime. TEC02. No performance degradation owing to SPF, and no failure propagation. TEC03. A reliability of 0.75 at EoM as defined in USR-SYS-02.
Safety + Protection	SAF01. The hazards the spacecraft poses associated with the manufacturing, operation (including end of life) as well as personnel, other property, and the environment are eliminated. PRT01. No debris is created during design, manufacturing, and operating of the spacecraft. PRT02. The orbiter and kickstage are disposed at end of operations.
Schedule	SCH01. The project schedule is compatible with the ready for launch delivery date of 2035 as defined in USR-MIS-01.
Cost	COS01. The development and production costs of the spacecraft are compatible with the budget of $750\,\mathrm{M\$}$ (FY2025) as defined in USR-SYS-06.

As shown in Chapter 15 the time until 2035 appears to be too short for the delivery of ELMO. Moreover, as shown in Chapter 17, the budget appears to be too tight for the development and production of the spacecraft.

16.4.2. Severity and Likelihood Categorisations

Risk are classified according to their impact domains. Risks will be assessed in terms of severity and probability. The severity of the risk is defined according to the worst-case impact with respect to the domains science, technical and safety, schedule cost, and mass on a scale of 1 to 5 in Table 16.7.

The probability of a risk is normalised on a scale of A to E in Table 16.8.

Table 16.7: Severity categorisation.

Score & Severity	Science	Technical / Safety	Schedule	Cost	Mass
5 Catastrophic	Failure leading to the impossibility of fulfilling the mission's scientific objectives	*Safety:* Loss of life, life-threatening or permanently disabling injury or occupational illness; Severe detrimental environmental effects. *Dependability:* Loss of ELMO spacecraft, launcher, or launch facilities	Delay of more than 48 months	Cost increase of more than $750\,\mathrm{M\$}$ (FY2025)	Increase of more than dry mass: $250\,\mathrm{kg}$, wet mass: $750\,\mathrm{kg}$
4 Critical	Failure results in a major reduction (70-90%) of mission's science return	*Safety:* Major damage to flight systems, major damage to ground facilities, or private property; Temporarily disabling but not life-threatening injury or temporary occupational illness; Major detrimental environmental effects *Dependability:* Major degradation of the system	Delay of 24-48 months	Increase in estimated cost of $500-750\,\mathrm{M\$}$ (FY2025)	Increase of dry mass: $100-250\,\mathrm{kg}$, wet mass $500-750\,\mathrm{kg}$
3 Major	Failure results in an important reduction (30-70%) of the mission's science return	*Safety:* Minor injury, minor disability, minor occupational illness. Minor system or environmental damage. *Dependability:* Partial degradation of the system	Delay of 6-24 months	Increase in estimated cost of $250-500\,\mathrm{M\$}$ (FY2025)	Increase of dry mass: $50-100\,\mathrm{kg}$, wet mass: $250-500\,\mathrm{kg}$
2 Significant	Failure results in a substantial reduction (10-30%) of the mission's science return	*Safety:* Impact less than minor *Dependability:* Minor degradation of the system (e.g., system is still able to control the consequences).	Delay of 3-6 months	Increase in estimated cost of $50-250\,\mathrm{M\$}$ (FY2025)	Increase of dry mass: $5-50\,\mathrm{kg}$, wet mass: $25-250\,\mathrm{kg}$
1 Minimum	No/minimal consequences (<10% impact)	No/minimal consequences	Delay of 1-3 months	<$50\,\mathrm{M\$}$ (FY2025)	dry mass: <$5\,\mathrm{kg}$, wet mass: <$25\,\mathrm{kg}$

Table 16.8: Probability categorisation.

Score	Probability	Definition
E	Maximum	Certain to occur, will occur once or more times per project.
D	High	Will occur **frequently**, about 1 in 10 projects
C	Medium	Will occur **sometimes**, about 1 in 100 projects
B	Low	Will occur **seldom**, about 1 in 1000 projects
A	Minimum	Will **almost never** occur, 1 in 10000 projects

16.4.3. Risk Index and Acceptance Policy

The risk index is the combination of the probability and impact of a risk. The risk indices are shown in Table 16.9. Risks that are too high need mitigation. The proposed actions for each risk index are shown in Table 16.10.

Table 16.9: Risk indices shown in a risk map.

	Probability				
Severity	A (min.)	B (low)	C (medium)	D (high)	E (max.)
5 (catastrophic)	A5	B5	C5	D5	E5
4 (critical)	A4	B4	C4	D4	E4
3 (major)	A3	B3	C3	D3	E3
2 (significant)	A2	B2	C2	D2	E2
1 (minor)	A1	B1	C1	D1	E1

Table 16.10: Risk indices and proposed actions.

Adopted Risk Index	Risk Magnitude	Proposed Actions
E4, E5, D5	**Very high risk**	**Unacceptable risk:** implement mitigation action(s) - either reduce likelihood or reduce severity through renegotiation of requirement
E3, D4, C5	**High Risk**	
E2, D3, C4, B5	**Medium Risk**	
E1, D1, D2, C2, C3, B3, B4, A5	**Low Risk**	**Acceptable risk:** control and monitor
C1, B1, A1, B2, A2, A3, A4	**Very Low Risk**	

16.4.4. Risk Log

The risks that have been preliminarily identified are shown in Table 16.11, along with their mitigation and new risk index. Distinct risk mitigations are denoted with letters.

Table 16.14 shows the risks before mitigation, Table 16.15 shows the risks post mitigation. Note that some risks have multiple mitigations, they do not suggest that more risks have been created.

Table 16.14: Risk map post-mitigation.

	Probability				
Severity	A (min.)	B (low)	C (medium)	D (high)	E (max.)
5 (catastrophic)	R9		R5		R1, R3, R4
4 (critical)					
3 (major)			R7	R6	
2 (significant)			R8		
1 (minor)	R2				

Table 16.15: Risk map pre-mitigation.

	Probability				
Severity	A (min.)	B (low)	C (medium)	D (high)	E (max.)
5 (catastrophic)	R9, R3b	R5a			R4a1, R4b1
4 (critical)			R4a2, R4b2		
3 (major)			R7	R6	R3a
2 (significant)			R8		
1 (minor)	R2, R1a, R4c				

Table 16.11: Risk log for the ELMO spacecraft.

Identified risk and preliminary risk assessment	Risk mitigation and preliminary assessment	Risk Index
R1 - Unrealistic schedule ready for launch date of 2035 specified by customer, the project schedule has to be in line with the ready for launch date. **Baseline risk:** **Schedule** - development/ production / testing / transport needs more time than available till 2035 probability: **maximum** / severity: **catastrophic** -> **very high risk**	**Baseline mitigation:** negotiation with customer to adopt ready for launch date a) no further mitigation needed **Remaining risk:** a) risk removed	baseline risk: R1 - E5 remaining risk: R1a - A1
R2 - Suboptimal launch window ELMO is designed for arrival before 2051 meaning no eclipse **Baseline risk:** Eclipse periods of 8% of orbit around Enceladus charging of batteries can be done during communications -> payload idled for at most 8% of mission Section 3.6 probability: minimum severity: minimum ->	**Baseline mitigation:** no mitigation required **Remaining risk:** no risk remaining	baseline risk: R2 - A1
R3 - Mass budget mass budget specified by customer (max. launch mass Ariane 64: $9600\,\mathrm{kg}$) **Baseline risk:** **Mass** ELMO design is exceeding given mass specification probability: **maximum** severity: **catastrophic** -> **very high risk**	**Baseline mitigation:** a) negotiation with customer for payload reduction b) negotiation with customer to launch with a different launch vehicle **Remaining risk:** a) **Science** decrease (30-70%) probability: **maximum** / severity: **major** -> **high risk** b) **Schedule** increase of more than 48 months probability: **minimum** / severity: **catastrophic** -> **low risk**	baseline risk: R3 - E5 remaining risk: R3a - E3 R3b - A5
R4 - Cost budget cost budget specified by customer ($750\,\mathrm{M\$}$ FY2025) **Baseline risk:** **Cost** Estimated costs of ELMO design are exceeding given cost specification probability: **maximum** severity: **catastrophic** -> **very high risk**	**Baseline mitigation:** a) outsource payload instrument costs to scientific institutions b) share development costs with other missions c) negotiation with customer to increase cost budget **Remaining risk:** a1*) **Cost** overrun (more than $750\,\mathrm{M\$}$ and **Schedule** probability: **maximum** / severity: **critical** -> **very high risk** a2*) **Schedule** delay of 24-48 months probability: **medium** / severity: **critical** -> **medium risk** b1*) **Cost** overrun ($500 - 750\,\mathrm{M\$}$ probability: **maximum** / severity: **critical** -> **very high risk** b2*) **Schedule** delay of 24-48 months probability: **medium** / severity: **critical** -> **medium risk** c) risk removed **Mitigations are included for completeness and can be used in combination with c*	baseline risk: R4 - E5 remaining risk: R4a1 - E5 R4a2 - C4 R4b1 - E4 R4b2 - C4 R4c - A1

R5 - Safe mode during critical phase normal failure handling is fail-safe **Baseline risk:** **Science** loss of mission due to safe mode during critical phase of transfer flight probability: **medium** / severity: **catastrophic** -> **high risk**	**Baseline mitigation:** a) selection of fail-operational strategy for critical phases **Remaining risk:** a) **Science** loss of mission probability: **low** / severity: **catastrophic** -> **medium risk**	baseline risk: R5 - C5 remaining risk: R5a - B5
R6 - Unknown micrometeorite resistance ELMO is exposed to an unknown flux of micrometeorites during transfer flight and in orbit around Enceladus **Baseline risk:** **Mass** the effects of micrometeorites on external components (MLI, louvers, SA, engine nozzles, ...) needs assessing. Further studies might conclude extra protection is required. Cassini uses a retractable engine cover to protect a thermal coating inside the main engine nozzles [114]. Elmo's main engines also use a film for cooling [a] probability: **high** / severity: **major** -> **medium risk**	**Baseline mitigation:** No mitigation yet, await further studies **Remaining risk:** **Mass** increase of dry mass (<100 kg) probability: **high** / severity: **major** -> **medium risk**	baseline risk: R6 - D3
R7 - Effect of E-ring unknown ELMO orbits Enceladus, situated in the E-ring of Saturn **Baseline risk:** **Mass** The E-ring contains particles expelled by Enceladus' cryovolcanoes. The effect of these particles on the solar intensity experienced by ELMO and on the payload instruments are unknown. Further studies might conclude extra SA area or protection of the payload is needed probability: **medium** / severity: **major** -> **low risk**	**Baseline mitigation:** No mitigation yet, await further studies **Remaining risk:** **Mass** increase of dry mass (<100 kg) probability: **high** / severity: **major** -> **low risk**	baseline risk: R7 - C3
R8 - Delayed SA deployment thermal management requires SA to stay in a non deployed configuration until after the hot phase of the transfer flightsubsection 11.1.2 **Baseline risk:** **Schedule** the delayed SA deployment is an unproven procedure. Studies into the delayed deployment might conclude this concept to be too unreliable, requiring redesign of the system, resulting in a delay of phase A of 3 to 6 months probability: **medium** / severity: **significant** -> **low risk**	**Baseline mitigation:** Acceptable risk, no mitigation **Remaining risk:** **Schedule** increase (6-24 months) probability: **low** / severity: **major** -> **low risk**	baseline risk: R8 - C2
R9 - Communications and science split For scientific value and to reduce the number of slews during operations, the mission has been split into three equal batches of science and communication orbits. Section 3.3 **Baseline risk:** **Science** the communications subsystem has one SPF, as it has only one HGA dish capable of downlinking scientific data. If the HGA fails in the first batch of science orbits, no scientific data can be downlinked. probability: **minimum** / severity: **catastrophic** -> **low risk**	**Baseline mitigation:** no mitigation required **Remaining risk:** **Science** probability: **minimum** / severity: **catastrophic** -> **low risk**	baseline risk: R9 - A5

16.4.5. Conclusions and Recommendations

The following risks should be discussed with the customer. For a more detailed proposition to alter the requirements, refer to Chapter 18:

- R1 - Unrealistic schedule
- R3 - Mass budget
- R4 - Cost budget

The following risks need further studies for more detail:

- R6 - Unknown micrometeorite resistance
- R7 - Effect of E-ring unknown
- R8 - Delayed solar array deployment

The following risks are recommended to be discussed, analysed, and mitigated in the coming phases:

- R5 - Safe mode during critical phase
- R6 - Unknown micrometeorite resistance, even though this risk requires further studies, the risk is of a level that some proactive mitigation is recommended.

17
Cost and Market Analysis

This chapter discusses the cost estimation of the ELMO spacecraft and the market analysis. In Section 17.2, a database containing dry mass and cost of spacecraft is used to select a cost estimation model. Section 17.3 gives several cost reducing methods. Finally Section 17.4 presents the findings and recommendations.

17.1. Requirements

Table 17.1: Cost requirements.

ID	Description
USR-SYS-06	The orbiter (including payload) shall cost equal or less than $750\,\mathrm{M\$}$ (FY 2025).

17.2. Cost Estimation

Since the project is in an early stage and cost data on components used in the spacecraft is not readily available, cost estimation is done parametrically. There are a number of cost estimation tools that rely on parametric estimation to determine spacecraft cost, all with different applicabilities, complexity, and training sets. Two models are considered for cost estimation for the ELMO spacecraft: the SVLCM for unmanned planetary spacecraft[1] and a model from ADSEE-1 reader [12], taken from a 1996 NASA study.[2]

17.2.1. Database

To evaluate the predictive capacity of the SVLCM and ADSEE model, a test set of data is needed. Therefore, a database has been formed, consisting of 29 spacecraft, documenting primarily the dry mass and spacecraft costs, the fiscal year of those costs, and where applicable, the total mission, launch service, and operations costs, with respective fiscal years. An important note to be made is that the spacecraft costs entail both the development and the production costs. In subsection 17.2.3, the estimated costs will be broken down into development and production costs.

The development costs, excluding launch service and operation costs, for each of the spacecraft, were determined in one of three ways:

1. Development cost was found directly. This was the case for VEX[3], MEX[4], Cassini [121], DAWN [122], Magellan [5] and MRO [123]

[1] Spacecraft/Vehicle Level Cost Model, Accessed on: 21-1-2025, URL: https://www.globalsecurity.org/military/intro/reference/calc/SVLCM.htm

[2] unfortunately, the reference in the reader seems to be incorrect.

[3] Venus Express, Accessed on: 21-01-2025, URL: https://nssdc.gsfc.nasa.gov/nmc/spacecraft/display.action?id=2005-045A

[4] European Space Agency's Mars Express, Accessed on: 21-01-2025, URL: https://www.space.com/18206-mars-express.html

[5] Magellan, Accessed on: 21-1-2025, URL: https://nssdc.gsfc.nasa.gov/nmc/spacecraft/display.action?id=1989-033B

2. Development cost was found by using the PEBD. This has been done for all spacecraft with a '*'. The development costs per year are multiplied by their conversion factor and summed. Often, the launch costs are included in the budget of the development (spacecraft with entries for 'LV cost'), if that is the case, they are subtracted from the spacecraft costs. If available, launch service cost and date from the news release are used. If a news release is not available, the cost reported in the PEBD with stated FY is used. If no FY is stated in PEBD, the launch year minus two years is used as FY, to account for the launch contract signed well in advance of launch.
3. Spacecraft costs were found by subtracting launch costs and operation costs from total mission costs. This has been done for JUICE, Rosetta, and BepiColombo. As all missions were launched by an Ariane 5 on an Earth escape orbit and were quite massive (lowest wet mass 3 tons), the launch costs are assumed to be $289\,\mathrm{M\$}$ FY2025[6], the most expensive configuration. The operation costs are estimated by averaging average operation costs per year ($50\,\mathrm{M\$}$ FY2023), determined using PEBD, of 10 spacecraft (see 'Avg. ops. costs per year') and multiplying by operational time, assumed $3\,\mathrm{years}$ for JUICE, $4\,\mathrm{years}$ for Rosetta and $3\,\mathrm{years}$) for BepiColombo.

A number of spacecraft have been excluded from the database. The exclusions and reason for exclusion are shown in Table 17.2.

Table 17.2: Excluded spacecraft from deep space spacecraft dataset.

Spacecraft	Reason for exclusion
Insight, Phoenix	Lander
Perseverance, MER (Opportunity), MSL Curiosity, Mars Pathfinder	Rover
Mariners, Pioneers, Ranger, Viking, Lunar orbiters	Considered too old
Mars sample return, NEO Surveyor, VERITAS	In the process of spacecraft
VIPER	Cancelled
GRAIL, Mars Odyssey	PEBD and officially reported LCC do not match

In Table 17.3, the data is shown, containing deep space spacecraft launched from 1989-2024. An online inflation calculator tool has been used to convert between fiscal years.[7] Most cost data comes from the Planetary Exploration Budget Dataset[8] (PEBD), this data set is based on public NASA budget estimates submitted to Congress, which list obligations, for the period 1959-1997 and from 2002 onwards. For the period of 1997-2001, the PEBD is based on [124] for the period 1997-2001. Dry mass data is from NASA's archive[9].

Validation of the cost data was done by comparing the total cost of the PEBD to the total costs reported in NASA's archive[10] for a number of spacecraft. The data mostly matched, spacecraft that had discrepancies were excluded from the database. One notable discrepancy is that of Cassini, the PBED reported a $3\,\mathrm{G\$}$ FY2023 spacecraft cost, whereas a slide from the 2008 SCEA-ISPA Joint Annual Conference and Training Workshop [121] stated a spacecraft cost of $2\,\mathrm{G\$}$ FY2023 for bus and payload.

[6]"Arianespace aims high in Asia-Pacific", Accessed on: 21-1-2025, URL: https://www.flightglobal.com/arianespace-aims-high-in-asia-pacific/120757.article

[7]US Inflation calculator, Accessed on: 21-1-2025, URL: https://www.usinflationcalculator.com/

[8]The Planetary Exploration Budget Dataset, Accessed on: 21-1-2025, URL: https://www.planetary.org/space-policy/planetary-exploration-budget-dataset

[9]NASA Space Science Data Coordinated Archive, Accessed on: 21-1-2025, URL: https://nssdc.gsfc.nasa.gov/

[10]NASA Space Science Data Coordinated Archive, Accessed on: 21-1-2025, URL: https://nssdc.gsfc.nasa.gov/

Table 17.3: Deep space spacecraft data set. *Spacecraft costs have been determined using The Planetary Exploration Budget Dataset.

Spacecraft	Avg. ops. costs per year [M$ FY2023]	LV FY [year]	LV cost [M$]	Spacecraft cost (can include LV & OPS) [M$]	FY [year]	Dry mass [kg]	Spacecraft costs [M$ FY2025]
BepiColombo (2x)	-	2025	289	1700	2023	2700	2047
Cassini	93	-	-	1009	1997	2523	1988
CONTOUR*	-	-	-	172	2023	328	178
DART*	-	2019	69	347	2023	483	274
DAWN	-	-	-	282	2007	747	429
Deep Space 1*	-	-	-	197	2023	374	204
Europa Clipper*	82	2021	178	4190	2023	3241	4129
Galileo*	87	-	-	2072	2023	2830	2145
Genesis*	-	-	-	282	2023	494	292
GRAIL*	-	2009	149	617	2023	265	432
JUICE	-	2025	289	1650	2023	2420	1419
Juno*	32	2007	190	1289	2023	1593	1045
LADEE*	-	2014	58	360	2023	248	296
Lucy*	-	2022	149	775	2023	821	641
Magellan	-	-	-	407	1991	1035	944
Mars Global Surveyor*	-	-	-	268	2023	1031	277
Mars Observer*	46	-	-	1205	2023	1125	1247
MAVEN*	-	2010	187	740	2023	903	495
MESSENGER*	19	2002	69	483	2023	485	379
MEX	-	-	-	195	1996	606	392
MRO	41	-	-	450	2005	1031	705
NEAR*	-	-	-	261	2023	487	270
New Horizons*	23	2004	182	906	2023	385	633
Osiris-Rex*	35	2013	184	1006	2023	880	793
Psyche*	-	2020	117	1059	2023	1400	953
Rosetta	-	2025	289	970	2023	1280	1125
Stardust*	-	-	-	249	2023	300	258
VEX	40	-	-	98	2005	670	158
Voyager* (2x)	-	-	-	1126	2023	1444	1165

17.2.2. Comparison of Cost Estimation Methods

Payload costs are often not financed by ESA or NASA, but by scientific institutions [42]. This is further supported by the specific reporting of instrument development costs for the Galileo and Voyager missions. It is assumed that SVLCM and ADSEE have been trained on spacecraft costs and dry mass excluding payload.

A plot of the dry mass versus spacecraft costs of the database can be seen in Figure 17.1, with the estimation curves of SVLCM and ADSEE. By visual inspection, it can be determined that ADSEE (blue) is quite good at estimating costs for spacecraft of low mass, whereas SVLCM (orange) estimates closer to the actual values for more massive spacecraft, but overestimates for lighter spacecraft.

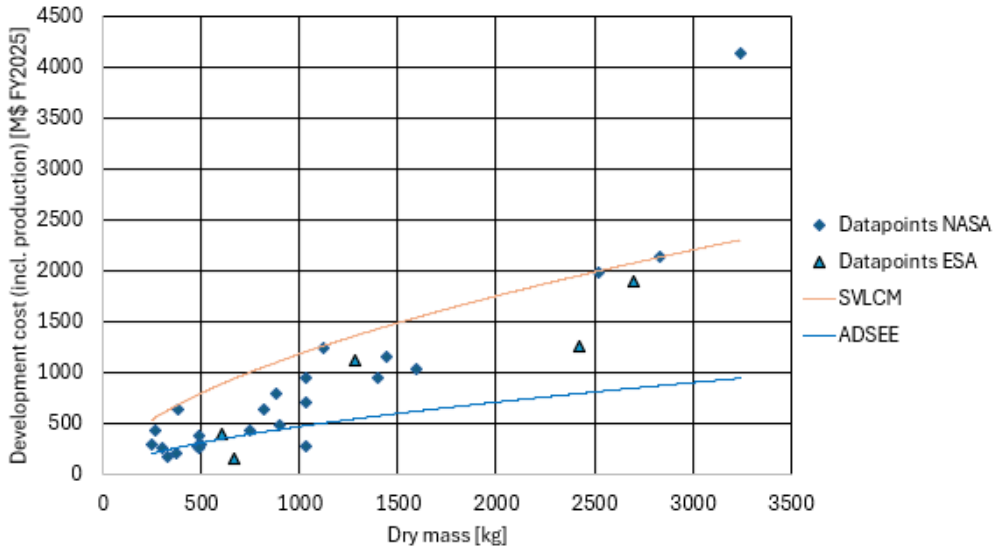

Figure 17.1: Dry mass versus spacecraft costs.

Figure 17.2 shows the actual costs and both estimations for each spacecraft. Relevant parameters of the performance of both models are shown in Table 17.4, the mean of actual spacecraft cost is $862\,\mathrm{M\$}$ and the standard deviation is $824\,\mathrm{M\$}$.

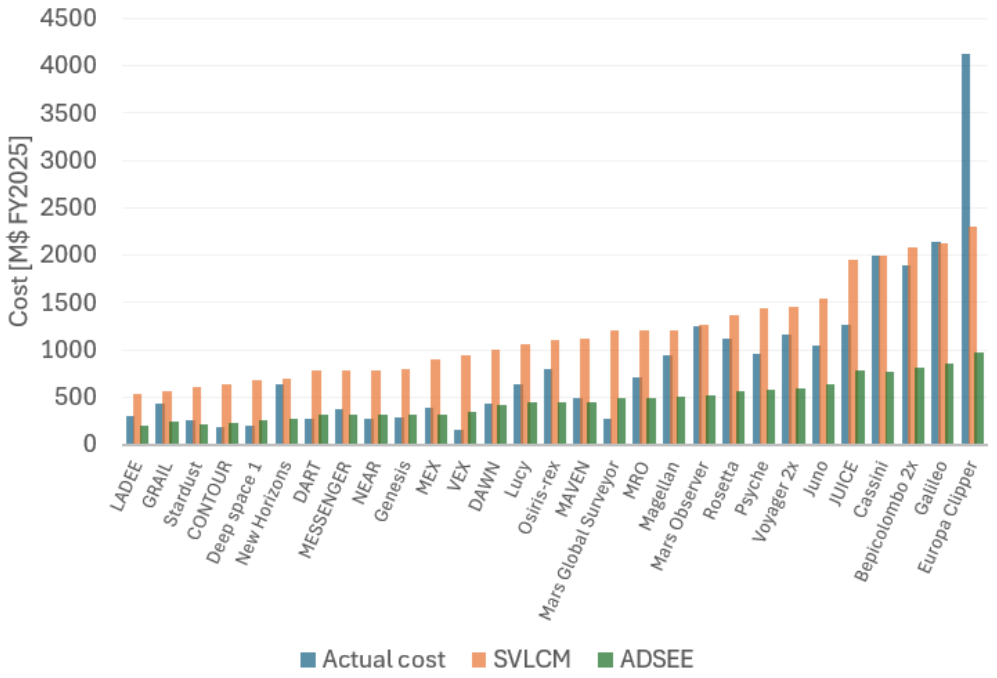

Figure 17.2: Estimated costs versus actual costs.

Table 17.4: Performance comparison between SVLCM and ADSEE.

Performance Parameter	SVLCM	ADSEE
R^2	0.54	0.15
RMSE [M$ FY2025]	560	758
Relative Standard Error of Estimate (RSE)	0.50	1.0

Considering the dry mass of ELMO excluding payload is $2290\,\mathrm{kg}$, it is in the more massive range. This fact, combined with the performances of the models, is the reason for the selection of the SVLCM model for the parametric cost estimation of ELMO.

17.2.3. Final Cost Estimate and Breakdown

The MLE of the spacecraft bus cost using SVLCM is $1892\,\mathrm{M\$}$ FY2025. Adding the payload costs including contingencies gives a total spacecraft cost of $2045\,\mathrm{M\$}$ FY2025. The MLE $2045\,\mathrm{M\$}$ budget is broken down into $1613\,\mathrm{M\$}$ for development of the bus, $279\,\mathrm{M\$}$ for production and $153\,\mathrm{M\$}$ for payload costs including contingencies. The RSE is a measure of the certainty of an estimate. It is similar to the standard deviation of a data set and follows the 66-95-99 rule. The probability of the actual cost being lower than the estimate is 82.5% for the MLE plus RSE. The MLE plus RSE estimation is $2846\,\mathrm{M\$}$ FY2025. The MLE + RSE $22\,846\,\mathrm{M\$}$ budget is broken down into $2426\,\mathrm{M\$}$ for development of the bus, $420\,\mathrm{M\$}$ for production and $153\,\mathrm{M\$}$ for payload costs including contingencies.

Two remarks need to be made on the cost estimate. One remark is that ELMO is in essence quite a small spacecraft with a big propulsion subsystem. This adds a lot of dry mass that usually is not very costly in terms of money. This suggests that the estimate is an overestimation.

The other remark is that SVLCM is a model relying on old data. Based on the last modification of the site, the youngest data is at best from 2005. As discussed in subsection 15.4.2, current trends for testing are shifting towards a protoflight approach. The protoflight approach entails refurbishing the testing model for use as the flight model, saving on production, integration, and testing costs. This is done at the cost of 30% non-recurring costs for refurbishment[58]. Considering development costs as non-recurring costs, the refurbishment costs are $484\,\mathrm{M\$}$. Some data could be found on the reduction of testing costs and integration costs due to the protoflight approach, but it could not be determined how those costs were related to the total development costs so, no estimate can be given. Since the industry seems to shift towards the protoflight approach due to it reducing costs, a good case can be made for the SVLCM approach overestimating costs due to the protoflight approach. The estimation of this cost reduction is recommended for further studies.

However, even if the MLE is reduced by one RSE, the estimated cost is still $1419\,\mathrm{M\$}$. The conclusion is that, with the current considerations USR-SYS-06 is unfeasible.

17.3. Market Analysis

Following the conclusion in subsection 17.2.3, it is clear that there is a need for cost reduction. The key stakeholders, presented in a stakeholders map in Figure 17.3 and the SWOT analysis, presented in Figure 17.4 are tools used in this process.

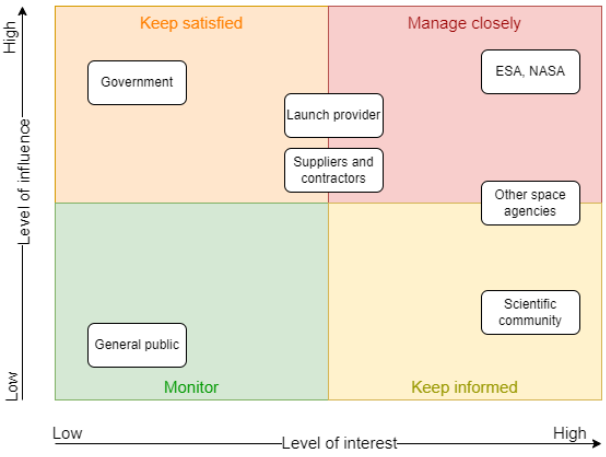

Figure 17.3: Stakeholders map for ELMO.

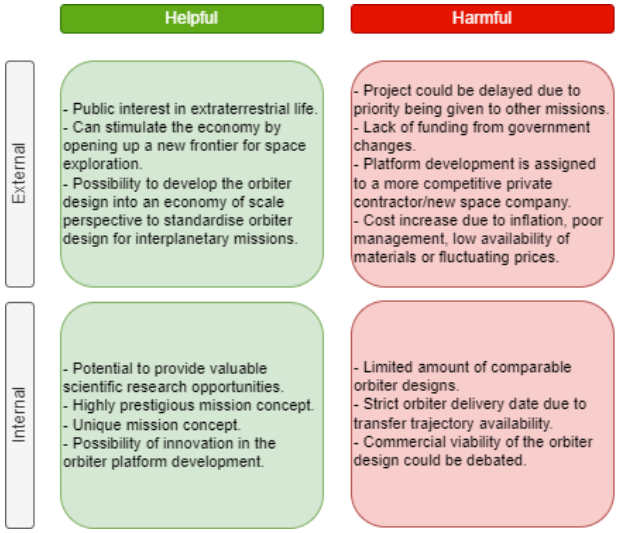

Figure 17.4: SWOT analysis for ELMO's market analysis.

One cost reducing method for a project is sharing development costs with other projects. The cost breakdown of $1613\,\mathrm{M\$}$ for the development of the spacecraft and $279\,\mathrm{M\$}$ for production, seems to suggest there is a lot of potential for cost reduction by sharing development costs.

An example of cost reduction by sharing development costs can be seen when one looks at the combined costs of the MEX and VEX missions. By using already developed components from MEX, ESA managed to save $180\,\mathrm{M€}$[11] FY2005 (determined by comparing total mission cost of the article to mission cost found in NASA's archive[12]). Dividing the amount of reduced costs by the spacecraft costs of VEX $158\,\mathrm{M\$}$, the cost reduction $405\,\mathrm{M\$}$ and the spacecraft costs of MEX $392\,\mathrm{M\$}$ (values come from Table 17.3 gives a reduction of 42% of spacecraft costs. This cost reduction method seems very promising. A reduction of 42% would mean costs would reduce from $2045\,\mathrm{M\$}$ to $1186\,\mathrm{M\$}$ FY2025. There is however a problem: since the requirements for ELMO were so constraining, the spacecraft is optimised for the niche of its particular mission. This means that the chances of other missions being able to share development costs with ELMO are quite slim. Nonetheless, some possibilities have been determined for development cost sharing:

- QUEST[125] - A mission concept of an orbiter of Uranus that considered a similar bus to Juno. The ELMO bus however is a more recent design, providing leaps in performance.
- COMPASS [126] - A mission concept for a Jovian orbiter that uses a newly designed spinning, 3 SA panel, bus. The opportunity of sharing development costs might alter the decision of the COMPASS team for the current envisioned design.

By sharing the development costs of 10% of components with one other mission, assuming equal split and no losses, costs for ELMO are reduced by 10% $\cdot$ 1613 $\cdot$ 1/2 = $81\,\mathrm{M\$}$, by sharing with two other missions, costs are reduced by 10% $\cdot$ 1613 $\cdot$ 2/3 = $108\,\mathrm{M\$}$.

The scientific community was identified to have a strong interest in the ELMO project. The purpose of the mission is to investigate signs of life on Enceladus, which could offer valuable insight in a variety of research fields. The scientific community might also offer opportunities for cost reduction. NASA and ESA often outsource development costs of payload instruments to scientific institutions, in exchange for exclusive rights to the data for a year [42]. The outsourcing of payload instruments can save up to the total cost of the payload, $152\,\mathrm{M\$}$ including contingencies.

[11]"Venus Express Frequently Asked Questions (FAQs)", Accessed on: 21-1-2025, URL: `https://www.esa.int/Science_Exploration/Space_Science/Venus_Express/Venus_Express_Frequently_Asked_Questions_FAQs`

[12]Venus Express, Accessed on: 21-01-2025, URL: `https://nssdc.gsfc.nasa.gov/nmc/spacecraft/display.action?id=2005-045A`

17.4. Conclusions and Recommendations

The estimated costs of the ELMO spacecraft are shown in Table 17.5. The bus cost is estimated using the dry mass of the bus $2290\,\mathrm{kg}$.

Table 17.5: Cost estimates ELMO in FY2025.

	Estimated cost bus [M$]	Payload costs incl. contingencies [M$]	Estimated costs spacecraft [M$]	Development costs [M$]	Production costs [M$]
MLE	1892	153	2045	1613	279
MLE + RSE	2846	153	2999	2426	420

It is clear that the cost requirement is not met, even when considering hypothetical cost reduction measures of joint development of 10% of components with another mission (-$81\,\mathrm{M\$}$) payload outsourcing (-$153\,\mathrm{M\$}$). It is recommended that the cost requirement be renegotiated with the customer.

Another recommendation in two fold, is refining the cost estimate by accounting for the effect of the kick stage on the cost estimation and the effect of a protoflight testing approach.

The high RSE shows the top-down cost estimation has a lot of uncertainty. For a better estimation of the cost, it is recommended that, if possible, a bottom-up approach be used to estimate the cost in the following stage. If there still is not enough data on the cost of individual components, it is recommended that NASA's PCEC software is used to come to a more accurate top-down estimation. [13]

By considering the orbiter (dry mass of $1633\,\mathrm{kg}$ and kick stage (dry mass of $922\,\mathrm{kg}$) as two separate systems, the ADSEE estimation method might be more applicable to either of the systems, reducing the cost estimate. If the cost of the orbiter is estimated using SVLCM and the cost of the kick stage with ADSEE, the MLE is $1925\,\mathrm{M\$}$ FY2025, if both systems are estimated using ADSEE, the MLE is $1183\,\mathrm{M\$}$ FY2025. It is recommended that this possibility be assessed in further studies.

[13] Project Cost Estimating Capability (PCEC), Accessed on: 21-1-2025, URL: https://software.nasa.gov/software/MFS-33187-2

18
Requirement Compliance and Recommendations

This chapter starts with assessing the requirements compliance of ELMO in Section 18.1, after which options that can improve the performance of a future design are explored in Section 18.2.

18.1. Requirements Compliance

In this section, the requirement compliance matrix is discussed. The compliance of all user requirements addressed in Section 3.1 has been examined and is displayed in Table 18.1. From this table, it is clear that most requirements have been met. A good example is requirement USR-PLD-02, which states: 'The orbiter shall be able to supply a maximum power of $97.5\,\mathrm{W}$ to the payload'. This requirement is used as an input for the electrical power system, resulting in the EPS complying with it (see Chapter 6).

In general, only small deviations from this rule exist. As an example, USR-MIS-03 is given, which states: 'The transfer orbit shall be of a similar trajectory to Cassini.' This requirement required investigation before the implications could be found and designed for using methods similar to those mentioned for USR-PLD-02. The only exception to the general rule for requirements that are met is the requirement for reliability, USR-SYS-02, which states: 'The orbiter reliability (including payload) shall be equal or better than 0.75 for EoM.' After extensive research and design efforts, this requirement is reasoned to be met (for details, see subsection 16.2.3).

Table 18.1: Requirement Compliance Matrix.

Compliance	IDs
Yes	USR-SYS-02, USR-SYS-03, USR-SYS-04, USR-SYS-05, USR-SYS-07, USR-SYS-08, USR-SYS-09, USR-MIS-02, USR-MIS-03, USR-MIS-04, USR-MIS-05, USR-MIS-08, USR-MIS-09, USR-PLD-01, USR-PLD-02, USR-PLD-03, USR-PLD-04, USR-PLD-05, USR-PLD-06, USR-PLD-07, USR-PLD-08, USR-PLD-09, USR-PLD-10, USR-PLD-11, USR-PLD-12, USR-PLD-13, USR-PLD-14, USR-PLD-15, USR-PLD-16, USR-PLD-17, USR-PLD-18, USR-PLD-19, USR-PLD-20, USR-PLD-21, USR-PLD-22, USR-PLD-23, USR-COM-01, USR-COM-02, USR-COM-03, USR-COM-04, USR-COM-05.
No	USR-SYS-01, USR-SYS-06, USR-MIS-06, USR-MIS-07.
At Risk	USR-MIS-01

Table 18.1 shows five requirements that are not met or are at risk of not being met. The first is the requirement related to the maximum launch mass, USR-SYS-01, stating: 'The spacecraft shall be compatible with the Ariane 64 launch vehicle'. The maximum launch mass for the Ariane 64 is

$9600\,\mathrm{kg}$ to put the spacecraft on an Earth escape trajectory. In Chapter 4, it can be seen that this requirement has not been met. In Section 17.4, it appears that the same is true for the requirement on the maximum cost, USR-SYS-06 which states: 'The orbiter (including payload) shall cost equal or less than $750\,\mathrm{M\$}$ (FY 2025).'

Another requirement that ELMO does not meet is USR-MIS-06, stating: 'A safety policy in accordance with ECCS-Q-ST-40C shall be established that aims to eliminate hazards associated with the manufacturing, operation (including end of life) as well as personnel, other property, and the environment.' This has not been met, as the current design has not incorporated ΔV for EoL, which is part of the safety philosophy in ECCS-Q-ST-40C. This specific customer request has been discussed in Section 13.2. The same is true for USR-MIS-07, which states: 'The orbiter shall comply with the Space Debris Guidelines of the Committee on the Peaceful Uses of Outer Space'. The final noteworthy requirement is USR-MIS-01, which states that 'The orbiter shall be delivered ready for launch in 2035'. This requirement has been placed under the category 'At Risk' as it is at high risk of not being met in the future, especially if other requirements are adhered to. This topic has been explained further in Chapter 15 and Section 16.4.

Failing to meet these requirements renders the current design unfeasible under the existing constraints. Section 18.2 discusses the recommendations regarding this feasibility study moving forward.

18.2. Recommendations for Future Design

As illustrated in Section 18.1, excluding the two requirements on safety and space debris, the ELMO orbiter design does not meet two important requirements namely the launch mass and maximum orbiter cost.

Throughout this feasibility study, many promising design options were rejected due to time constraints or violations of requirements. To improve the feasibility of the mission, the following recommendations and design exploration suggestions are provided for future development of both the orbiter and the mission. Design options are evaluated by qualitatively analysing the benefits of implementing them in future iterations of the ELMO spacecraft.

System Design

As mission requirements evolve and design choices are reassessed, several subsystem design options for future development could be explored. For power generation, the large solar array could be optimised. Further research into newer cell models and lighter support materials could contribute to the overall subsystem mass reduction. Solar panel mechanisms were rejected due to the difficulty of pointing four separate wings, as 2 of the wings would need to flap upwards and downwards with the respective to the spacecraft's longitudinal axis. If two solar panel wings are used instead, they can be made to rotate about their principal axis which enables ELMO to optimise the angle of incidence of the solar arrays. In terms of larger EPS changes, the use of RTGs could also be evaluated, as their mass-to-power production ratio is significantly higher than that of a solar array. The design with RTGs showed promising performance in the previous design phase but was discarded per the request of the customer.

Integration of the ADCS subsystem with the propulsion subsystem may allow for a more efficient ADCS that uses more powerful and higher specific impulse thrusters. This option was rejected early in the design due to reliability and complexity concerns but would eliminate the need for independent ADCS propellant tanks, and this configuration is not uncommon in previously flown spacecraft.

CFRP propellant tanks were rejected as the hypergolic propellants would be too reactive for such a material, however, the feasibility of CFRP tanks with a titanium liner still warrants further investigation. The integration of the fuel tanks in the orbiter's support structure should also be explored, as this could help reduce the structural mass of the spacecraft.

Regarding the structural mass, there would be the possibility to make the truss structure lighter by employing a generative truss design, however, as this technology is more recent it would likely be more difficult to qualify for space applications. Nonetheless, further investigation on lighter structures is suggested. Moreover, the attachment design could also be evaluated further, as the current estimation is larger than the projected one.

It is recommended to explore whether the design of the T&RC subsystem could have a better performance considering its high relative mass compared to that of Cassini's. This improvement would be reached by increasing the MLI mass. This is worth investigating as this increase could lead to a large decrease in the required heater and louver mass. Moreover, the radiative effects of the RHU on the system should be evaluated. Furthermore it should be investigated how to ensure that the kick-stage does not go below allowable temperature limits (as the eclipsing of the entire spacecraft the heatshield may cause extreme local temperature variations). Finally the choice of coating for the heatshield should be reconsidered in future designs as the absorptivity of the gold coating is too high.

A design change could be considered at a payload level, where the design of the instruments could be optimised focusing on mass as well as power consumption reductions, which would lead to the transmission orbits becoming the critical ones for the design. Consequentially, the communication performance could also be increased: optical communications offer higher bandwidth but face challenges such as lower technology readiness and the need for high-precision antenna alignment. Maintaining RF transmission while addressing the assumptions in the ELMO design would result in power consumption too high for the EPS to sustain. More advanced transmission modulation schemes could increase the achievable data rate with the same transmission power, but robust error correction needed to maintain reliability will also increase power requirements. Therefore, a lower required data rate, coupled with further optimisation of subsystem parameters (such as antenna size, gain, and transmission efficiency), would be necessary to have a feasible design, though it would limit the downlink science data rate.

When lowering the data rate, the value of the acquired science data could be preserved by enabling the onboard data processing unit to evaluate the significance of measurements, selectively choosing data for transmission thus reducing the overall required data rate without reducing the gathered data. It is recommended to explore the option of reducing the data rate by selecting non-redundant data from the second and third orbit batches with respect to the first. This would lead to a negligible increase in mass for C&DH for enhanced processing, but also a significant decrease in mass of the communication subsystem. Furthermore, it is recommended to evaluate the use of the standardised Advanced Data Handling Architecture (ADHA) in development by ESA which could be adapted to the specific requirements of the ELMO mission.

Transfer flight

The sensitivity analysis showed that ΔV is the most driving factor for the spacecraft launch mass. A reduction of $600\,\mathrm{m\,s^{-1}}$ still did not bring the total launch mass below the launch mass requirement. ΔV reductions seem necessary and can be obtained by further studies in trajectory optimisation, for example by making use of additional gravity assists in the inner solar system, to follow a trajectory more similar to that of JUICE [1].

Several advantages of delaying the launch were identified. The 2035 launch timeline was deemed too short and unrealistic compared to the development time of similar missions. Additionally, it was found that if ELMO launches in 2035, the South Pole of Enceladus, where its mission-critical tiger stripes are located, would be in a polar night for the next decade. If the launch is delayed by 15 years, the South Pole will be in permanent sunlight and will be able to be photographed by the HRC. Due to Saturn's orbital eccentricity, delaying the mission by 15 years would have Saturn 1

[1] https://sci.esa.int/web/juice/-/58815-juices-journey-to-jupiter

AU closer to the Sun, resulting in a 20% increase in solar power which would snowball into a major mass reduction. Delaying the mission would allow for key technologies to achieve readiness such as storable cryogenic propellants which have much higher specific impulses which would also snowball into significant mass reductions. Finally, delaying the launch would increase the time for RTGs to become more readily available as a power source; RTGs were found to be more optimal for mass and reliability but were rejected primarily due to their low availability and sustainability considerations.

For further mission definitions, it is relevant to note that if ELMO was permitted to launch aboard other launchers such as Falcon Heavy[2], the mass requirement would be met, as the Falcon Heavy is capable of sending a mass of 16.8 tons on an Earth escape trajectory.

The specific impulse value of the non-toxic green propellant mention in Section 14.3, should be revised for as [3] shows thrusters able of provide a specific impulse from around $280\,\mathrm{s}$, with the given specific impulse of the bi-propellant itself being $319\,\mathrm{s}$. However, this is without considering the usage of the gelling agent used at the thruster in Section 14.3. Investigation can be done on finding a more accurate specific impulse value, which will probably be way higher, leading to the usage of green propellant becoming less unfeasible.

End of Life

A more developed ELMO mission will need to consider an end of life in accordance with the planetary protection protocols followed by ESA and NASA. Furthermore, crashing into Enceladus will not be a viable option. Tethys is the closest moon to Enceladus, and it was calculated that with a Hohmann transfer, Tethys would be the least demanding celestial body that ELMO could impact into other than Enceladus. Tethys is much less significant in the study of extraterrestrial life. Crashing into it would allow ELMO to comply with planetary protection policy. This manoeuvre would take roughly $550\,\mathrm{m/s}$ of additional ΔV. However, this could potentially be reduced with gravity assists.

The kick stage must also have its end-of-life procedure. This was not studied extensively as there are a significant number of unknowns about the transfer flight to Enceladus, but the most likely option for disposal of the kick stage will be to detach it while in a Saturn impact trajectory or to have it directed into such a trajectory by solid rocket motors.

This shows that there are still a lot of possibilities for performance gain for ELMO. However, it needs to be stressed that, even with the performance improvements allowed by the requirements, considering the current technology and the technology available in the reasonably near future, under the current set of constraints, the chances of converging to a feasible design meeting all requirements are low. The current set of requirements needs to be reevaluated and altered to enable a future design team to come to a feasible design.

[2] https://www.spacex.com/vehicles/falcon-heavy/

[3] http://www.astronautix.com/h/h2o2kerosene.html

19
Conclusion

This report has detailed the feasibility study for the ELMO (Enceladus Life and Mechanisms Explorer) orbiter, which aims to send an orbiter to Enceladus to investigate biosignatures and analyse the moon's unique environment. The mission concept involves the orbiter carrying a payload suite of five scientific instruments and two hopper vehicles, designed to conduct in-depth investigations of the moon's south pole geysers.

While the design process introduced several mass and cost-saving measures such as using a truss structure, opting for a two-stage design and incorporating off-the-shelf components where possible, several critical challenges emerged. Chief among them is the high total ΔV requirement of $6\,\mathrm{km/s}$, which is significantly greater than comparable missions such as Cassini-Huygens. This requirement contributed to the projected launch mass of $13.5\,\mathrm{tons}$, significantly exceeding the Ariane 64's maximum allowable mass of $9.6\,\mathrm{tons}$ by $3.8\,\mathrm{tons}$. Similarly, the estimated mission cost of 2.0 B$ more than doubles the allocated 750 M$ budget. Further iterations of the mission design are necessary to address these issues, making the already challenging ambitious 2035 launch date, increasingly unfeasible.

To address these issues, the ELMO orbiter design team recommends several strategies, including trajectory optimization to reduce ΔV, leveraging additional gravity assists, and extending the timeline to be able to integrate emerging technologies in the design. Delaying the launch to 2050 could also ensure optimal sunlight conditions on Enceladus' south pole, maximizing scientific output. Additionally, the addition of emerging technologies afforded by a delayed launch could provide further mass and cost-saving opportunities.

Despite these challenges, this study concludes that the ELMO mission holds immense scientific value and potential. By refining the spacecraft design and mission parameters, ELMO can become a transformative step in humanity's search for life beyond Earth. Continued development, informed by the findings of this study, will be critical to advancing this ambitious mission concept toward realization.

Bibliography

[1] Coin News Media Group, “Inflation Calculator,” , 2025.

[2] “ENCELADUS LIFE & MECHANISM EXPLORER (ELMO) Orbiter design,” , 2024.

[3] NASA, “Cassini Mission: Scenic Route to Saturn,” , 2017. Accessed: 2025-01-16.

[4] G. Neukum and R. Jaumann, “HRSC: the High Resolution Stereo Camera of Mars Express,” , 2002.

[5] Shin, D. K., “Frequency and Channel Assignments,” Tech. Rep. JPL 810-005-201 Rev. F, NASA Jet Propulsion Laboratory, 2022.

[6] NASA, “Cassini Mission: Quick Facts,” , 2025. Accessed: 2025-01-19.

[7] NASA, “Cassini Mission: Spacecraft Navigation,” , 2025. Accessed: 2025-01-19.

[8] NASA, “Cassini Program Status Report,” , 2025. Accessed: 2025-01-20.

[9] Brown, C. D., *Elements of Spacecraft Design*, American Institute of Aeronautics and Astronautics, Reston, Virginia, 2002.

[10] Zak, A., “Fregat upper stage,” , 2024.

[11] SRE-PA & D-TEC staff, “Margin Philosophy for Science Assessment Studies,” Tech. Rep. SRE-PA/2011.097, European Space Agency (ESA), Noordwijk, The Netherlands, 2012. Prepared by ESA’s SRE-PA and D-TEC staff for assessment studies.

[12] Zandbergen, B., *AE1222-II: Aerospace Design & Systems Engineering Elements I*, 6th ed., TU Delft, 2020.

[13] Viasat Inc., “HI-BEAM Modem: High-Throughput Satellite Communications,” , 2021.

[14] L3 Harris Technologies, “High Data Rate Transmitters,” , 2020. IMS Datasheet.

[15] Taylor, J., Sakamoto, L., and Wong, C.-J., “Cassini orbiter/huygens probe telecommunications,” *DESCANSO Design and Performance Summary Series*, 2002.

[16] Thales Group, “Radio Frequency and Microwave Sources for Space,” , n.d.

[17] Stellant Systems, “86160HX Traveling Wave Tube,” , n.d..

[18] SatCatalog, “SGSL-100 S-Band Transponder,” , n.d.

[19] Stellant Systems, “8412HXR Traveling Wave Tube,” , n.d..

[20] European Space Agency, “Radio Frequency Distribution Network for Spacecraft Communication Systems,” Tech. rep., European Space Agency (ESA), 2025.

[21] Roddy, D., *Satellite Communications Systems*, 4th ed., McGraw-Hill, New York, 2006.

[22] NASA Jet Propulsion Laboratory, “Chapter 2: Deep Space Communications,” , 2014. Monograph Series 13.

[23] Chang, C., “Deep Space Network Document 810-005: Telecommunications Link Design Handbook,” Tech. rep., NASA Jet Propulsion Laboratory, 2020.

[24] Stelzried, C. T., Freiley, A. J., and Reid, M. S., “System noise concepts with DSN applications,” *Low-Noise Systems in the Deep Space Network, MS Reid, Ed. Jet Propulsion Laboratory*, 2008, pp. 13–94.

[25] Labelle, R., and Rochblatt, D., “Ka-band high-rate telemetry system upgrade for the NASA deep space network,” *Acta Astronautica*, Vol. 70, 2012, pp. 58–68.

[26] Taylor, J., Cheung, K.-M., and Seo, D., “Galileo Mission: A Summary of the Galileo Mission to Jupiter,” , 2005. DPSummary Document.

[27] Lazio, J., “The Deep Space Network Radio Astronomy User Guide,” *Jet Propulsion Laboratory, California Institute of Technology*, 2021.

[28] Zhu, X., Jin, K., Hui, Q., Gong, W., and Mao, D., “Long-range wireless microwave power transmission: A review of recent progress,” *IEEE Journal of Emerging and Selected Topics in Power Electronics*, Vol. 9, No. 4, 2020, pp. 4932–4946.

[29] Schiavon, G., Ferraxxoli, P., Guerriero, L., Jorgensen, R., Badessi, S., De Maagt, P., and Fenech, H., “Improving satellite antenna temperature estimation by high-resolution emission model of the earth,” *IEEE Antennas and Propagation Society International Symposium. 1999 Digest. Held in conjunction with: USNC/URSI National Radio Science Meeting (Cat. No. 99CH37010)*, Vol. 3, IEEE, 1999, pp. 2174–2177.

[30] Laboratory, N. J. P., “Voyager Mission Summary,” , 2014.

[31] Speretta, S., “AE2111-II Telecommunications - Lecture S4,” , 2024.

[32] Liu, C., Yang, S., and Nie, Z., “Design of a parabolic reflector antenna with a compact splash-plate feed,” *2013 Cross Strait Quad-Regional Radio Science and Wireless Technology Conference*, 2013, pp. 241–244. https://doi.org/10.1109/CSQRWC.2013.6657398.

[33] Nessel, J., “Propagation Terminal Design and Measurements,” *mm-wave Satellite Communications Workshop*, Vol. GRC-E-DAA-TN27748, 2015.

[34] Huang, J., and Imbriale, W., “Spacecraft antenna research and development activities aimed at future missions,” *Spaceborne Antennas for Planetary Exploration*, Citeseer, 2006, pp. 485–536.

[35] Reznik, S., Prosuntsov, P., and Novikov, A., “Comparison of space antennas mirror reflectors parameters made of composite materials,” *MATEC Web of Conferences*, Vol. 110, EDP Sciences, 2017, p. 01072.

[36] Larson, W. J., and Wertz, J. R., *Space Mission Analysis and Design*, 2nd ed., Springer, 2013.

[37] European Space Agency, “Cassini-Huygens Engineering,” , n.d.

[38] Henry, C. A., “An introduction to the design of the Cassini spacecraft,” *Space science reviews*, Vol. 104, No. 1, 2002, pp. 129–153.

[39] Spectrolab, Inc., “XTE-LILT (Low Intensity Low Temperature) Space Qualified Triple Junction Solar Cell,” , 2019.

[40] QiOptics, “Qioptiq Space-Qualified Cover Glass Datasheet,” , n.d.

[41] M. Kroon et al., “Solar arrays for Jupiter missions Europa Clipper and JUICE,” , 2019.

[42] Jameux, D., January 2025. Personal communication.

[43] Tounsi, R., Zouari, B., Chaari, F., Haugou, G., Markiewicz, E., and Dammak, F., "Experimental study of aluminium honeycomb behaviour under dynamic multiaxial loading," *EPJ Web of Conferences*, Vol. 26, 2012.

[44] Ibeos, "B50-412/825/1237 50-Volt Modular Battery," , 3 2024.

[45] Scheidegger, R., and Soeder, J., "Spacecraft Bus Voltage Selection 2015 Space Power Workshop," , 5 2015.

[46] Airbus Defence and Space, "Datasheet PureLine Pearl V2," , 2 2022.

[47] AZUR SPACE Solar Power GmbH, "30% Triple Junction Solar Cell Assembly, Type: 3G30A 8x8," , 2 2019.

[48] Carrara, V., and Kuga, H. K., "Torque and Speed Control Loops of a Reaction Wheel," *Proceedings of the 11th International Conference on Vibration Problems (ICOVP)*, Lisbon, Portugal, 2013, pp. 1–10.

[49] Strange, N. J., Lam, T., Russell, R. P., and Spilker, T. R., "Study on the Stability of Science Orbits at Enceladus," *AAS/AIAA Spaceflight Mechanics Meeting*, 2006. Jet Propulsion Laboratory, California Institute of Technology.

[50] R. Schmehl, J. S., "Flash-evaporation of oxidizer spray during start-up of an upper-stage rocket engine," , 2003.

[51] Smith, I. D., and Dhooge, P. M., "Triple Point Determinations of Monomethylhydrazine and Nitrogen Tetroxide (2.2 Percent by Weight Nitric Oxide)," , 1977.

[52] Megyesy, E. F., *Pressure vessel handbook*, 12th ed., Pv Pub Inc., 2001.

[53] Agusril, A. M. A. Z., Norazman M. Nor, "Failure Analysis of Carbon Fiber Reinforced Polymer (CFRP) Bridge Using Composite Material Failure Theories," , 2012.

[54] ASM Aerospace specification metals inc., "Titanium Ti-6Al-4V (Grade 5), Annealed," , n.d.

[55] Sutton, G. P., *Rocket Propulsion Elements*, 7th ed., Wiley, 2001.

[56] Kurien, J., and R-Moreno, M. D., "Costs and Benefits of Model-based Diagnosis," , 2017.

[57] Space, A., "ARIANE 6 USER'S MANUAL," , 2021.

[58] Wertz, J. R., and Larson, W. J., *Space Mission Analysis and Design*, 3rd ed., Microcosm Press, 2005.

[59] Annarella, C., Fraser, D., Kleespies, H., and Vasicek, C., "Spacecraft Structures," , 1991.

[60] Skullney, W. E., Kreitz, H. M., Harold, M. J., Vernon, S. R., Betenbaugh, T. M., Hartka, T. J., Persons, D. F., and Schaefer, E. D., "Structural Design of the MSX Spacecraft," *JOHNS HOPKINS APL TECHNICAL DIGEST*, Vol. 17, 1996, pp. 59–76.

[61] Akau, R. L., Behr, V. L., and Whitaker, R., "Thermal Design of the Fast-On-Orbit Recording of Transient Events (FORTE) Satellite'," *Small Satellite Conference*, 1994.

[62] Rudolph, D., "Design and development of the Cassini Main engine assembly gimbal mechanism," Tech. rep., NASA, 1996.

[63] Spectrolab, "Space Qualified Triple Junction Solar Cell," , n.d.

[64] Karam, R., *Satellite thermal Control for Systems Engineers*, American Institute of Aeronautics and Astronautics, 1998.

[65] Henninger, J., "Solar Absorbance and Thermal Emmitance of Some Common Spacecraft Thermal Control Coatings," , 1984.

[66] NASA, "Saturn Fact Sheet," , 2024.

[67] NASA, "Venus Fact Sheet," , 2024.

[68] National Institute of Standard and Technology, "Stefan-Boltzmann constant," , n.d.

[69] NASA, "Radioisotope Heater Units," , n.d.

[70] Summer, I., "Thermal Performance of Gaseous-Helium purged Tank-Mounted Multilayer Insulation System During Ground-Hold and Space-Hold Thermal Cycling and Exposure to Water vapor." , 1978.

[71] Nyman, L., "Coatings on Metals and Plastics for Lunar Habitats and Equipment," , 2019.

[72] B.E. Hardt, R. E., R.D. Karam, "Spacecraft Thermal Control Handbook," , 2002.

[73] Thyssenkrupp, "Density of Aluminium," , n.d.

[74] Hetherington, O., December 2024. Personal communication.

[75] Menicucci, A., December 2024. Personal communication.

[76] R. Peyrou-Lauga, P. G., "JUICE (Jupiter Icy Moon Explorer) Spacecraft Thermal Control," , 2021.

[77] SierraSpace, "Passive Thermal Louvers," , n.d.

[78] Kurth, B., "Juno Spacecraft Description," , 2012.

[79] eoPortal, "BepiColombo Mission," , 2018.

[80] SYSTEMS, E., "Evolution and Application of MIL STD 1553 in Modern Technology," , 2014. Accessed: 2025-01-16.

[81] ESA, "The history and basics of the Milbus 1553b," , 2001. Accessed: 2025-01-20.

[82] Bouwmeester, J., "AE3534 Spacecraft Technology: Command and Data Handling Lecture Notes," , n.d.

[83] STAR-Dundee, "An Overview of the SpaceWire Standard," , n.d.

[84] Parkes, S., "The SpaceWire on-board data-handling network," , n.d.

[85] The European Space Agency, "Architectures of Onboard Data Systems," , n.d.

[86] BAE SYSTEMS, "RAD750® radiation-hardened PowerPC microprocessor," , n.d..

[87] BAE SYSTEMS, "RAD750® 6U CompactPCI single-board computer," , n.d..

[88] eoPortal, "LRO (Lunar Reconnaissance Orbiter)," , 2013. Accessed: 2025-01-19.

[89] Berger, R., and Dennis, A., "Session: SpaceWire Onboard Equipment and Software Short Paper," , n.d.

[90] BAE Systems, "Monolithic 64M radiation-hardened SRAM," , n.d.

[91] Mercury, “440 GB 3U VPX Rad-Tolerant SSDR,” , n.d.

[92] United Nations Office for Outer Space Affairs, “Treaty on Principles Governing the Activities of States in the Exploration and Use of Outer Space, including the Moon and Other Celestial Bodies,” , 1966.

[93] Agency, E. S., “BepiColombo overview,” , n.d.

[94] K. Olsson-Francis et al., “The COSPAR Planetary Protection Policy for robotic missions to Mars: A review of current scientific knowledge and future perspectives,” *Life Sciences in Space Research*, Vol. 36, 2023, pp. 27–35. https://doi.org/10.1016/j.lssr.2022.12.001.

[95] “Nedelin’s disaster,” , 2024.

[96] COSPAR, “About COSPAR,” , 2024.

[97] Peter Doran, e., “Planetary Protection of Icy Worlds,” , 2024.

[98] Neveu, M., and Rhoden, A. R., “Age of Enceladus and its ocean,” , 2019.

[99] C. D. Parkinson et al., “Habitability of enceladus: Planetary conditions for life,” *Origins of Life and Evolution of Biospheres*, Vol. 38, 2008, pp. 355–369.

[100] LabXchange, “Europa Clipper: Mission Timeline,” , 9 2024.

[101] ESA, “The Making of JUICE: The Film,” , 11 2023.

[102] Poehler, H. A., “Cassini Cancers,” , 8 1997.

[103] Chun, M., “Hawai’i County Green Party v. Clinton,” , 1997.

[104] Huh, J., Jyoti, B. V. S., Yun, Y., Shoaib, M. N., and Kwon, S., “Preliminary Assessment of Hydrogen Peroxide Gel as an Oxidizer in a Catalyst Ignited Hybrid Thruster,” , 2018.

[105] ESA, “VENUS EXPRESS ANNOUNCEMENT OF OPPORTUNITY,” , 1 2006.

[106] NASA, “Cassini Launch Press Kit,” , 10 1997.

[107] Berner, C., Bernardi, G. D., Giordano, P., and Ferri, P., “The Rosetta Spacecraft: Verification Approach, Testing And Related Analysis With MATED Tool,” , n.d.

[108] NASA, “How to Ship the World’s Largest Space Telescope 5,800 Miles Across the Ocean,” , Sep 2023.

[109] Johnson, W., and Stephens, J., “NASA’S CRYOGENIC FLUID MANAGEMENT TECHNOLOGY DEVELOPMENT ROADMAPS,” *NASA*, 2018.

[110] Airbus, “JUICE,” , Nov 2024.

[111] ECSS, “ECSS-E-ST-10-03-Rev.1,” , 5 2022.

[112] Roig, A., Etchevery, C., and Etienne, K., “Satellite Reliability Model Supporting End-of-Life Operations Success,” *35th Annual Small Satellite Conference*, 2021.

[113] Grile, T. M., and Bettinger, R. A., “Reliability analysis of deep space satellites launched 1991–2020: Bulk population and deployable satellite performance analysis,” *Quality and Reliability Engineering International*, 2024. https://doi.org/10.1002/qre.3600.

[114] Henry, C. A., “An introduction to the design of the Cassini spacecraft,” , 2002. https://doi.org/10.1023/A:1023696808894.

[115] Jaffe, L. D., and Herrell, L. M., "Cassini/Huygens Science Instruments, Spacecraft, and Mission," *Journal of Spacecraft and Rockets*, Vol. 34, No. 4, 1997, pp. 509–521. https://doi.org/10.2514/2.3241.

[116] Bayer, T., and Bittner, M., "Europa Clipper Mission: Preliminary Design Report," , 2019.

[117] Ecale, E., Torelli, F., and Tanco, I., "JUICE interplanetary operations design drivers and challenges," *15th International Conference on Space Operations, 2018*, 2018. https://doi.org/10.2514/6.2018-2493.

[118] Castet, J. F., and Saleh, J. H., "Satellite and satellite subsystems reliability: Statistical data analysis and modeling," *Reliability Engineering and System Safety*, Vol. 94, 2009, pp. 1718–1728. https://doi.org/10.1016/j.ress.2009.05.004.

[119] ECSS, "Space product assurance Safety ECSS Secretariat ESA-ESTEC Requirements & Standards Division Noordwijk, The Netherlands," , 2 2017.

[120] ECSS, "Space project management Risk management," , 7 2008.

[121] Zandbergen, B., "Slide from the 2008 SCEA-ISPA Joint Annual Conference and Training Workshop," , January 2025. Received via email, unpublished material.

[122] NASA, "Dawn Launch Mission to Vesta and Ceres," , 9 2007.

[123] Beasley, D., Underwood, J., Webster, G., and Diller, G., "Mars Reconnaissance Orbiter Launch," , 8 2005.

[124] Callahan, J., "Budgeting for Exploration: the History and Political Economy of Planetary Science," *AAS/Division for Planetary Sciences Meeting Abstracts #45*, AAS/Division for Planetary Sciences Meeting Abstracts, Vol. 45, 2013, p. 108.01.

[125] et Al., S. J., "QUEST: A New Frontiers Uranus orbiter mission concept study," *Acta Astronautica*, Vol. 170, 2020, pp. 6–26. https://doi.org/10.1016/j.actaastro.2020.01.030.

[126] et. al, G. C., "Comprehensive Observations of Magnetospheric Particle Acceleration, Sources, and Sinks (COMPASS): A Mission Concept to Jupiter's Extreme Magnetosphere to Address Fundamental Mysteries in Heliophysics," , 2 2023.

A

Astrodynamic Calculations

Estimating the True Anomaly

Calculating the eclipse time due to Saturn and the Saturn-sun distance requires knowing where Saturn is in its orbit. However, due to Saturn's eccentricity, using a circular orbit approximation is inaccurate. Specifically, assuming a constant speed of Saturn around the sun leads to a position error of 6 months at certain points of Saturn's orbit. These are the equations relating the true anomaly, eccentric anomaly and mean anomaly. The interval between Saturn's equinoxes oscillates between 13.7 and 15.7 years instead of the 14.7 years predicted by the circular orbit approximation. To fix this problem, a new and more accurate approximation of true anomaly will be derived and subsequently used in the following sections. The derivation starts by highlighting the following 2 equations, relating the true, eccentric and mean anomalies. True anomaly is related to eccentric anomaly in Equation A.1:

$$\tan(\frac{\theta}{2}) = \sqrt{\frac{1+e}{1-e}}\tan(\frac{E}{2}) \tag{A.1}$$

Mean anomaly is related to eccentric anomaly in Equation A.2

$$E - e\sin E = M \tag{A.2}$$

The problem is that these equations cannot be transformed to find an exact explicit equation of the true anomaly as a function of the mean anomaly (which can easily be related to time). For small eccentricities (e<0.1), it is possible to find an equation for true anomaly as a function of time. This is done by deriving a first order approximation of the exact equations. The derivation starts by approximating $M \approx E$ in Equation A.2, leading to this equation:

$$E = M + e\sin M \tag{A.3}$$

The square root term can be approximated as follows.

$$\sqrt{\frac{1+e}{1-e}} = \sqrt{(1+e)\cdot\frac{1}{1-e}} \approx \sqrt{(1+e)\cdot(1+e)} = 1+e \tag{A.4}$$

$$\theta = 2\arctan[(1+e)\tan(\frac{M+e\sin M}{2})] \tag{A.5}$$

It is possible to simplify this equation by finding the first-order Taylor series expansion around e = 0 of the following function:

$$f(e) = \arctan[(1+e)\tan(x)] \tag{A.6}$$

Which is:

$$f(e) = x + \frac{\tan(x)}{1 + (1+e)^2 \tan^2(x)} \cdot e \tag{A.7}$$

Because this is a first order approximation, it is possible to set $1 + e \approx 1$ in this equation

$$f(e) = x + \frac{\tan(x)}{1 + \tan^2(x)} \cdot e \tag{A.8}$$

Using Pythagoras' formula of tangents and secants $sec^2(x) = 1 + tan^2(x)$ and several trigonometric identities, it is possible to deduce the next equation.

$$f(e) = x + \sin x \cos x \cdot e \tag{A.9}$$

Leading to this Taylor expansion approximation

$$\arctan[(1+e)\tan(x)] \approx x + \frac{e}{2}\sin 2x \tag{A.10}$$

Using this equation to simplify A.5 yields:

$$\theta = 2[\frac{M + e\sin M}{2} + \frac{e}{2}\sin(M + e\sin M)] \tag{A.11}$$

Because this is a first order approximation: $\sin(M + e\sin M) \approx \sin(M)$. It leads to the final equation relating the true anomaly as a function of mean anomaly.

$$\theta = M + 2e\sin(M) \tag{A.12}$$

The approximation can be verified by plotting it against the true function in Figure A.3

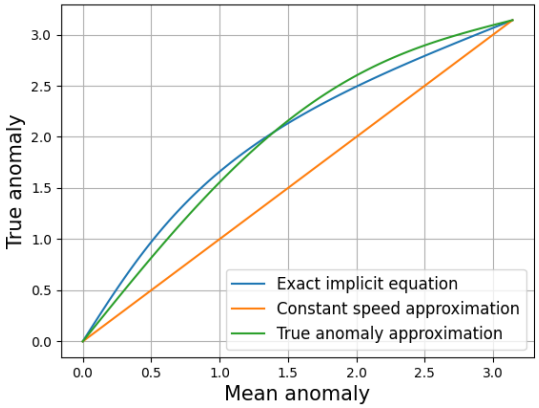

Figure A.1: High eccentricity (e = 0.33)

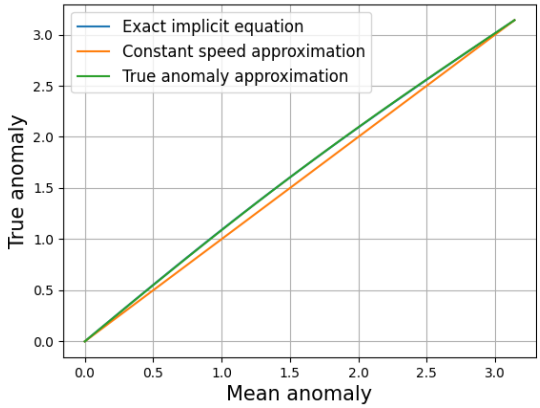

Figure A.2: Saturn eccentricity (e = 0.052)

Figure A.3: Verification of the true anomaly approximation

The newly derived approximation is plotted against the constant speed approximation and the exact formulas. On the left figure they are plotted for a high eccentricity of 0.25 and on the right they are plotted for the smaller eccentricity of Saturn of 0.052. On the left, it can be seen that the newly derived

approximation is already much better than the constant speed approximation but shows significant deviation from the true values. The newly derived approximation truly shows its use on the right where it is so close to the exact function, it becomes hard to see any deviation. The newly derived approximation has a maximum position error of around 5 days out of the 29.45 year Saturnian orbit, and will turn out very useful in the next sections.

Calculations for the Eclipse time around Saturn

First, you define a planar orbit around Saturn. Then you transform it using 3D rotation and projection matrices. Finally, you track what fraction of the orbit is behind Saturn. A circular orbit is defined representing Enceladus orbiting around Saturn on the XY plane.

$$\vec{O} = \begin{bmatrix} a_{enc}\cos(\lambda) \\ a_{enc}\sin(\lambda) \\ 0 \end{bmatrix}$$

Two rotation matrices are applied. R_x rotates the orbit around the x-axis by the inclination of the Saturn system ($i = 26.7°$). R_z is a rotation that represents the fact that Enceladus' orbit can be viewed from different directions depending on where Saturn is in its orbit. The two matrices are depicted below

$$R_x = \begin{bmatrix} 1 & 0 & 0 \\ 0 & \cos(i) & -\sin(i) \\ 0 & \sin(i) & \cos(i) \end{bmatrix} \quad R_z = \begin{bmatrix} \cos(\Omega) & -\sin(\Omega) & 0 \\ \sin(\Omega) & \cos(\Omega) & 0 \\ 0 & 0 & 1 \end{bmatrix}$$

Ω is the right ascension of the ascending node and is set equal to $\Omega = -(\theta + \Delta\theta)$. $\Delta\theta$ corresponds to the difference of the true anomaly between Saturn's perihelion and equinox. Using the fact that Saturn's equinox occurs on the 6th of May 2025, $\Delta\theta$ can be found to be $98.5°$. The true anomaly can be calculated using Equation A.12.

Lastly, the 3D vector (x,y,z) is projected to a 2D vector, removing the depth coordinate x. This can be done using this projection matrix:

$$P = \begin{bmatrix} 0 & 1 & 0 \\ 0 & 0 & 1 \end{bmatrix}$$

When the magnitude of the projected vector is smaller than the radius of Saturn, Either Enceladus is in front of Saturn or Saturn is in front of Enceladus, leading to an eclipse. Therefore, half the time that the vector's magnitude is smaller than the radius, Enceladus will be eclipsed.

$$|P \cdot R_z(\Omega) \cdot R_x(i) \cdot \vec{O}| < r_s \tag{A.13}$$

r_s is Saturn's radius and was set equal to $62\,268\,\mathrm{km}$, which is Saturn's equatorial radius plus a margin of 2000 km. This accounts for the fact that Saturn's equatorial radius is determined to be where Saturn's atmosphere has the density of 1 bar, which would still cause significant attenuation of the solar flux. The 2000 km above Saturn's defined surface has a similar gas density as in LEO. This was calculated using Saturn's atmosphere halving parameter of 59.5km.

B

Task Division

Table B.1: Distribution of the workload

Report Chapter	Task	Student Name(s)
Executive Summary	Writing	Nelson
Introduction	Writing	Alice
Payload Description	Writing	Farris
Mission Analysis	Requirements and Constraints	Jeroen
	Launch and Transfer Phase, Mission Profile	Farris
	Payload Data Analysis	Farris, Elena
	Astrodynamics (Sections 4,5,6,7,8)	Nelson
System Overview	System Engineering and Writing	Jeroen
	Power Budget	Alice, Visini
	Configuration	Nelson
	Margins iterations	Elena, Matyas, Jeroen
	Functional Analysis	Farris, Christian
Communications	Design, Writing and Diagram	Elena
Power	Design, Diagrams and Writing	Alice
	Back Panel Structural Analysis	Nelson
ADCS	Design, Diagrams and Writing	Sherif
	Previous Phase Design	Jeroen
Propulsion	Design, Diagrams and Writing	Jochem
Structures	Design, Reporting	Visini
Mechanisms	Design, Reporting	Nelson
Thermal and Radiation Design	Design and Writing	Christian
C&DH	Design and Writing	Farris
	Previous Phase Design	Elena
Sus. Dev. Strategy and EoL Plan	Research and Writing	Matyas
Sensitivity Analysis	Writing	Jeroen, Matyas
Further Mission Development	Research and Writing	Matyas
Reliability, Safety, and Risk	Research and Writing	Hidde

Continued on next page

Report Chapter	Task	Student Name(s)
Cost and Market Analysis	Research and Writing	Hidde
Requirement Compliance and Recommendations	Writing	Jeroen, Matyas, Elena, Alice, Hidde
Conclusion	Writing	Sherif
Appendix A	Writing	Nelson
	3D Model	Matyas
	Document Design and Layout	Visini